

# DEFORMATION AND BEARING CAPACITY OF BUCKET FOUNDATIONS IN SILT AND SAND

---

MASTER'S THESIS | 2017



Master's Program in Structural and Civil Engineering

School of Engineering and Science | Aalborg University

Vinojan Vethanayagam





**AALBORG UNIVERSITY**  
STUDENT REPORT

**School of Engineering and Science**  
Department of Civil Engineering  
Thomas Manns Vej 23  
9220 Aalborg Ø  
<http://www.civil.aau.dk>

## Master's Thesis

**Title:**

Deformation and Bearing Capacity of Bucket  
Foundations in Silt and Sand

**Project period:**

September 2016 - June 2017

**Written by:**

Vinojan Vethanayagam


**Supervisor:**

Professor Lars Bo Ibsen

**Number of pages:** 121

**Appendix:** files in folder

**Finished:** 08-06-2017

  
Vinojan Vethanayagam

*The report and its content is freely available, but publication (with source reference) may only happen after agreement with the authors.*

*Front page image is from Universal Foundation A/S.*





## Preface

This report is the Master's Thesis for the Master's Program in Structural and Civil Engineering under the School of Engineering and Science at Aalborg University. It is a long thesis of 60 ECTS points, and the project period spans from September 1<sup>st</sup> 2016 to June 8<sup>th</sup> 2017.

The purpose of this thesis is to develop new analytical design formulas and gaining knowledge by a comprehensive study within the chosen topic.

The student would like to thank the supervisor, Professor Lars Bo Ibsen, for inspiring and motivational academic guidance throughout the whole project period. The motivational and moral support from family and friends is likewise thankfully appreciated.

## Reading guide

The written work of the project will consist of this main report and include a scientific paper produced by the student and supervisor. After the bibliography list different appendices are found. Appendices for the thesis are differentiated by written appendices and a folder containing files such as scripts, calculation sheets and documents. Appendix A contains the article produced in connection to this thesis.

The appendix folder is named 'Appendix Folder', and files are found in sub-folders. References to a file in the appendix folder will be made as: [Appendix Folder, 'sub folder', 'file/folder'].

Throughout the report source references will appear, these will be assembled in a bibliography list at the end of the main report. The system used to refer to a source is the Harvard method. Therefore sources will be referred with [Surname, Year], where the reference leads to the bibliography list.

Figures, tables and equations are numbered according to the chapter, i.e. the first figure in Chapter 7 will have number 7.1, the second will have number 7.2 etc. Captions for figures are found below the figures, and for tables captions are found above the tables.

Roundings of the calculations are made in the report to make the report easier to read. The roundings are made in the extent, which is considered acceptable for the specific case.



The increasing focus on the environment and climate changes both among the population and the politicians means, that alternatives to fossil fuels are sought. Due to the location of Denmark on the northern hemisphere, where hours of sun are scarce, but where there are a lot of wind, wind turbines have gained a footing. Though, the politicians have had problems with the population concerning onshore wind turbines due to the noise nuisance, which the wind turbines generate, and their significant visual impact in the nearby surroundings. Therefore, offshore wind turbines are a more popular solution, where larger offshore wind farms are being established and planned all around the world.

Before offshore wind turbines can become one of the best and most favourable solutions, where demands are not only set from a climate-political perspective, it has to be cheap to design, install, operate and dismantle. The efficiency improvement is clearly seen, as wind turbines are becoming bigger with time. From an engineering perspective the bigger wind turbines mean, that the design of the foundation is complicated. This is due to the fact, that the soil has to have enough bearing capacity to withstand the greater forces, which leads to bigger foundation designs and cost increasements.

The alternative to the analytical formulas is to use finite element models, which can be very time-consuming, thereby increasing costs. Thus, there is an incentive to develop new p-y formulations, which are valid for suction bucket foundations, as the old formulations are valid for slender small-diameter piles. By changing the diameter of the bucket and the soil parameters, 12 numerical models are analysed for both drained and undrained silt with use of the finite element program PLAXIS 3D AE. To simplify the work a number of horizontal displacements of the buckets are made, where the relation between the displacement,  $y$ , and the soil pressure,  $p$ , is found afterwards.

Data from the numerical models is at first compared to former p-y formulations, which are covered in the literature review. The former formulations are not applicable though, thus new are sought. Inspiration to the development of the new p-y formulations are found in some of the former formulations.

As there is a difference in the physical response and the soil parameters between the two, there are some differences in the sub-formulations as well. The soil pressure for the p-y curves for the drained models rise to an ultimate soil pressure and stays there, whereas the undrained models reach the ultimate soil pressure, after which the soil pressure decreases. The drained silt is described with use of a tanh-function, where the undrained silt is described in fragments; until the ultimate soil pressure the curve is described with a tanh-function like the one used for the drained soil, after which the soil pressure is described by a linear decreasing function. The developed p-y formulations are based on the 12 numerical models, which are governed by the diameter of the bucket, the effective in-situ vertical stress, soil stiffness and either the friction angle (for drained silt) or the undrained shear strength (for undrained silt).

Since data from a similar project is available, where sand has been studied, the developed p-y formulation is used to examine its validation for drained sand as well. It is shown, that the p-y formulation for sand can be developed with the same basic formulation and method used for the drained silt. It is also concluded, that precision of the reconsidered p-y formulation is higher than the formulation developed in the original project for sand.

The governing parameters for the p-y formulation for the drained silt is governing for the drained sand as well.

A natural and important direction for the further work should be to study more models with more variations of soil parameters and geometry of the bucket to ensure the validation of the p-y formulations. Furthermore, an interesting objective for the further work would be to examine if clay can be described in similar manner.

Det øget fokus på miljøet samt klimaforandringer blandt befolkningen og politikkerne betyder, at alternativer til fossile brændstoffer eftersøges. Grundet Danmarks placering på den nordlige halvkugle, hvor antallet af soltimer er knappe, men hvor der er en del vind, vinder vindmøller større indpas. Dog har politikkerne problemer med befolkningen vedrørende onshore vindmøller grundet støjgenen, som møllerne generer, samt deres markante visuelle aftryk i de omkringliggende omgivelser. Derfor er offshore vindmøller en mere populær løsning, hvor større havvindmølleparker bliver etableret og planlagt rundt omkring i verden.

Før offshore vindmøller kan blive en af de bedst og mest eftragtede løsninger, hvor kravene ikke kun stilles fra et klimapolitisk perspektiv, skal det være billigt at projekttere, installere, operere og afinstallere. Effektiviseringen ses tydeligt, da vindmøllerne bliver større med tiden. Fra et ingeniørmæssigt perspektiv betyder de større vindmøller, at projekteringen af fundamentet kompliceres. Dette skyldes, at jorden skal have tilstrækkelig bæreevne til at modstå de større kræfter, hvilket resulterer i større fundamenter og øget omkostninger.

Alternativet til de analytiske formler er at bruge finite element modeller, som dog ofte er tidskrævende, hvilket øger omkostningerne. Derfor er der et incitament for at udvikle nye p-y formuleringer, som er gældende for bøttefundamenter, da de gamle formuleringer er gældende for slanke pæle med små diametre. Ved at ændre diameteren af bøtten samt jordparametrene er der analyseret 12 numeriske modeller i silt i drænet samt udrænet tilstand ved at bruge finite element programmet PLAXIS 3D AE. For at simplificere arbejdet påføres bøtten en række horisontale flytninger, hvorefter relationen mellem flytningen,  $y$ , og jordtrykket,  $p$ , findes.

Data fra de numeriske modeller er først sammenholdt med tidligere p-y formuleringer, som er gennemgået i litteraturstudiet. De tidligere formuleringer er dog ikke anvendelig, og derfor søges nye udviklet. Inspiration til udviklingen af de nye p-y formuleringer er fundet ved nogle af de tidligere p-y formuleringer.

Siden der er en forskel i den fysiske respons samt jordparametrene for det drænet og udrænet silt, er der ligeledes forskel i nogle af elementerne i formuleringerne. Jordtrykket for den drænet silt steg til et ultimativt jordtryk og forblev på det niveau ved fortsat flytning, hvorimod det udrænet silt steg til et ultimativt jordtryk, hvorefter jordtrykket faldt ved en fortsat flytning. Den drænet silt er beskrevet ved en tanh-funktion, hvor det udrænet silt er beskrevet i to dele; indtil peaket i jordtryk er kurven beskrevet med en tilsvarende tanh-funktion, hvorefter kurven beskrives med en lineær aftagende funktion for den aftagende del. De udviklede p-y formuleringer er afhængige af bøttediameteren, den effektive vertikale in-situ spænding, jordens stivhed og enten friktionsvinklen (for drænet silt) eller den udrænet forskydningsstyrke (for udrænet silt).

Siden data fra et lignende projekt er tilgængeligt, hvor drænet sand er undersøgt, undersøges den nye p-y formuleringens gyldighed for sand også. Det er vist, at p-y formulering for sand kan udvikles med samme basale formulering og metode som anvendt for den drænet silt. Det er konkluderet, at den reevalueret p-y formulering for sand er mere præcis end den oprindelig formulering, og den er derudover afhængig af de samme parametre som den drænet silt.

En naturlig og vigtig kurs for det videre arbejde bør være at undersøge flere modeller med flere variationer af jordparametre og bøttediametre for at validere og sikre gyldigheden af p-y formuleringerne. Ydermere vil et interessant punkt være at undersøge, om ler kan beskrives på samme vis som sandet og silten.

# Contents

---

<b>Chapter 1</b>	<b>Introduction</b>	<b>1</b>
1.1	Basis of Thesis . . . . .	2
<b>Chapter 2</b>	<b>Literature Review</b>	<b>5</b>
2.1	Numerical Modelling . . . . .	5
2.1.1	Soil . . . . .	5
2.1.2	Structure . . . . .	7
2.1.3	Mesh . . . . .	8
2.1.4	Staged Construction . . . . .	8
2.2	Results . . . . .	9
2.2.1	Method of Stress Integration . . . . .	9
2.2.2	Methods of Data Extraction . . . . .	10
2.3	Data Processing . . . . .	11
2.3.1	Drained p-y Formulations . . . . .	11
2.3.2	Undrained p-y Formulations . . . . .	14
<b>Chapter 3</b>	<b>Numerical Modelling</b>	<b>17</b>
3.1	Model Overview . . . . .	17
3.2	Soil . . . . .	18
3.2.1	Model Domain . . . . .	18
3.2.2	Material Model . . . . .	19
3.2.3	Input Parameters for the Numerical Models . . . . .	22
3.3	Structure . . . . .	26
3.3.1	Material Properties . . . . .	26
3.3.2	Loading of Structure . . . . .	26
3.3.3	Interface . . . . .	27
3.4	Mesh . . . . .	27
3.4.1	Convergence Analysis . . . . .	28
3.5	Staged Construction . . . . .	29
<b>Chapter 4</b>	<b>Results and Comparison of Former p-y Formulations</b>	<b>31</b>
4.1	Data Extraction and Integration of Stresses . . . . .	31
4.2	P-y Curves of the Numerical Models . . . . .	32
4.3	Comparison of Reviewed p-y Formulations and FE Data . . . . .	32
4.3.1	Drained Models . . . . .	33
4.3.2	Undrained Models . . . . .	34
<b>Chapter 5</b>	<b>Formulation of p-y Curves for Silt</b>	<b>37</b>
5.1	Drained Silt . . . . .	37
5.1.1	Normalisation . . . . .	37
5.1.2	Mathematical Model . . . . .	41
5.2	Undrained Silt . . . . .	45
5.2.1	Normalisation . . . . .	45
5.2.2	Mathematical Model . . . . .	48

<b>Chapter 6 Formulation of p-y Curves for Sand</b>	<b>53</b>
6.1 Normalisation . . . . .	53
6.1.1 Formulation of Ultimate Soil Pressure . . . . .	54
6.2 Mathematical Model . . . . .	55
6.2.1 Formulation of Model Parameters . . . . .	55
<b>Chapter 7 Conclusion</b>	<b>59</b>
<b>Bibliography</b>	<b>63</b>
<b>Appendix A Article</b>	<b>65</b>
<b>Appendix B Hardening Soil Small Strain</b>	<b>83</b>
<b>Appendix C Undrained Shear Strength</b>	<b>87</b>
<b>Appendix D Guide for Numerical Modelling and Data Extraction</b>	<b>91</b>
<b>Appendix E Convergence and Model Domain Analysis</b>	<b>95</b>
<b>Appendix F P-y curves of Numerical Models</b>	<b>103</b>
<b>Appendix G Plot of p-y Curves for Silt</b>	<b>109</b>
<b>Appendix H Plot of p-y Curves for Sand</b>	<b>115</b>



Political powers in countries all over the world are trying to reduce the amount of energy consumption consisting of fossil fuels due to climate changes. In countries placed in the northern hemisphere such as Denmark, where the number of hours of sun are limited, solar panels and cells are not an optimal solution. On the other hand, the windy weather in the northern hemisphere can be utilised by wind turbines to produce green energy.

In Denmark wind turbines are already a popular solution regarding renewable energy, but people do not want onshore wind turbines near them, due to them being significant in their surroundings. Thus offshore wind turbines have become a more popular solution on a national scale, as it is seen in Figure 1.1. Globally offshore wind turbines are also popular, which is seen by the increasing investments in offshore wind farms around the world. Beside contributing to the increased amount of energy produced by renewable energy sources, offshore wind turbines are also more productive than onshore wind turbines due to a higher mean wind velocity and a lower surface roughness at sea. [DWIA and Offshoreenergy.dk, 2015]

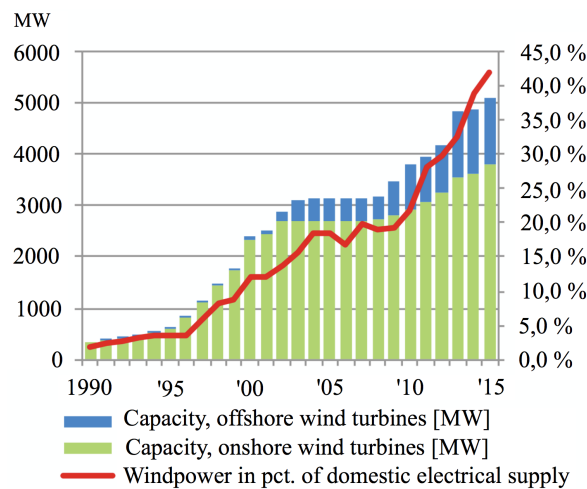


**Figure 1.1:** Wind power capacity and percentage of domestic electricity supply produced by wind turbines in Denmark [Energistyrelsen, 2016].

Wind turbines becomes bigger and bigger due to the continued increasing cost-effective requirements, where the bigger sizes cause problems for the engineers. One of the problems is regarding the foundation of the wind turbine, which must withstand the enormous forces, e.g. from waves, wind and during operation. 2/3 of the cost price of a wind turbine is made up by the foundation and cable, thus the foundations also have to be relatively easy and cheap to install.

To meet the demand to decrease price regarding design, installation, operation and decommission, the recently developed foundation type; *suction bucket* is a good alternative to the gravitational foundation and the monopile, which are typically used. Figure 1.2 shows an example of the suction bucket installed offshore.

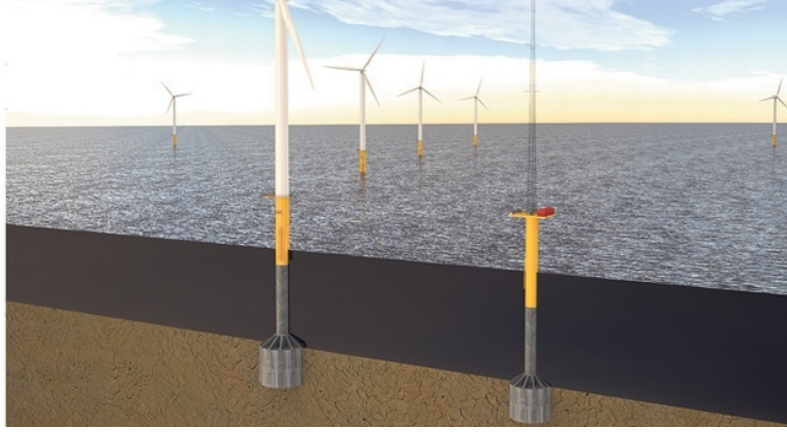


**Figure 1.2:** Suction bucket installed for offshore structures [Recharge News, 2014].

As long as the soil is suitable, the bucket foundations can be used at water depths from near shore to approximately 55m and with 8 MW plus wind turbines. Furthermore, the bucket uses approximately 25 % of the material of a monopile, and the installation is at the same time easier because heavy machinery is not needed, and the process is noise-free due to the suction method. The bucket can be dismantled by reversing the installation process, thus the steel can be recycled, where e.g. monopiles cannot be pulled up and are therefore left in the seabed. [Ibsen et al., 2005] [DWIA and Offshoreenergy.dk, 2015]

## 1.1 Basis of Thesis

When a pile is loaded in either the  $y$ - or  $z$ -direction, there are three stresses appearing from the soil-structure interaction:  $\sigma_N$ ,  $\tau_1$  and  $\tau_2$ , which is also as seen in Figure 1.3

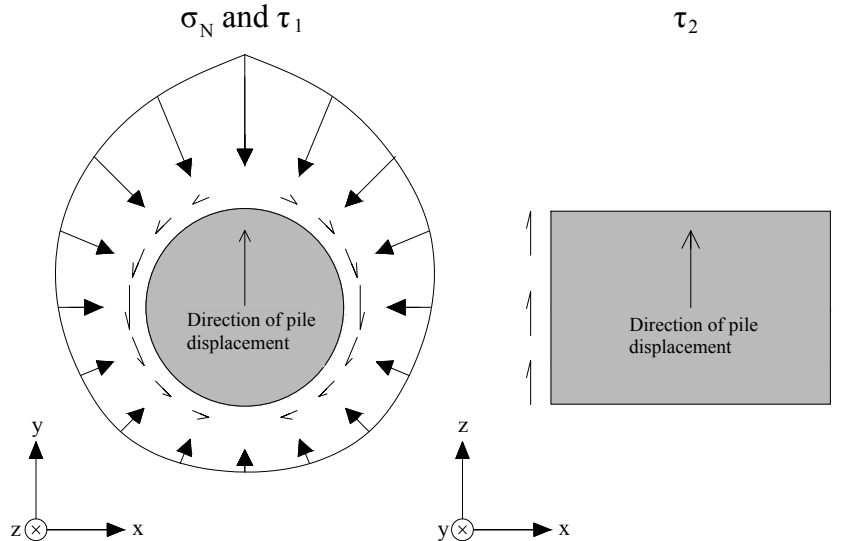


**Figure 1.3:** Displacement of pile in  $y$ - and  $z$ -direction with associating stresses working on the skirt of the suction bucket.

$\sigma_N$  and  $\tau_1$  are taken into account by the  $p$ - $y$  curves, where the two stresses are represented by the lateral soil pressure,  $p$ , while  $\tau_2$  is taken into account by  $t$ - $z$  curves. The  $p$ - $y$  curves describes the relation between a lateral displacement,  $y$ , and the associating lateral soil

pressure,  $p$ . Figure 1.4 shows the principal of a p-y curve, where the figure also shows the ultimate soil pressure,  $p_u$ .

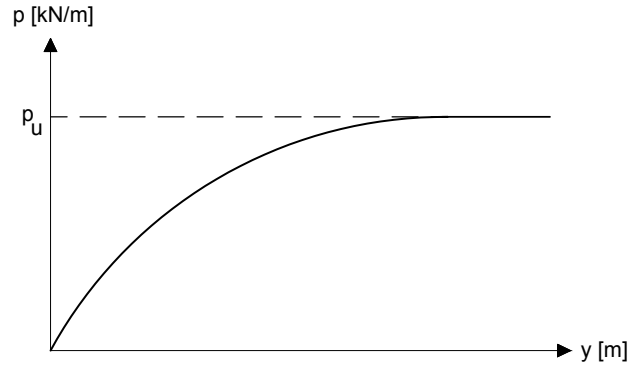


**Figure 1.4:** P-y curve showing the relation between lateral displacement,  $y$ , and the associating lateral soil pressure,  $p$ .

The p-y formulation mentioned in the offshore design code, Det Norske Veritas [2013], for clay was empirically developed by Matlock [1970], where field tests were conducted in Lake Austin, USA. The test pile had a length of 13 m and a diameter of 0.3 m, where it was embedded into inorganic clay and laterally loaded. Cox et al. [1974] developed the p-y formulations for sand, which are based on tests conducted on 0.61 m diameter pile with a length of 21 m in clean fine sand at Mustang Island, USA.

The problem with the formulations of the p-y curves is, that the tests were conducted on piles with a  $L/D > 30$ . It is in contrast to suction bucket foundations of today, which have a slenderness ratio of 0.5-1. The slenderness ratio has a significant impact on the pile behaviour during loading, as slender piles tend to have a flexible behaviour, whereas bucket foundations are less slender and have a rigid movement, as illustrated in Figure 1.5. [Ibsen et al., 2005]

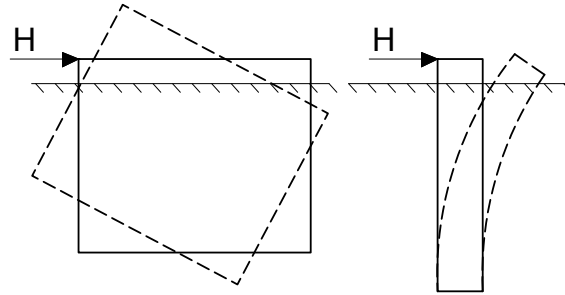


**Figure 1.5:** Rigid behaviour of a bucket foundation and flexible behaviour of a slender pile when laterally loaded.

Achmus et al. [2016] studied monopiles in clay using finite element (FE), where it was shown, that the FE results were closer to the Lake Austin test results, than the formulation developed by Matlock [1970], despite the fact Matlock [1970] calibrated the p-y method on the field tests. Thus Achmus et al. [2016] concluded FE could be used as a tool to obtain p-y curves for large diameter monopiles.

Even though Achmus et al. [2016] concludes, that the formulations developed by Matlock [1970] result in soil with less bearing capacity than results obtained by FE, it cannot

be considered as conservative design estimations in all design senses. The significantly incorrect estimations of the bearing capacity of the soil affects the determination of the eigen-frequencies of the structure, which has to be designed outside the windows of the load-frequencies. Therefore, it is important to be able to estimate the bearing capacity of the soil precisely, as it affects the stiffness.

FE models might result in precise and cost-efficient designs, but a significant drawback is the fact, they are time-consuming, as a single model can run for several days. Hence analytical methods with precise estimations of the bearing capacity are desirable in practical design work. Thus, in the light of work done by Achmus et al. [2016] for monopiles, it is assumed, that FE can be used for suction buckets to develop new and more precise p-y relations as well.

Vahdatirad et al. [2016] modelled a suction bucket in sand by an analytical method; the Winkler method, where springs along the skirt and bottom are modelled, cf. Figure 1.6, to estimate the soil pressure, when the bucket is loaded. The lateral resistance, governed by the p-y springs, was based on the p-y formulation suggested by Østergaard et al. [2015], where FE was used to interpret a number of numerical modelled suction buckets exposed to lateral displacements in drained sand. Vahdatirad et al. [2016] compared the analytical model to results from a field test, from where it was concluded, that the analytical method was fairly precise, but behaved softer than the field test at small strains. The model parameters from the p-y formulation were believed to be the reason of deviating prediction. To obtain more precise estimations, the soil stiffness is sought implemented, thereby making the p-y formulation more versatile as well.

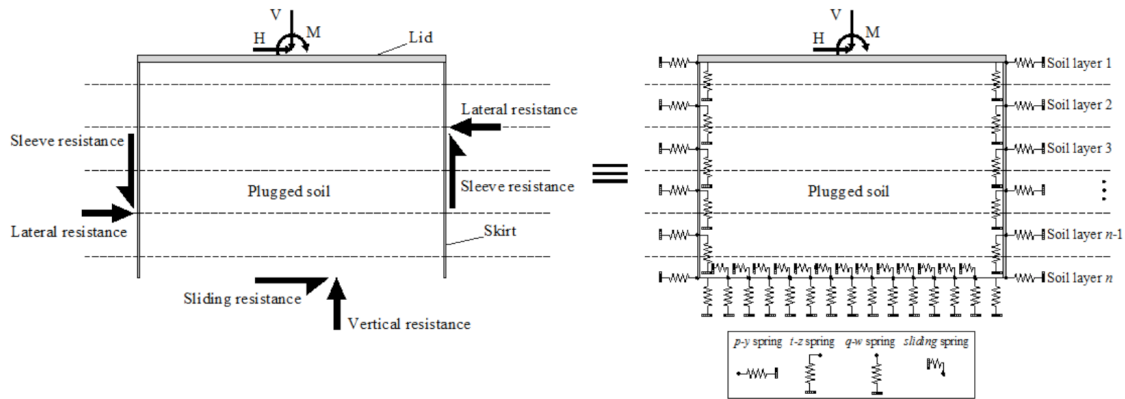


**Figure 1.6:** The principle of the Winkler method, where the suction bucket is modelled with springs along the skirt and bottom [Vahdatirad et al., 2016].

From the abovementioned elements, this thesis aims to develop p-y formulations, where soil stiffness is implemented, for bucket foundations in undrained and drained silt by simulating a number of numerical models in the commercial FE program PLAXIS 3D Anniversary Edition. With use of the data available from Østergaard et al. [2015], a reconsidered p-y formulation for sand is sought as well. Favourably, the formulation should be as simple and practically applicable as possible, and have the same basic formulations regardless of soil type to obtain continuity.

# Literature Review 2

---

To be make sure the thesis becomes a frontier within the scope of this study, knowledge and experiences from earlier studies have to be reviewed and taken advantage of. Thus, a literature review will be a part of this project, and relevant knowledge and conclusions from these studies will be presented in this chapter. The chapter will consist of three overall sections: *numerical modelling*, *results* and *data processing*.

## 2.1 Numerical Modelling

The numerical modelling is about the process of the model setup in the FE program. Hence, the topics within numerical modelling will be displayed by describing, how the different examined studies have handled following general elements:

- Soil
- Structure
- Mesh
- Staged Construction

The four abovementioned elements are the general "mode tabs" in PLAXIS. These elements are only general, but the more detailed sub-elements will be presented and reviewed as well.

Østergaard et al. [2015], who studied suction buckets in sand, and Achmus et al. [2016], who studied monopiles in clay, will be reviewed for the numerical modelling, as they are found most relevant concerning the numerical modelling. Furthermore, Wolf et al. [2013] will be used as well, as the objective of the study was assessment of numerical methods for non-slender monopiles.

### 2.1.1 Soil

In the review of the soil the following topics will be looked at: *model domain*, *material model* and *soil type*.

#### Model Domain

The model domain defines the overall size of the model. How the model domain was defined by Østergaard et al. [2015] and normalised to the dimensions of the bucket is shown in Figure 2.1. The model domain was verified by a model domain analysis with the condition, that edges of the domain could not be affected significantly by the stresses compared to the magnitude of the stresses close to the bucket. Furthermore, only half of the model was modelled due to symmetry of both geometrical and load conditions.

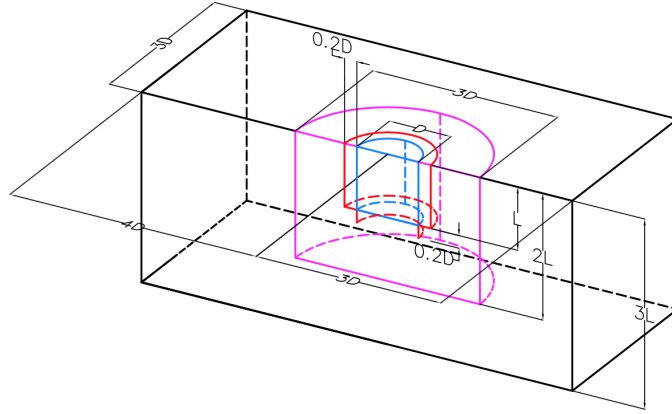


**Figure 2.1:** Model domain normalised to bucket dimensions. Size of model domain shown with black lines. The bucket itself is shown with blue lines, the volume with refined mesh is shown with pink lines, and the extended interfaces are shown with red lines [Østergaard et al., 2015].

Achmus et al. [2016] defined the model domain as shown in Figure 2.2, which was determined from an analysis similar to the one made by Østergaard et al. [2015]. Furthermore, half of the system was modelled due to symmetry of both geometrical and load conditions.

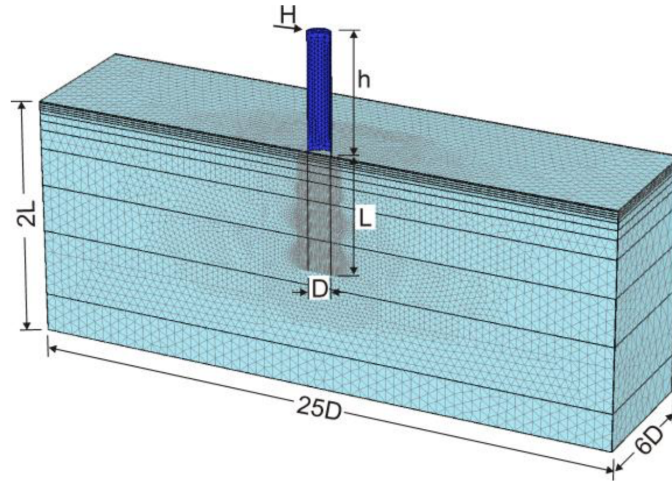


**Figure 2.2:** Size of model domain normalised to the length and diameter of the monopile [Achmus et al., 2016].

### Material Model

HSsmall was used in Østergaard et al. [2015], as it was considered the best material model due to its real-life behaviour compared to the alternatives.

In Achmus et al. [2016] the HSsmall material model was also used due to the same above-mentioned reasons.

## Soil Type

In Østergaard et al. [2015] the studied soil type was sand, and three different strengths were considered:  $\phi = 30^\circ$ ,  $35^\circ$  and  $40^\circ$  - all modelled as drained. Furthermore, the study considered two cases for the bucket dimension;  $L/D=0.5$  and  $1$ , where  $D=10$  m,  $15$  m and  $20$  m, which gave a total of 18 different numerical models.

In Achmus et al. [2016] several types of clay were studied. As of first Achmus et al. [2016] studied different soils using FE, including the clay studied by Matlock [1970] to validate FE as a reliable tool for soil-structure modelling. After the validation, Achmus et al. [2016] studied both soft and medium soft clay, where the drainage type was set to Undrained (B). In total 148 numerical models were studied.

### 2.1.2 Structure

In the review of the structure, the following topics will be looked at: *material properties*, *loading* and *interface*.

#### Material Properties

As only the soil response was of interest in Østergaard et al. [2015], the thickness and stiffness of the bucket were set higher than normal. By doing so, the bending stiffness of the bucket was increased, thereby decreasing the likeability of the bucket deforming.

In Achmus et al. [2016] the modelled monopile was divided into two separate parts, when it came to the material properties. The part of the monopile beneath the mudline was given realistic properties, while the part above the mudline was made nearly rigid by increasing the Young's modulus to a higher value. This was not considered to have any influence on the study, as the part of the monopile above mudline was used as a tool to make sure, that the load was directly led to the part below mudline.

#### Loading

In Østergaard et al. [2015] the whole bucket was given a completely lateral predescribed displacement, which is in contrast to the real loading case, where both lateral and moment load would occur. Meanwhile this was not a problem, as only the lateral soil responses was of interest, as Wolf et al. [2013] also mentions.

In Achmus et al. [2016] the rigid part of the monopile, which was above the mudline, was applied with a lateral load, which resulted in a real-life load case with both lateral and moment loads.

#### Interface

In Wolf et al. [2013] it was shown, if interfaces were not used to model the soil-structure interaction, and instead the stresses were taken from the soil element, the stress points would be further from the pile. Hence, the stresses would be applied to a larger area, which would lead to lower magnitude of the stresses, and thereby resulting in inconvenient p-y curves. By defining interfaces for the structure, the soil-structure interaction would be modelled better, and stresses would be taken at the correct points. [Wolf et al., 2013]

In Østergaard et al. [2015] the study made use of interfaces, which were applied to the bucket, as seen in Figure 2.1. This was done, as both Brinkgreve et al. [2015] and Wolf et al. [2013] recommend it, if realistic soil-structure interaction is wanted. Furthermore, the study also made use of extended interface at the end of the bucket skirt, as stress concentrations at such ends can occur, due to the mesh elements having difficulties with abrupt change in geometry according to Brinkgreve et al. [2015].

In Achmus et al. [2016] it is not mentioned whether interfaces were used or not, but as the study used PLAXIS, where interfaces are highly recommended to be used, it is assumed that this lies implicitly in the modelling description of the study.

### 2.1.3 Mesh

Wolf et al. [2013] discussed the importance of enough stress points being represented in each layer and integration area for the average value to be representative. Another problem with having too few elements is the difficulties, which occurs, when the plate elements has to simulate a cylindrical shape. These element will peak out with sharp edges, as they cannot model the cylindrical shape well enough, which results in stress concentrations. Hence, if only few stress points are represented in certain areas, reliable and representative p-y curves cannot be obtained. Therefore, the study recommends the use of proximity volumes, where a volume confining the structure is defined and given a finer mesh to make sure, an efficient amount of stress points are obtained. In this way enough stress points are introduced, and increasing the calculation time unnecessarily by applying a finer mesh to the whole model domain is avoided.

Østergaard et al. [2015] made use of the recommendation of a proximity volume made by Wolf et al. [2013], as seen in Figure 2.1, where the mesh density was made finer than the rest of the soil volume. To find the optimal solution, where results from numerical simulations were precise and at the same time, where calculation time was kept down to a minimum, a convergence analysis was made. From the analysis it was decided to set the overall coarseness of the model to coarse, while the refinement factor of the proximity volume was set to 0.15.

In Achmus et al. [2016] the fineness of the mesh was optimized to obtain precise results with a minimum number of elements.

### 2.1.4 Staged Construction

In Østergaard et al. [2015] the first phase set the initial stress state of the soil by a  $K_0$ -consolidation procedure. Thereafter the second phase was introduced, where the bucket was installed. In the third phase (plastic nil-step phase), the displacements caused by installation were reset, as only lateral displacements were of interest. After displacements were reset, the first loading phase was defined by a certain magnitude of the prescribed displacement. A loading phase was always followed by an unloading phase. This way of loading (loading followed by an unloading phase) continued with an increased displacement for every load step until reaching the prescribed displacement or soil failure occurred.

Achmus et al. [2016] made use of an initial phase, where the stress state in the soil was set by an  $K_0$ -procedure, as in Østergaard et al. [2015]. Hereafter, the pile geometry was



activated. Lastly, the load was applied to the monopile, which was done by applying a horizontal point load at the part of the monopile above mudline.

The numerical modelling from different studies has been reviewed, hence a review of different approaches of processing the data to obtain the p-y curves, which in this case are considered as the result from the numerical method, is needed.

## 2.2 Results

The literature review regarding results will focus on, how p-y curves are obtained from the data output from the numerical models. This is done, as p-y curves are considered as the results from the numerical models, even though the direct results from the numerical models are given as deformations and stresses.

Wolf et al. [2013] will be the basis of the literature review regarding results, as the study both examines, how the data can be processed, and from where data should be extracted to obtain p-y curves. As Østergaard et al. [2015] made use of the suggested approaches given by Wolf et al. [2013], Østergaard et al. [2015] will be reviewed as well.

### 2.2.1 Method of Stress Integration

Wolf et al. [2013] suggested a method of integrating the stresses to obtain p-y curves, as stresses are the output of the numerical models. The stresses around the circumference of the pile were the ones needed to be integrated. The elements in the mesh were not of the same size, thus a cumbersome study was needed, if the stresses were supposed to be integrated for each element. In stead it was suggested to divide the circumference of the pile into smaller rectangular areas. This was done by firstly dividing the pile into horizontal slices along the pile, thereby the number of horizontal slices is equal to the number of curves in the p-y plot. Thereafter a number of vertical slices around the pile were defined, as shown in Figure 2.3.

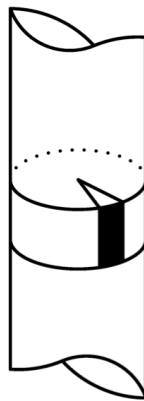


**Figure 2.3:** Integration of stresses at a given depth and area of the pile [Wolf et al., 2013].

In each of these areas, as the black marked area in Figure 2.3, several elements, hence also stress points, were represented. To obtain the force,  $p$ , given for the area, the stresses

within each area were averaged and then multiplied by the area. Thereafter, the resulting force for a given depth (horizontal slice) was calculated as the sum of the forces of all the areas in the layer divided by the height of the layer. Wolf et al. [2013] also stresses the importance of having enough stress points represented in each of the area defined, as too few stress points could result in stress concentrations, as the average would be highly affected thereby. Thus the mesh should be adequately dense.

Mathematically the expression of the integration is defined in Eq. (2.1) [Østergaard et al., 2015].

$$F_y = \int_A (\sigma'_N \sin \theta + \tau_1 \cos \theta) dA \quad (2.1)$$

$\sigma'_N$  is the effective normal stress, where  $\tau_1$  is the shear stress working around the circumference of the pile.  $\tau_2$  is the shear stress working along the pile length vertically. As the soil pressure,  $p$ , is defining the lateral soil pressure,  $\tau_2$  was disregarded by Østergaard et al. [2015].

### 2.2.2 Methods of Data Extraction

Wolf et al. [2013] examined two different approaches of how the data output could be processed to obtain useful and reliable p-y curves. The two different examined approaches for extracting data were from *soil* and *interface* elements.

#### Extraction from Soil

When stresses were extracted from the stress points of the soil elements, the accuracy of the extraction around the circumference of the pile was not good enough. To obtain more sufficient number of stress point in each area of integration, stress points at a given distance from the pile must be taken, as seen in Figure 2.4. Furthermore it is seen from the figure, that the force, due to the distance from the pile, will be distributed onto a larger area resulting in lower stresses.

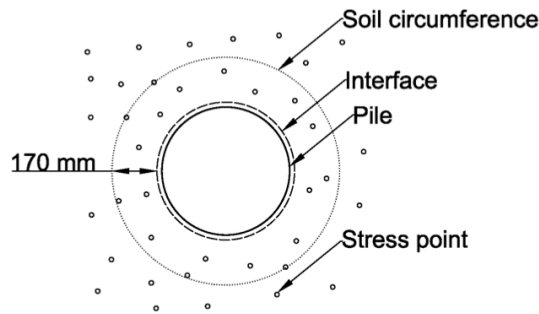


**Figure 2.4:** Stress points for soil elements, and visualisation of extraction from soil vs. interface elements [Wolf et al., 2013].

#### Extraction from Interface

As recommended by Brinkgreve et al. [2015], interfaces should be used, when soil-structure interaction is studied, which is also the conclusion made by Wolf et al. [2013]. The interfaces

was defined between the soil and structure and made infinitely thin. Therefore, Wolf et al. [2013] concluded from comparison to the extraction from soil elements, that extraction from interface elements was better, as the elements were sufficiently close to the pile circumference, cf. Figure 2.4.

## 2.3 Data Processing

In the data processing it will be looked at, how different studies have addressed their p-y curves to develop formulations for p-y curves, and which normalisations have been used with success.

The reviewed studies, concerning the data processing, are:

- Østergaard et al. [2015]
- Thieken et al. [2015]
- Matlock [1970]
- Sullivan et al. [1980]

Notice Achmus et al. [2016] is not reviewed, as the project is fairly new, and a p-y formulation valid for the studied case has not yet been developed. The authors intend to develop the p-y approach similar to the formulation for monopiles in sands developed by Thieken et al. [2015], where the formulation depend on the pile geometry and soil stiffness. Therefore, Thieken et al. [2015] will be included in this literature review.

### 2.3.1 Drained p-y Formulations

In Østergaard et al. [2015] the depth dependency, which is seen in the left graph in Figure 2.5 with increasing pressure,  $p$ , with increasing depth,  $z$ , was eliminated by normalising the data to the Rankine pressure,  $p_R$ . While the displacements was normalised to the diameter of the bucket,  $D$ . As seen in the right graph in Figure 2.5, the normalisations merge the p-y curves for different depths into one curve fairly well. The data of the graph showing the normalised state has been trimmed by excluding data points at the bottom and top of the skirt, as edge effects occurs close to these ends.

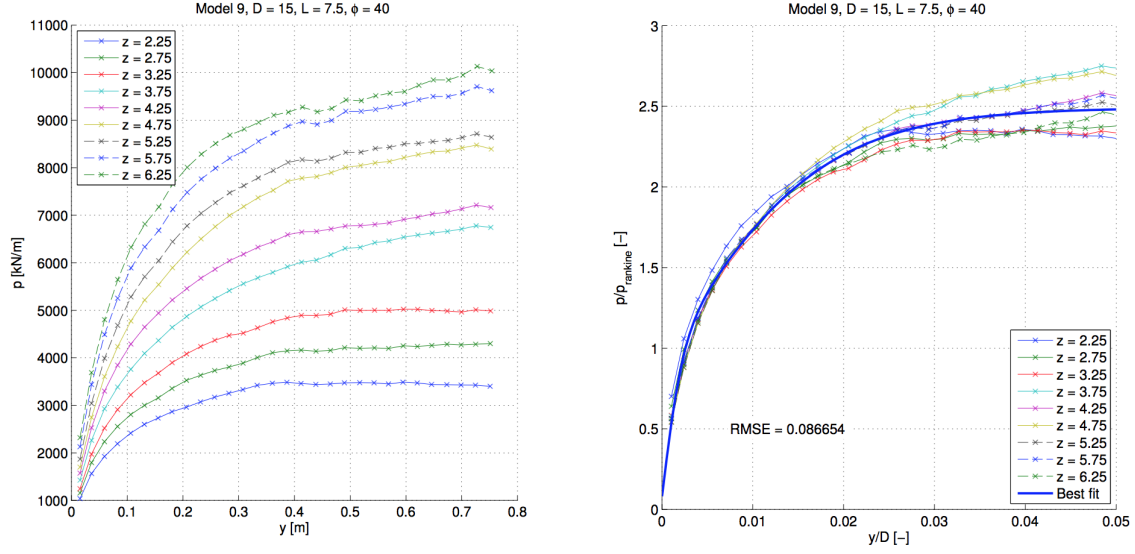


**Figure 2.5:** Left graph: raw data of  $p$ - $y$  curve for Model 9. Right graph: trimmed and normalised  $p$ - $y$  curve for Model 9 [Østergaard et al., 2015].

After the normalisation the data was fitted with Eq. (2.2).

$$\frac{p}{p_R} = \beta_1 \tanh\left(\beta_2 \frac{y}{D}\right) + \beta_3 \tanh\left(\beta_4 \frac{y}{D}\right) + \frac{K_0}{K_\gamma^p - K_\gamma^a} \quad (2.2)$$

where:

- $\beta_1, \beta_3$  control the maximum soil pressure
- $\beta_2, \beta_4$  control the gradient towards the ultimate soil pressure
- $\frac{K_0}{K_\gamma^p - K_\gamma^a}$  accounts for the soil pressure at rest at  $y = 0$

Østergaard et al. [2015] defined the model parameters to be governed by the bucket geometry ( $D$  and  $L$ ) and the soil strength ( $\phi$ ). The model parameters were plotted as the sum,  $\beta_1 + \beta_3$ , and the product,  $\beta_1 \cdot \beta_3$  against  $D, L$  and  $\phi$ , to study if any trends occurred. Afterwards  $\beta_1$  and  $\beta_3$  were defined as two equations with two unknowns, as shown in Eq. (2.3).

$$\begin{aligned} \beta_1 + \beta_3 &= a_1 \frac{\phi}{L} + a_2 \\ \beta_1 \cdot \beta_3 &= b_1 \frac{\phi}{L} + b_2 \end{aligned} \quad (2.3)$$

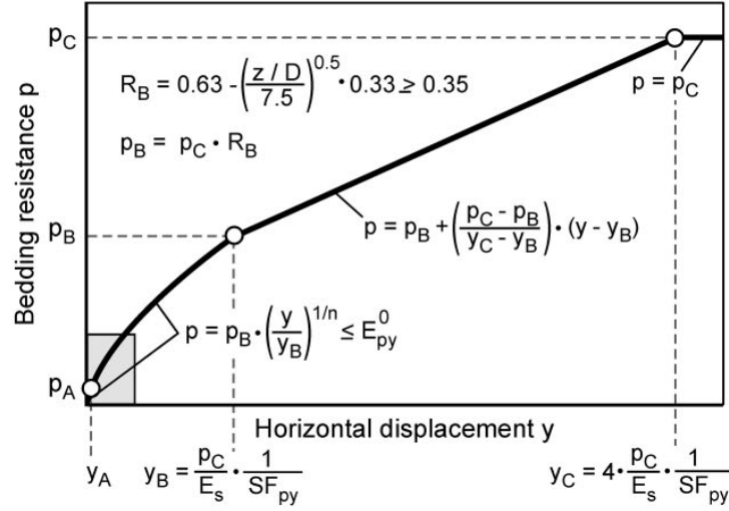
$\beta_2$  and  $\beta_4$  were examined in a similar way, where the only difference was the use of a non-linear fit instead, as seen in Eq. (2.4). The coefficients are given in Table 2.1.

$$\begin{aligned} \beta_2 + \beta_4 &= c_1 \left(\frac{\phi}{L}\right)^2 + c_2 \left(\frac{\phi}{L}\right) + c_3 \\ \beta_2 \cdot \beta_4 &= d_1 \left(\frac{\phi}{L}\right)^2 + d_2 \left(\frac{\phi}{L}\right) + d_3 \end{aligned} \quad (2.4)$$

**Table 2.1:** Coefficients in the fit of  $\beta_{1-4}$ .

$a_1$	0.041 m/°	$c_2$	-13.12 m/°
$a_2$	2.050	$c_3$	66.24
$b_1$	0.107 m/°	$d_1$	936.5 (m/°) <sup>2</sup>
$b_2$	0.560	$d_2$	-4579 m/°
$c_1$	8.900 (m/°) <sup>2</sup>	$d_3$	5989

Thieken et al. [2015] studied monopiles in sand with use of FE to develop a new formulation for p-y curves. A graphic illustration and equations for the formulation can be seen in Figure 2.6 and 2.7.

**Figure 2.6:** P-y curve developed by Thieken et al. [2015].

From Figure 2.6, it is seen, that the curve is divided into three connecting sub-parts. The first part being a non-linear function followed by a linear function. Lastly the ultimate bedding resistance (ultimate soil pressure),  $p_C$ , is reached, from where the curve becomes constant to an increasing horizontal displacement.

Ultimate bedding resistance  $p_C$ :

$$p_C = p_C^{\text{Basic}} \cdot [3 - 2 \cdot (z / (2.5 \cdot D))^{0.25}] \geq p_C^{\text{Basic}}$$

$$p_C^{\text{Basic}} = \frac{11}{16} \cdot \gamma \cdot z^{1.5} \cdot K_{\text{pgh}} \cdot (1 + 2 \cdot \tan \phi) \cdot \sqrt{D}$$

$$K_{\text{pgh}} = \sqrt{\frac{\left(\frac{1 + \sin \phi'}{1 - \sin \phi'}\right) \cdot (1 - 0.53 \cdot \delta_p)^{0.26 + 5.96 \cdot \phi'}}{1 + (\tan \delta_p)^2}}$$

$$\delta_p = -2/3 \cdot \phi'$$

Stretching factor  $SF_{py}$ :

$$SF_{py} = SF_{py, \text{bend}} + SF_{py, \text{tip}}$$

$$SF_{py, \text{tip}} = 5 \cdot \left(\frac{z - L}{2 \cdot D} + 1\right)^5 \quad \text{if } z \geq L - 2 \cdot D$$

$$SF_{py, \text{tip}} = 5 \cdot \left(\frac{z - L}{2 \cdot D} + 1\right)^5 + 3 \quad \text{if } z \geq L - 0.1 \cdot D$$

$$\text{Basic curves: } SF_{py} = 1.0$$

**Figure 2.7:** P-y formulation developed by Thieken et al. [2015].

From the formulation it is seen, that it depends on  $D$ ,  $L$ ,  $\phi$  and soil stiffness,  $E_s$ . Thieken et al. [2015] concluded, the formulations were easy to use and implement, as they are similar to the formulations suggested in the offshore guidelines. Furthermore it is seen, that the formulation includes a "stretching factor",  $SF_{py}$ , which accounts for the deflection

line and pile tip effect, as seen in Eq. (2.5).

$$SF_{py} = SF_{py,bend} + SF_{py,tip} \quad (2.5)$$

Thieken et al. [2015] lastly concluded, that the developed p-y formulation predicted the load bearing behaviour of the homogeneous sand better than the formulation suggested by the offshore guidelines.

### 2.3.2 Undrained p-y Formulations

Matlock [1970] did not investigate clay by FE. Instead full scale field tests were conducted with the use of circular steel piles with  $D=0.32$  m and  $L=12.8$  m. The tests were conducted in Lake Austin, USA in soft inorganic clay by laterally loading a steel pile. From the tests Matlock [1970] formulated the p-y curves with a parabolic function, which was limited to a ultimate soil pressure,  $p_u$ , at the displacement  $8 \cdot y_c$ . The formulations are given in Eq. (2.6) and (2.7), and a graphical view of the formulation is shown in Figure 2.8.

$$p = 0.5 \cdot p_u \left( \frac{y}{y_c} \right)^{1/3} \quad \text{for } y \leq 8 \cdot y_c \quad (2.6)$$

$$p = p_u \quad \text{for } y > 8 \cdot y_c \quad (2.7)$$

Where  $y_c$  is given in Eq. (2.8).

$$y_c = 2.5 \cdot \epsilon_{50} \cdot D \quad (2.8)$$

$\epsilon_{50}$  in Eq. (2.8) is the strain at half the principal stress difference,  $q$ , at an undrained triaxial test.

The ultimate soil pressure,  $p_u$ , is given in Eq. (2.9)

$$p_u = \min \begin{cases} (3 \cdot c_u + \gamma' \cdot z) \cdot D + J \cdot c_u \cdot z \\ 9 \cdot c_u \cdot D \end{cases} \quad (2.9)$$

The empirical constant,  $J$ , is usually defined between 0.25-0.5, where 0.5 is recommended for soft clays. The developed formulation of p-y curves for clays from Matlock [1970] is a function of the undrained shear strength,  $c_u$ , the diameter,  $D$ , the depth below mudline,  $z$ , and the effective unit soil weight,  $\gamma'$ .

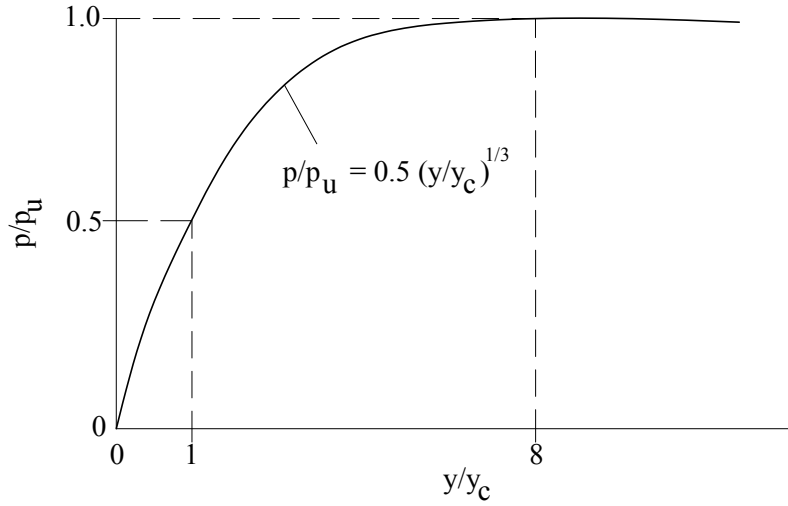


**Figure 2.8:** P-y curve by Matlock [1970] normalised to  $y_c$  and  $p_u$ .

Sullivan et al. [1980] proposed a approach to the development of p-y curves valid for any clay soil by conducting lateral load tests. The formulation suggested by Sullivan et al. [1980] are as follows:

$$p = 0.5 \cdot p_u \left( \frac{y}{y_c} \right)^{1/3} \quad \text{for } y \leq 8 \cdot y_c \quad (2.10)$$

$$p_r = \begin{cases} p_u & \text{for } z > 12D \text{ and } y \geq 30 \cdot y_c \\ p_u \cdot \left( F + (1 - F) \cdot \frac{z}{12D} \right) & \text{for } z \leq 12D \text{ and } y \geq 30 \cdot y_c \end{cases} \quad (2.11)$$

From Eq. (2.10) it is seen, that the initial non-linear part of the p-y curve is dependent on the critical deflection,  $y_c$ , which is given in Eq. (2.12), and is quite similar to the critical deflection described by Matlock [1970]. The empirical factor,  $A$ , is set to 2.5 for soft clays as in Matlock [1970] and 0.35 for stiff clays, while the parameter  $F$  is set to 1.0 and 0.5 for soft and stiff clays respectively.

$$y_c = A \cdot \epsilon_{50} \cdot D \quad (2.12)$$

The ultimate soil pressure is defined in Eq. (2.13).

$$p_u = \min \begin{cases} \left( 2 + \frac{\gamma'}{c_{u,avg}} \cdot z + \frac{0.833}{D} \cdot z \right) \cdot c_{u,avg} \cdot D \\ \left( 3 + \frac{0.5}{D} \cdot z \right) \cdot c_u \cdot D \\ 9 \cdot c_u \cdot D \end{cases} \quad (2.13)$$

From Eq. (2.13) it is seen, that two undrained shear strengths are used, where  $c_{u,avg}$  is the average undrained shear strength until the depth  $z$ , and  $c_u$  is the undrained shear strength at the depth  $z$ .

Figure 2.9 shows p-y curve suggested by Sullivan et al. [1980] with the developed p-y formulation labelled.

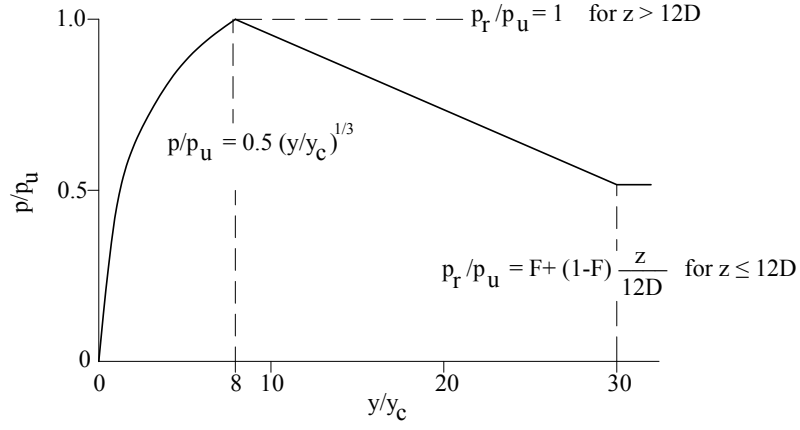


**Figure 2.9:** P-y curve developed by Sullivan et al. [1980] normalised to  $y_c$  and  $p_u$ .

A review of relevant studies has been given. By use of the applicable elements from the different studies, it is possible to begin the numerical modelling of suction buckets in silt.



# Numerical Modelling 3

To develop precise and applicable p-y formulations, great work has to be put into the numerical modelling of the examined models. Therefore, the general steps to define the models, determine their properties and the different assumptions and choices made will be described in this chapter. If a more thorough description of the numerical modelling in PLAXIS is wanted, readers are referred to look at the PLAXIS script files, which are found in [Appendix Folder, Numerical Model, P-y Scripts]. Only the script of the first model has been commented, so the reader has a better chance of understanding the commands used in the numerical modelling. Furthermore, a step-by-step guide is available in Appendix D.

The structure of the chapter will follow the relevant overall modelling procedure in PLAXIS given by the "Mode tabs":

- Soil
- Structure
- Mesh
- Staged construction

As only silt is needed to be numerically modelled, the sand will not be presented in this chapter. The different numerical models and input parameters for the sand used in Østergaard et al. [2015] will be presented in Chapter 6, where a reconsidered p-y formulation is sought for the drained sand.

## 3.1 Model Overview

Table 3.1 shows the geometry of the studied models with the corresponding drainage and soil type.

**Table 3.1:** Model overview.

Model no.	Drainage type	D and L [m]	Soil type
1	Drained	10	Soft
2	Drained	15	Soft
3	Drained	20	Soft
4	Drained	10	Stiff
5	Drained	15	Stiff
6	Drained	20	Stiff
7	Undrained	10	Soft
8	Undrained	15	Soft
9	Undrained	20	Soft
10	Undrained	10	Stiff
11	Undrained	15	Stiff
12	Undrained	20	Stiff

As it is seen from Table 3.1, three different diameters are set, and the only slenderness ratio studied for this project is  $L/D=1$ . This is chosen, since Østergaard et al. [2015]

studied two cases regarding the slenderness ratio;  $L/D=0.5$  and 1, but they concluded, that the length of the bucket did not have an affect on their normalisations. Furthermore it is seen, that two silt types are studied; *soft* and *stiff*, which are then further divided into drained and undrained silts. Hence, a total of 12 different models will be used to develop p-y formulations for bucket foundations in silt.

## 3.2 Soil

In this section the main elements regarding the numerical modelling of the soil are addressed. The main elements are *soil contour* as well as the *material model* and its properties.

### 3.2.1 Model Domain

The contour of the soil depends on the geometry of the suction bucket. The geometry of the model normalised to the bucket dimensions is shown in Figure 3.1.

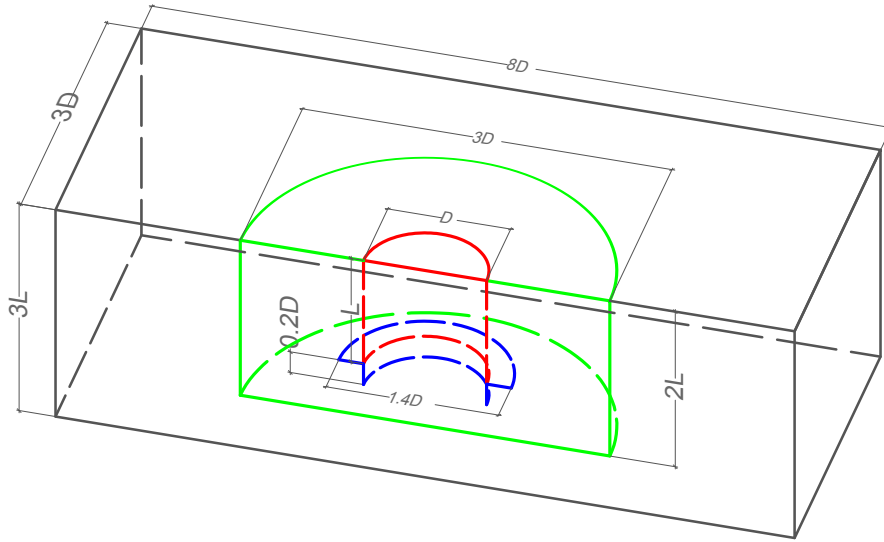


**Figure 3.1:** Overall model geometry normalised to the bucket diameter and length. Indication of line colors: black: soil contour/model domain, green: proximity volume with refined mesh, blue: interface extension and red: suction bucket [Østergaard et al., 2015].

### Model Domain Analysis

The model domain, shown in Figure 3.1, is determined from a model domain analysis. The aim of the analysis is to determine the size of the model, which is big enough to only be affected by stresses at the edges in an insignificant manner compared to the stresses close to the bucket. On the other hand, the model domain cannot be unnecessarily big, as calculation time will increase.

The analysis results in acceptable results, as the boundaries are not affected by stresses in a significant manner, as seen in Figure 3.2 and 3.3.



*Figure 3.2:*  $\sigma'_{yy}$  for a loading phase.

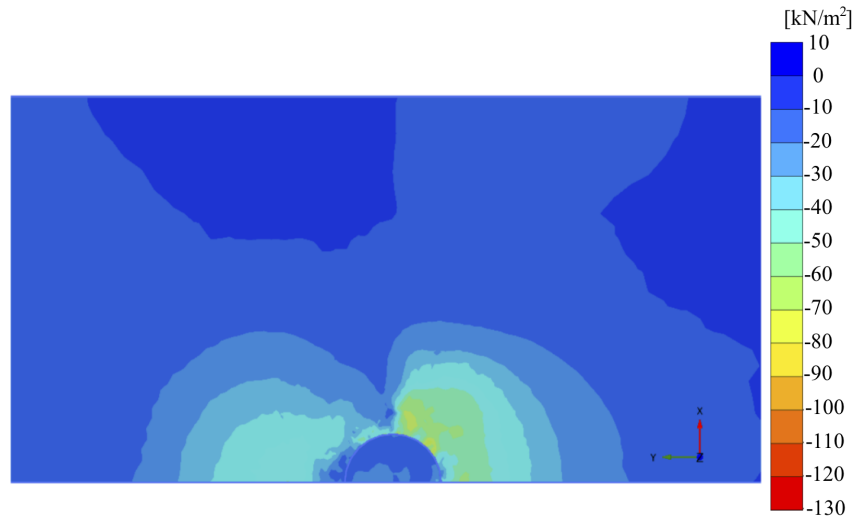


*Figure 3.3:*  $\sigma'_{yy}$  for an unloading phase.

### 3.2.2 Material Model

There are different material models, which has their individual pros and cons. To establish p-y formulations the soil-structure behaviour has to be simulated well by using an accurate material model. Østergaard et al. [2015] studied bucket foundations in sand with use of the HSsmall model due to its advanced material model and relatively real-life behaviour. Furthermore Achmus et al. [2016] used the HSsmall model as well, where monopiles in clay were studied, hence it is considered suitable for this study as well. A brief exposition of the HSsmall model is therefore made to highlight its modelling features and interpretation capabilities of soil behaviour.

#### HSsmall

The HSsmall model, compared to the well-known Mohr-Coloumb (MC) model, has considerable advantages, since it takes both shear and isotropic hardening into

consideration by a shear locus and a yield cap respectively. The failure envelopes in effective principal stress space is seen in Figure 3.4.

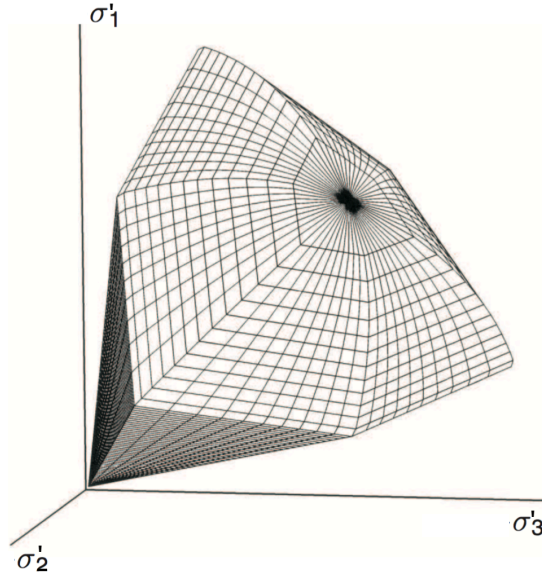


**Figure 3.4:** Failure envelope of HSsmall model in effective principal stress space [Brinkgreve et al., 2015].

Even though Figure 3.4 is similar to the MC model regarding the hexagonal shaped shear locus, they have very different interpretation capabilities of the soil stiffness due to the hardening considered in the HSsmall model. In the MC model the strains are entirely elastic until reaching the failure envelope, from where the material will behave perfectly plastic due to its bi-linear curve. The shear locus and yield cap of the HSsmall model can expand, where the locus at maximum shearing, with continued straining, will reach MC failure line, as shown in Figure 3.5. When this stage of the shear locus is reached, the material will undergo similar material behaviour as the MC model, namely perfectly plastic behaviour.

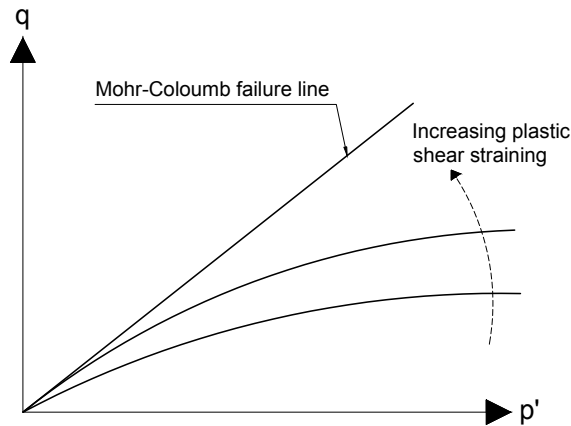


**Figure 3.5:** Development of shear locus with increasing plastic shear straining [Brinkgreve et al., 2015].

The hardening of the material, as shown in Figure 3.5, causes change in stiffness parameters, when the stress state changes. This is possible due to the use of a power law with the exponent  $m$ , which describes the amount of stress-dependency. Power  $m$  can be defined in an interval of 0.5-1, where 1 is used for soft soils indicated with a straight locus, and 0.5 for hard soils with a curved locus. Depending on the exponent,  $m$ , and at which stress state the soil is at, the model uses a certain stiffness modulus. Eq. (3.1) shows how the stiffness moduli for the HSsmall model depends on the power  $m$  and reference pressure,  $p^{ref}$  ( $= 100$  kPa).

$$\begin{aligned}
 E_{oed} &= E_{oed}^{ref} \cdot \left( \frac{c \cdot \cos \phi + \sigma'_1 \cdot \sin \phi}{c \cdot \cos \phi + p^{ref} \cdot \sin \phi} \right)^m \\
 E_{50} &= E_{50}^{ref} \cdot \left( \frac{c \cdot \cos \phi + \sigma'_3 \cdot \sin \phi}{c \cdot \cos \phi + p^{ref} \cdot \sin \phi} \right)^m \\
 E_{ur} &= E_{ur}^{ref} \cdot \left( \frac{c \cdot \cos \phi + \sigma'_3 \cdot \sin \phi}{c \cdot \cos \phi + p^{ref} \cdot \sin \phi} \right)^m \\
 G_0 &= G_0^{ref} \cdot \left( \frac{c \cdot \cos \phi + \sigma'_3 \cdot \sin \phi}{c \cdot \cos \phi + p^{ref} \cdot \sin \phi} \right)^m
 \end{aligned} \tag{3.1}$$

The model also takes the effect of small strain stiffness into account. For larger strains the stiffness is affected by a decrease in stiffness with a non-linear progress. Thus the soil cannot fully recover from large strains, which is shown in Figure 3.6, where e.g.  $E_{ur}$  is smaller than  $E_0$  or at the un- and reloading part, where hysteresis is observed. Figure 3.6 furthermore shows another important aspect of the HSsmall model, which is the hyperbolic relationship between the strain,  $\epsilon_1$ , and deviatoric stress,  $q$ . [Brinkgreve et al., 2015]

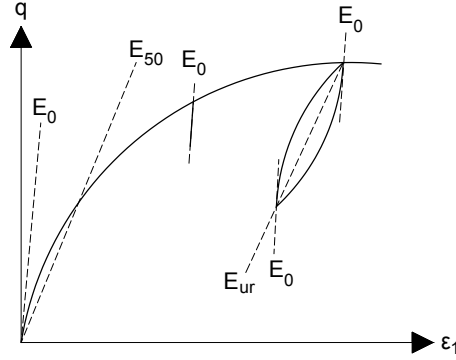


**Figure 3.6:** Stress-strain curve for HSsmall model with the different stiffness moduli [Brinkgreve et al., 2015].

Figure 3.7 shows decreasing stiffness with increased strain magnitude. It is seen that the stiffness decreases non-linearly and is dependent on the strain magnitudes. This is the small strain part of the HSsmall model, which differentiate it from the hardening soil model.

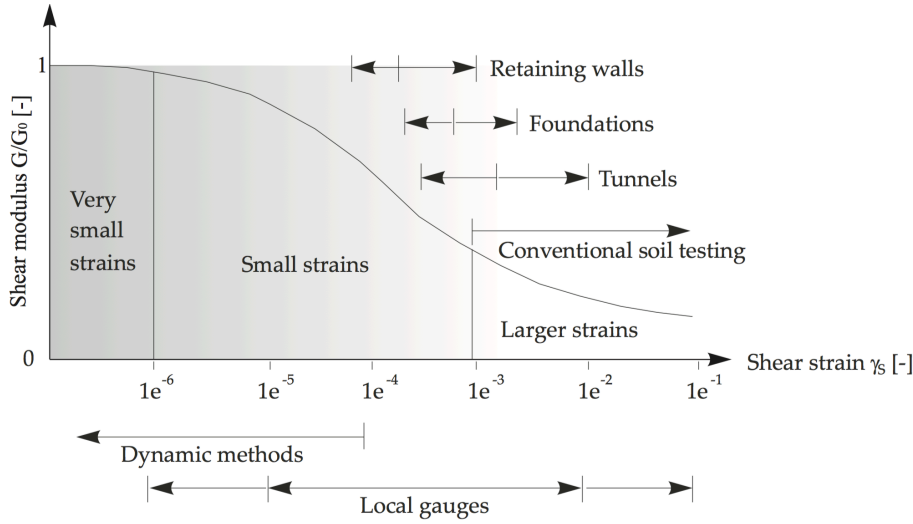


**Figure 3.7:** Change of stiffness ratio of  $G/G_0$  as the magnitude of the strain changes [Brinkgreve et al., 2015].

### Undrained Modelling

The drainage type for Model 7-12 are undrained and affects the modelling, as two different opportunities are available for modelling undrained numerical models with use of the HSsmall model; *Undrained (A)* and *Undrained (B)*, where Achmus et al. [2016] made use of the latter.

#### Undrained (A)

Strength parameters in Undrained (A) are set with effective parameters. Thereby the undrained shear strength,  $c_u$ , is not an input parameter, but is instead an output parameter. The undrained shear strength should be controlled and compared to known values. [Brinkgreve et al., 2015]

#### Undrained (B)

When using Undrained (B) the input are given as a total strength parameter, hence the undrained shear strength is an input parameter, while stiffness parameters are effective. [Brinkgreve et al., 2015]

Since the undrained shear strength has to be checked, when the Undrained (A) is used, as it is an output parameter, it is considered troublesome. Therefore, Undrained (B) will be used to model the undrained numerical models.

### 3.2.3 Input Parameters for the Numerical Models

Table 3.2 shows the different input parameters of the soft and stiff silt needed for the numerical models.

**Table 3.2:** Strength and stiffness parameters for the soft and stiff silt.

Silt type		Soft	Stiff
$c_u$	[kPa]	56	475
$\phi'$	[°]	29	33
$\psi$	[°]	0	3
$c'$	[kPa]	1	15
$E_{50}$	[MPa]	3.8	10.2
$E_{oed}$	[MPa]	5	14
$E_{ur}$	[MPa]	11.4	30.6
$m$	[-]	0.5	0.5
$\gamma_{0.7}$	[mm/m]	0.19	0.19
$\nu$	[-]	0.29	0.26
$G_0$	[MPa]	76.9	102.4
$K_0$	[-]	0.52	0.46

Originally the parameters given for the soft and stiff silt were given as effective parameters for both stiffness and strength. As some of the numerical models are run as undrained, the undrained shear strength is needed, thus the SHANSEP method is used.

### Undrained Shear Strength

The process of determining the undrained shear strength with use of SHANSEP is briefly described, but more detailed look at the calculations are found in [Appendix Folder, Numerical Models, Model and Parameters.xlsx].

The SHANSEP formula given in Eq. (3.2), where the only unknown part is  $(c_u/\sigma'_1)_{nc}$ , which can be obtained by consolidated undrained (CU) triaxial tests performed at different values of OCR. Notice the consolidation phase of the triaxial test is performed with  $K_0$ -consolidation, why  $\Lambda$  is set to 0.8, as recommended by Jensen et al. [2015].

$$\left(\frac{c_u}{\sigma'_1}\right)_{oc} = \left(\frac{c_u}{\sigma'_1}\right)_{nc} \cdot OCR^\Lambda \quad (3.2)$$

In PLAXIS triaxial tests can be modelled and performed both undrained and drained. Whether the soil is defined with only effective or total strength parameters does not matter, thus several consolidated undrained triaxial tests for different OCR values are performed to determine  $(c_u/\sigma'_1)_{nc}$ . In Table 3.3 the results from the performed triaxial tests are shown.

**Table 3.3:** Triaxial test results.

Stiff silt				Soft silt			
OCR	$\sigma'_{1,nc}$	$\sigma'_{3,nc}$	$c_{u,nc}$	OCR	$\sigma'_{1,nc}$	$\sigma'_{3,nc}$	$c_{u,nc}$
[-]	[kPa]	[kPa]	[kPa]	[-]	[kPa]	[kPa]	[kPa]
1.0	1080	497	448	1.0	80	42	31
1.4	1512	696	624	1.4	112	58	43
2.0	2160	994	885	2.0	160	83	60
4.0	4320	1987	1750	4.0	320	166	120
Average of $(c_u/\sigma'_1)_{nc} = 0.41$				Average of $(c_u/\sigma'_1)_{nc} = 0.38$			

In PLAXIS the input of the undrained shear strength has to be in relation to the reference pressure,  $p^{ref} = 100$  kPa. Hence the undrained shear strength for the numerical models for the stiff and soft silt are 475 kPa and 56 kPa respectively.

#### Remark concerning the undrained shear strength:

Before deciding to go with the use of SHANSEP, different studies and methods were reviewed, as relation between the undrained shear strength and the rest of the input parameters for Undrained (B) is not given by Brinkgreve et al. [2015].

#### *From Undrained Shear Strength to Stiffness Parameters*

In the beginning the aim was to determine the stiffness parameters from a given undrained shear strength, as this should be governing for the rest of the input parameters in the same way, the friction angle was in Østergaard et al. [2015]. They were able to determine all the necessary parameters by the friction angle alone, which was not an opportunity in this case, as the formulas were only for sands, hence other studies were looked at.

Andersen and Schjetne [2013] studied the consolidation characteristics of sand, clay and silt. The different deformation parameters studied were mostly valid for sand, and the silt was only considered in cases, where the soil was described as "silty sand". To determine the different parameters, the water content and  $D_{10}$  particle size were needed as well. Furthermore, it is mentioned lastly in the study, that the correlations should be used with caution, as they were only rough estimates. These limitations were considered as drawbacks, thus another approach was sought.

#### *From Stiffness Parameters to Undrained Shear Strength*

Unfortunately no direct nor valid relation was to be found between undrained shear strengths and the sought stiffness parameters. Furthermore, different people and companies, with expertise within the area, were contacted. One of them was PLAXIS Support, who was not aware of any such parameter relation. Instead they recommended, if possible, that CPTs or triaxial tests should be used to obtain the necessary parameters.

Lars Bo Ibsen gave the parameters needed for a drained numerical model, meaning that all the parameters (stiffness and strength parameters) were effective. The parameters given can be found on [Appendix Folder, Numerical Model, Soil Data.pdf]. Therefore, the undrained shear strength had to be found from the effective parameters, which was then done by using SHANSEP as aforementioned.

The use of physical triaxial tests were the initial plan, but due to problems with the geotechnical laboratory, this was not possible. This would indeed have been the most favourable approach to obtain all the input parameters for the HSsmall material model, as suggested by PLAXIS Support.

### **Shear Modulus and Threshold Shear Strain**

It is evident from [Appendix Folder, Numerical Model, Soil Data.pdf], that the parameters given is only enough for a HS model. As it is wanted to run the numerical models as the more refine HSsmall model, the two additional parameters; shear modulus,  $G_0$ , and



threshold shear strain,  $\gamma_{0.7}$ , have to be defined. The values for the parameters can be determined from similar soils or experience figures, but as soil often is unique from soil to soil, a more theoretical approach is wanted.

According to Brinkgreve et al. [2015]  $G_0$  and  $\gamma_{0.7}$  can be calculated in Eq. (3.3) and (3.4).

$$G_0^{ref} = 33 \cdot \frac{(2.97 - e)^2}{1 + e} \quad (3.3)$$

$$\gamma_{0.7} = \frac{1}{9G_0} \cdot (2c' (1 + \cos(2\phi')) - \sigma'_1 (1 + K_0) \sin(2\phi)) \quad (3.4)$$

To calculate the two parameters only the void ratio,  $e$ , is needed. According to Det Norske Veritas [1992] the void ratio depends on the modulus number,  $m$ , which is defined in intervals:

Loose:  $m = 40 - 60$   
Medium:  $m = 60 - 80$   
Dense:  $m > 80$

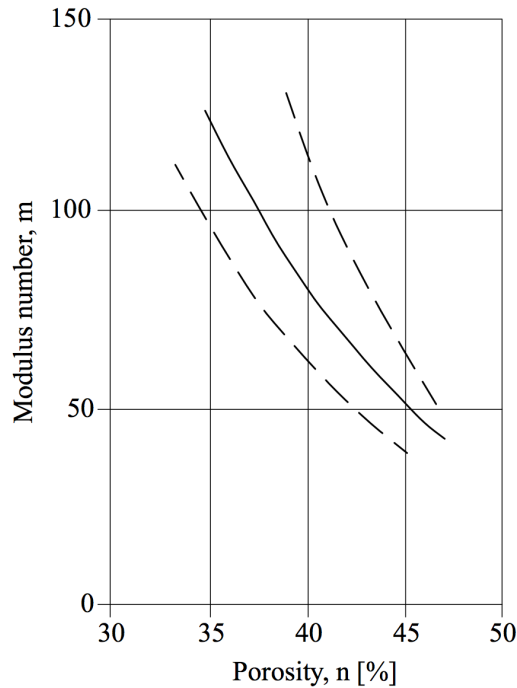


**Figure 3.8:** Relation between modulus number,  $m$ , and porosity,  $n$  [Det Norske Veritas, 1992, Fig. 5.9, Sec. 5.3.3.8].

The relation between the porosity and modulus number is given in Figure 3.8. By knowing whether the soil is loose, medium or dense, the modulus number can be determined, thus the porosity, and thereby the void ratio, can be determined as well. The assumed modulus number and the related void ratio are given in Table 3.4, where the calculated values for  $G_0$  and  $\gamma_{0.7}$  are given for the soft and stiff silt.

**Table 3.4:** Values of  $G_0$  and  $\gamma_{0.7}$  for the soft and stiff soil studied.

Soil	m [-]	e [-]	$G_0$ [kPa]	$\gamma_{0.7}$ [mm/m]
Soft	40	0.88	76891	0.19
Stiff	70	0.70	102358	0.19

Based on the stiffness moduli of the stiff silt, it is considered to be too low to be classified as a stiff silt concerning the intervals of the modulus number. Hence it is assumed to be a medium silt. Nevertheless, it will still be referred to as the stiff silt. The soft silt is considered to be very soft, thus the modulus number is set at the lowest value possible.

### 3.3 Structure

This section will describe the decisions made regarding the properties of the bucket foundation together with its interfaces. Furthermore, how the bucket is loaded to obtain useful output data is described as well.

#### 3.3.1 Material Properties

The skirt and top of the bucket are defined as plates, which afterwards have to be given its material properties. The plate is defined as steel, and the properties of the plate material can be seen in Table 3.5.

**Table 3.5:** Material properties for bucket foundation.

$d$	$E$	$\nu$
[m]	[MPa]	[-]
0.3	$6 \cdot 10^5$	0.3

As seen in Table 3.5, the bucket has both been given a thickness,  $d$ , greater than the approximate 20 mm, suction buckets are, and Young's modulus is set much higher than the 210.000 MPa, as steel is. This is done to increase bending stiffness, hence the bucket is stiff enough to resist deformations during loading. If the bucket is modelled with realistic values of the stiffness and thickness, it might deflect and thereby absorb some of the stresses, hence the results will not be usable to develop p-y formulations.

#### 3.3.2 Loading of Structure

Achmus et al. [2016] and Wolf et al. [2013] loaded their models with a horizontal and moment load. A moment causes the foundation to rotate, which will result in a rotation point, hence zero displacement will occur at this point. Furthermore, the displacement towards this rotation point from beneath and above the point causes the displacements and forces to vary.

Wolf et al. [2013] concluded it was not worth to apply realistic load cases to the structure, as the rotation point differed from every load amplitude, thereby making it troublesome to work with. Instead, as they also studied, a totally horizontal displacement of the structure were both easier to work with and useful, when p-y curves were considered. It was also

from Wolf et al. [2013], that Østergaard et al. [2015] got inspiration to displace the bucket by a completely uniform lateral displacements with a so called predescribed displacement. Because of the convenience of displacing the bucket by a completely lateral displacement, the whole bucket is modelled with a predescribed horizontal displacement.

### 3.3.3 Interface

Correct interpretation of the soil-structure interaction is very important for this study and due to intensive shearing close to the bucket, it is important to make use of interfaces. If interfaces are not used around the bucket, the soil-structure is not captured properly according to Brinkgreve et al. [2015]. Furthermore, Brinkgreve et al. [2015] recommends the use of interfaces around corners by extending the interface length, as non-physical stress oscillations will arise around the end of the skirt due to abrupt change in geometry without them.

Østergaard et al. [2015] extended the interface around their modelled bucket foundations by  $0.2D$ , which will be used for the numerical models in this thesis as well, as seen in Figure 3.1.

The properties for the interfaces are basically the same as the soil. But as seen in Table 3.2, the interface strength,  $R_{inter}$  is set to less than one, where  $R_{inter}=1$  would indicate interface strength is equal to the soil strength. This is because the interface at soil-structure interaction in reality is weaker than the adjacent soil. The interface strength for the soft and stiff silt in this project is set equal 0.66 and 0.56 respectively. [Brinkgreve et al., 2015]

## 3.4 Mesh

Fast computation of the model can be obtained by a coarse mesh, but on the other hand it will result in imprecise results. To obtain more precise results, a finer mesh can be used, but this will increase calculation time. Thus, a compromise between fast computation and precise results has to be made.

As mentioned regarding the use of interfaces, the magnitude of strains and stresses are greater close to the bucket. Thus, a cylindrical proximity volume, which encloses the bucket, can be given a finer coarseness factor than the rest of the soil to obtain both faster computation and precise results. Figure 3.1 shows the cylindrical proximity volume normalised to the overall geometry of the bucket, while Figure 3.9 shows a meshed model. To define an optimal refinement factor for the proximity volume, a convergence analysis is made.

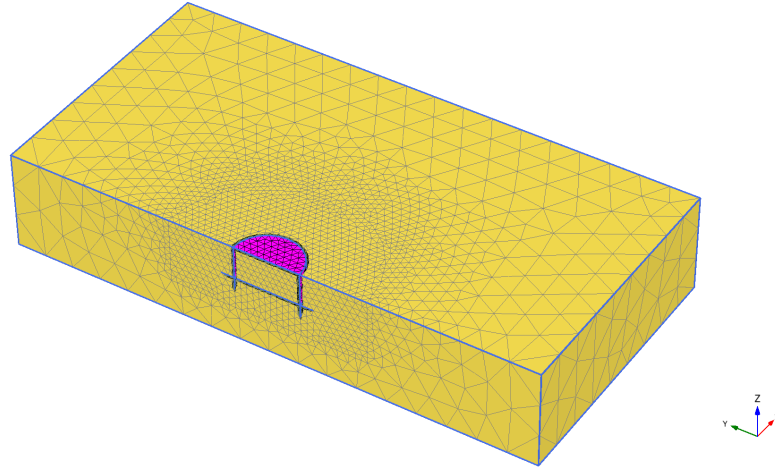


**Figure 3.9:** Meshed model.

### 3.4.1 Convergence Analysis

By the use of input parameters and geometry of Model 5, the convergence analysis was performed by only changing the refinement factor of the proximity volume.

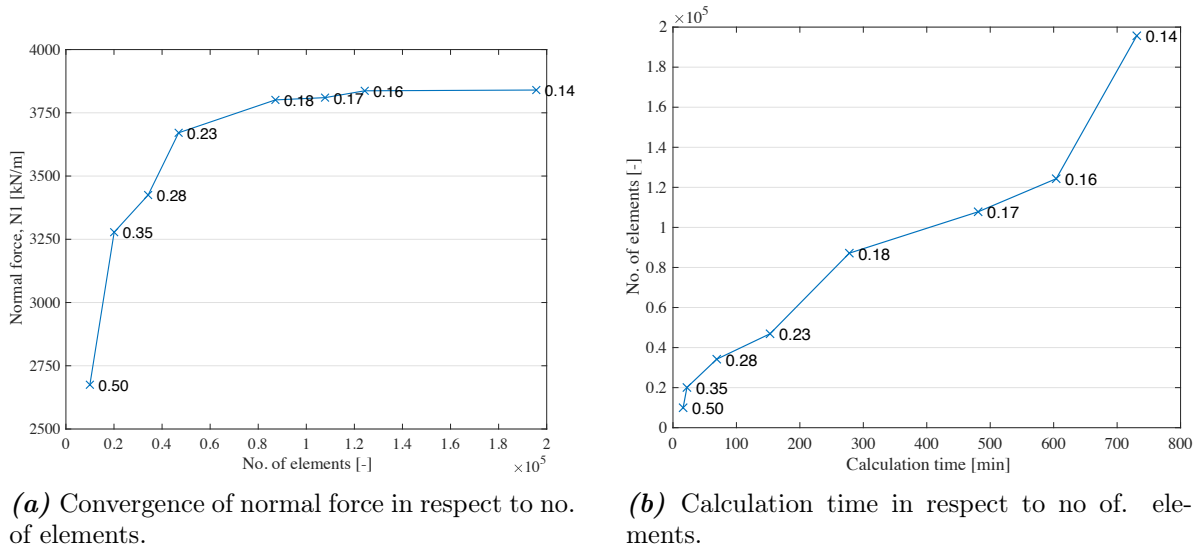


**Figure 3.10:** Result of convergence analysis. Numbers on the curve indicate the refinement factor of the different convergence models.

Figure 3.10 shows that the model converges at a refinement factor of 0.18. Furthermore it is seen, that a further refining of the proximity volume increases the calculation time significantly as expected.

Problems occurred with the undrained models, as it was seen from the p-y curves, that soil pressure did not increase with depth as expected. To troubleshoot the problem, about 30 different models were run, where the the numerical model, soil, displacements and refined mesh factor were changed in different combinations. From the troubleshooting, it seemed to help to increase the amount of elements within the proximity volume. Wolf et al. [2013] also explains the importance of having enough stress points represented in each area,

where the stresses are integrated up upon to determine the soil pressure,  $p$ . Therefore, the refinement factor of the proximity volume is set to  $0.16$  with a overall fineness factor of the mesh set to *medium*.

An exposition of the convergence analysis is given in greater detail in Appendix E.

### 3.5 Staged Construction

As mentioned earlier, the loading is applied as a prescribed displacement of the whole bucket, since only lateral displacements and the related forces are of interest. To load the bucket in steps, PLAXIS has in the *Staged construction* mode tab made it possible to define multiple calculation phases, where the phases are defined as followed:

- Phase 0: Initial phase
- Phase 1: Installation of bucket
- Phase 2: Plastic nil-step
- Phase 3: Loading by the prescribed displacement
- Phase 4: Unloading
- ⋮
- Phase n-1: Reloading by increased prescribed displacement
- Phase n: Unloading

In *initial phase* (Phase 0) the initial stress state is set with a  $K_0$ -procedure, and in the next phase (Phase 1) the bucket is installed. Installation of the bucket will cause vertical displacements of the soil, but these are not of interest. Thus the displacements are reset in the *plastic nil-step* phase (Phase 2). Afterwards the first prescribed displacement (Phase 3) is applied to the bucket. Since only plastic deformations is of interest, an *unloading* phase (Phase 4) is defined. Thereby data for the displacements,  $y$ , can be extracted from unloading phases, while the soil pressure,  $p$ , is extracted from the loading phases. Every load phase is set with an increased displacement compared to the prior load step.

Hereby the factors and assumptions made during the numerical modelling are highlighted, hence the models can be simulated in PLAXIS. The next step is to process the data to gain the p-y curves for the numerical models.



# Results and Comparison of Former p-y Formulations

## 4

In this chapter the results from the numerical models will be presented. Results are considered to be the p-y curves, which can be derived from the data of the numerical models. Additionally the former p-y formulations, which are described in the literature review, are compared to the data to evaluate their validity for bucket foundations in silt.

The direct data output for the numerical models are given as stresses and deformations, which cannot be plotted to obtain p-y curves directly, hence a description of the process of calculating the soil pressure will be given at first.

### 4.1 Data Extraction and Integration of Stresses

As recommended by both Brinkgreve et al. [2015] and Wolf et al. [2013], stress points will be extracted from the interface elements due to its precision. Furthermore, the bucket skirt will be divided in a number of horizontal and vertical slices, which results in smaller areas all around the skirt, cf. Figure 4.1. All stress points within the black marked area is averaged and multiplied by the area. All areas within the same layer are then summed and divided by the height of the layer to obtain the soil pressure,  $p$ , as kN/m. In principle the integration of the stresses follows Eq. (4.1).

$$p = \int_A (\sigma'_N \sin \theta + \tau_l \cos \theta) dA \quad (4.1)$$

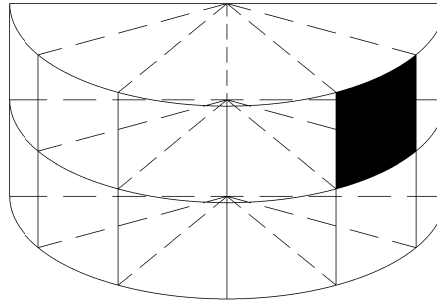


**Figure 4.1:** Principle of horizontal and vertical divisions of the skirt to define integration areas [Østergaard et al., 2015].

A step-by-step guide of the data extraction from PLAXIS 3D can be found in Appendix D.

It has been determined, from where stress points are extracted, and how they are processed to calculate the soil pressure to generate the p-y curves. Therefore, the p-y curves for the numerical models can be derived.

## 4.2 P-y Curves of the Numerical Models

The p-y curves for the numerical Model 5 and 11 are shown in Figure 4.2, while the p-y curves for all 12 models are presented in Appendix F.

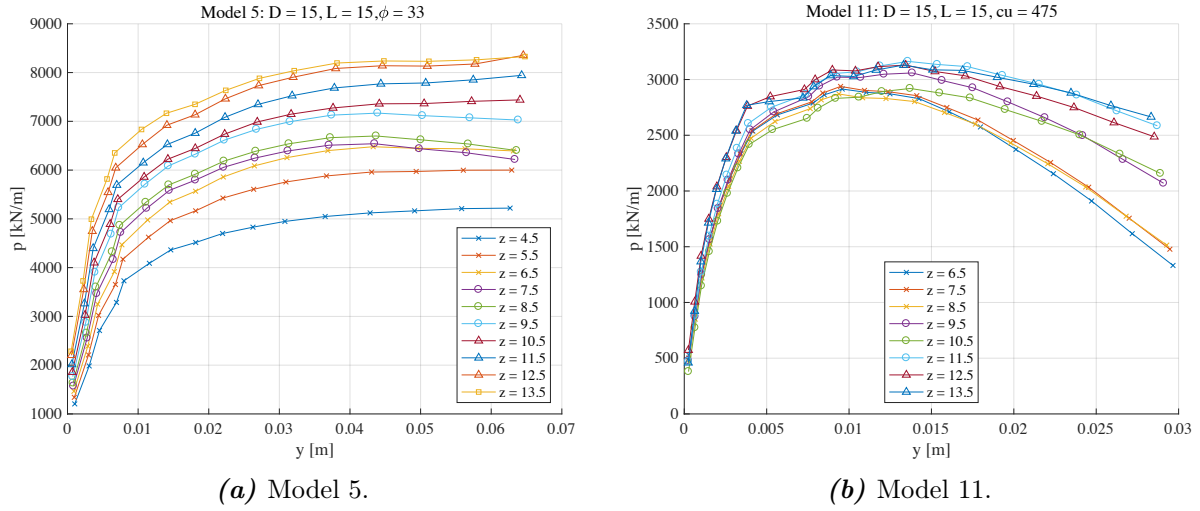


**Figure 4.2:** P-y curves of the numerical models.

As seen by the p-y curves, there is a significant difference between the drained and undrained models, hence distinction is made between the data processing of the drained and undrained models.

Since the results, in form of p-y curves for the numerical models, have been derived, the next step is to examine the validity of former p-y formulations in relation to the FE data of the silt.

## 4.3 Comparison of Reviewed p-y Formulations and FE Data

The FE data of the silt is at first examined in relation to former p-y formulations, which were addressed in the literature review, to evaluate their validity for the silt. The different approaches will be evaluated for all the numerical models, but only Model 2, 5, 8 and 11 will be shown, since showcasing all 12 models require many pages. All models are accessible through [Appendix Folder, MATLAB, masterloop.m].

As mentioned before, distinction is made between the drained and undrained models. The approaches suggested by Østergaard et al. [2015] and Thieken et al. [2015] will be compared to the drained models, while the formulations suggested by Matlock [1970] and [Sullivan et al., 1980] will be applied for the undrained models.

To evaluate the usability of the different approaches, the results from the numerical models are plotted in two ways:

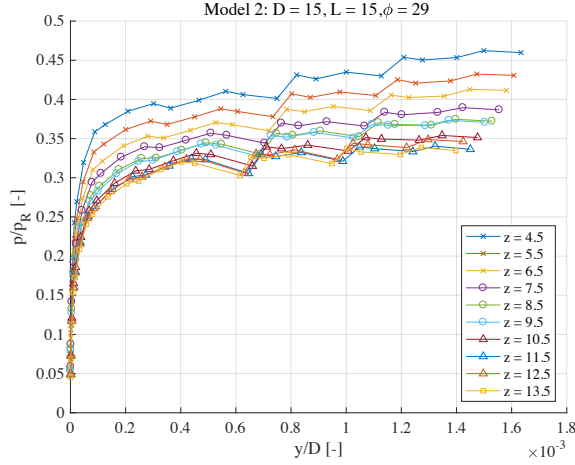
- Normalised p-y curve with use of suggested approach for the specific study.
- P-y data for FE models compared to the formulations suggested by the specific study at a given depth,  $z$ , which is considered to be free of edge effects and representative in general.



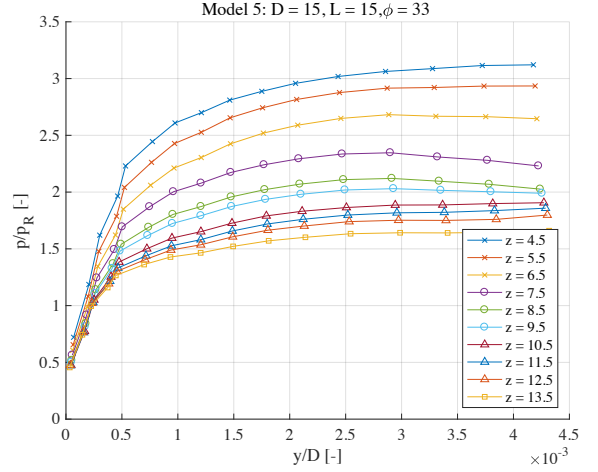
Only Thiesen et al. [2015] will not be shown as a normalised p-y plot, as a general normalisation was never presented in the study.

#### 4.3.1 Drained Models

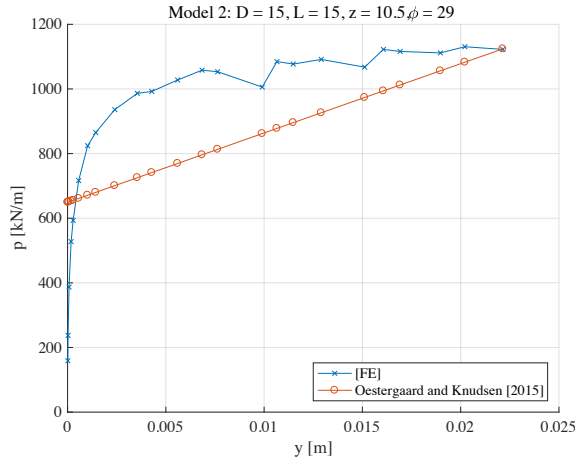
##### Østergaard et al. [2015]



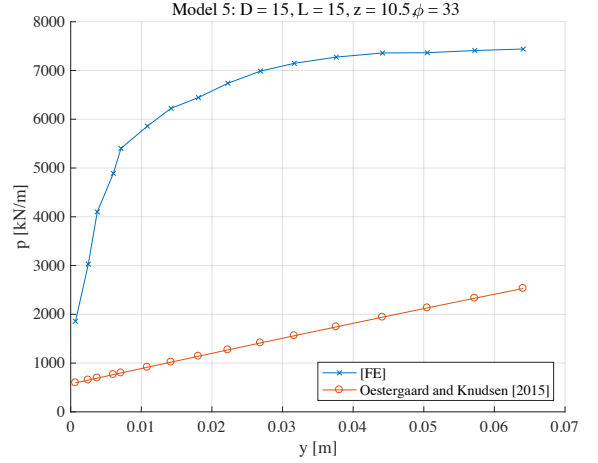
**Figure 4.3:** Normalised Model 2.



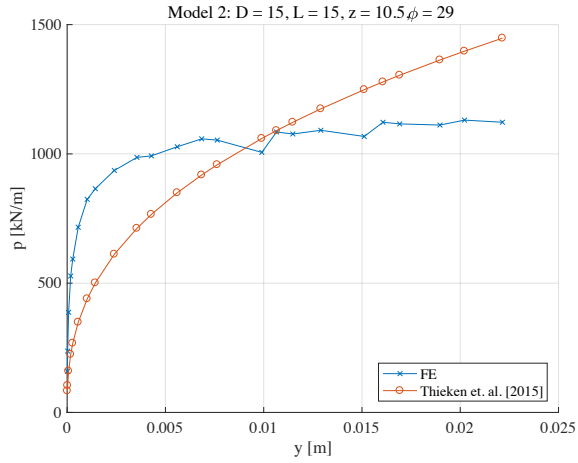
**Figure 4.4:** Normalised Model 5.



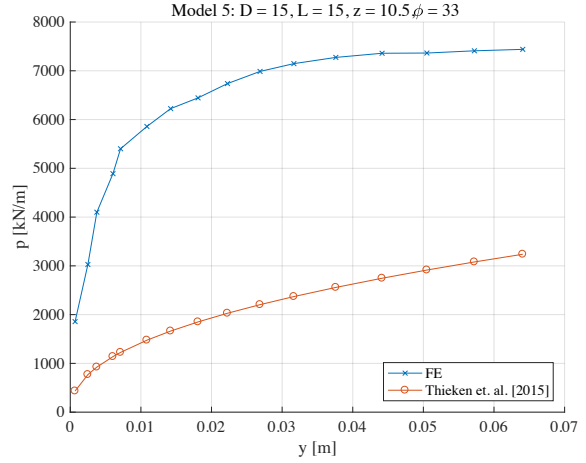
**Figure 4.5:** Østergaard et al. [2015] vs FE for Model 2.



**Figure 4.6:** Østergaard et al. [2015] vs FE data for Model 5.

**Thiessen et al. [2015]**

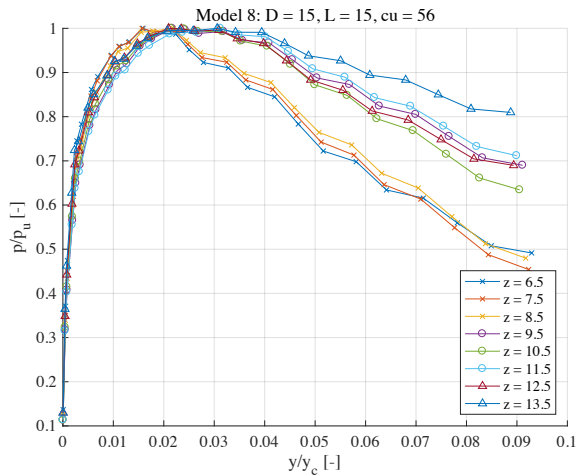
**Figure 4.7:** Thiessen et al. [2015] vs FE data for Model 2.



**Figure 4.8:** Thiessen et al. [2015] vs FE for Model 5.

**Conclusion**

A good normalisation should merge the curves into one curve and thereby making it independent of depth. Østergaard et al. [2015] suggested normalising the soil pressure to the Rankine pressure, which does not fit well for the drained silt, cf. Figure 4.3 and 4.4. When looking at the p-y curves for both Østergaard et al. [2015] and Thiessen et al. [2015] at a depth of 10.5 m, significant difference is seen between the reviewed approaches and the results from the FE simulation. The silt reaches the ultimate soil pressure,  $p_u$ , at lower displacements than former p-y formulations allows for. Østergaard et al. [2015] and Thiessen et al. [2015] are not considered applicable due to the significant differences in soil pressure estimations and unsuitable normalisations. Hence it is necessary to develop new p-y formulations for drained silt.

**4.3.2 Undrained Models****Matlock [1970]**

**Figure 4.9:** Normalised Model 8.

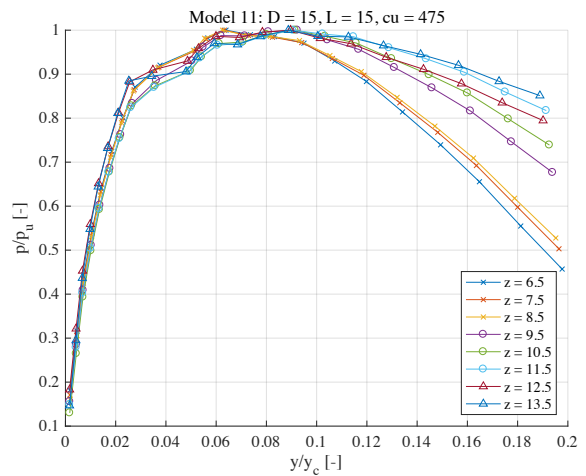


**Figure 4.10:** Normalised Model 11.

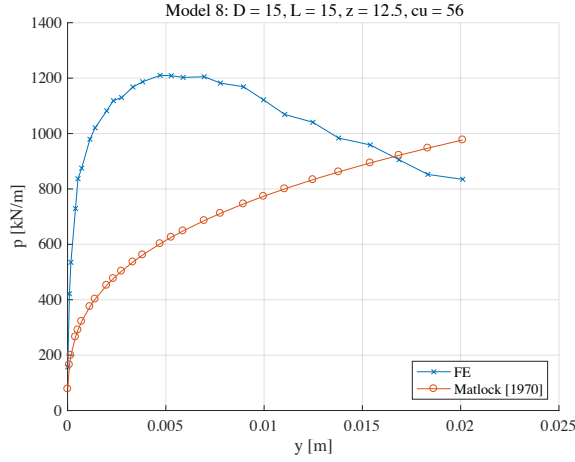


**Figure 4.11:** Matlock [1970] vs FE for Model 8.

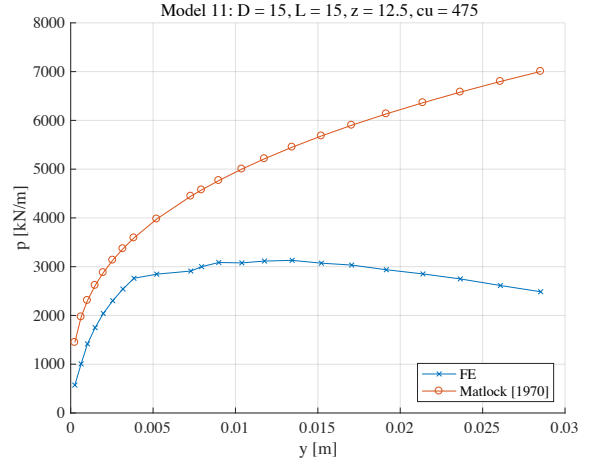


**Figure 4.12:** Matlock [1970] vs FE data for Model 11.

#### Sullivan et al. [1980]

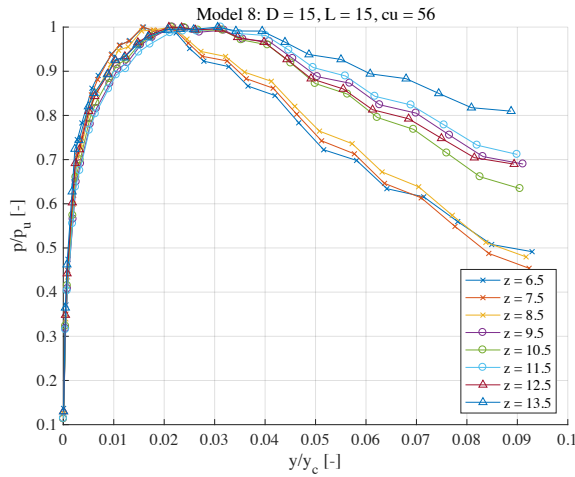


**Figure 4.13:** Normalised Model 8.

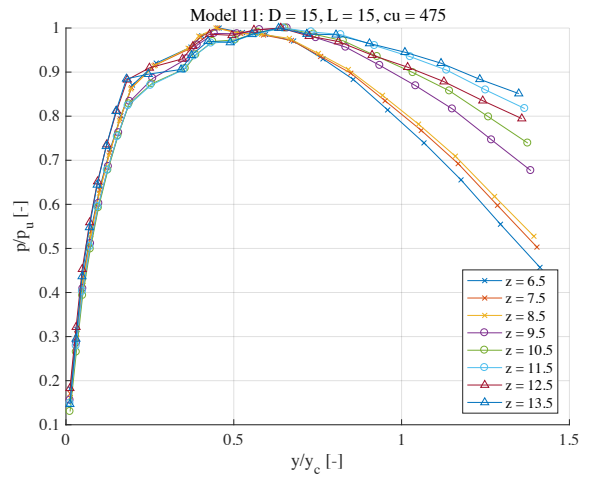


**Figure 4.14:** Normalised Model 11.

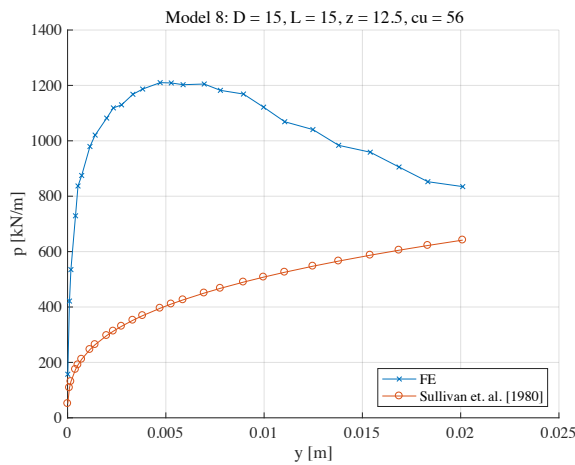


**Figure 4.15:** Sullivan et al. [1980] vs FE data for Model 8.

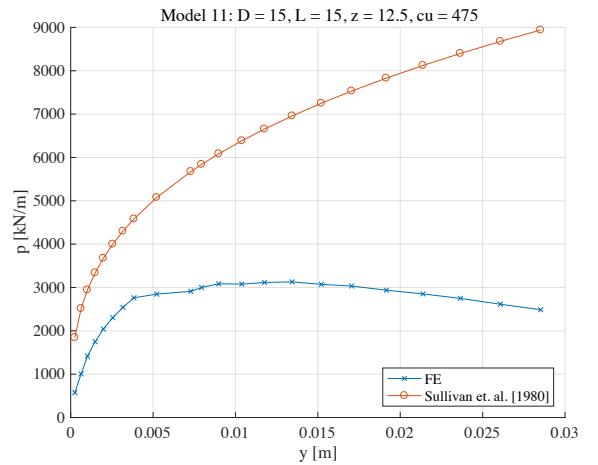


**Figure 4.16:** Sullivan et al. [1980] vs FE for Model 11.

**Conclusion**

As for the drained models, the undrained models cannot be described by the reviewed approaches; Matlock [1970] and [Sullivan et al., 1980]. Even though normalising the soil pressure by the ultimate soil pressure gives the wanted depth-independent p-y curve, problems occur for the formulation of the ultimate soil pressure. The FE data peaks at a lower value of the displacement, and starts to decrease in soil pressure, while the two applied formulations keep increasing for the same displacement. Since none of the reviewed studies for both the drained and undrained silt are considered to be directly applicable, new p-y formulations are needed to be developed. Furthermore, the behavioural difference between the drained and undrained silt is significant, thus they have to be separately addressed, when defining the p-y formulations.

# Formulation of p-y Curves for Silt

# 5

---

The aim of the p-y formulation is a short and simple formulation without too many sub-formulations, as the formulation should be convenient to use in practice, while still maintaining precision. A way to simplify the formulation from the beginning is to define the formulations by reusing some elements from the reviewed studies and adjusting them to the silt.

The overall steps taken to define the p-y formulation are:

- Normalise soil pressure,  $p$ , and displacement,  $y$ .
- Fit a suitable general mathematical function to the FE data.
- Define a p-y formulation based on the normalisation and fitted function.

The p-y formulation for drained and undrained silt will be separately addressed due to the significant behavioural difference as mentioned in Chapter 4. Calculations are mostly carried out in the developed MATLAB scripts, which can be found in [Appendix Folder, MATLAB, masterloop.m]. Few elements are calculated elsewhere, which will be referred to when addressed.

## 5.1 Drained Silt

The approach to define the p-y formulation for the drained silt will be similar to the approach taken by Østergaard et al. [2015]. The only different will be the implementation of soil stiffness as a governing parameter for the model parameters instead of the friction angle, as Vahdatirad et al. [2016] showed, the imprecision of soil pressure estimations were due to the model parameters.

The data processing to develop a p-y formulation for the drained silt models can be found in [Appendix Folder, Data Processing, Fitting Drained Silt.xlsx].

### 5.1.1 Normalisation

From Chapter 4 it was concluded, normalising the data to the Rankine pressure did not give an acceptable normalisation, while normalising the displacement,  $y$ , with the diameter of the bucket,  $D$ , seemed acceptable.

Matlock [1970] normalised the soil pressure by the ultimate soil pressure,  $p_u$ , and thereby merging the curves into one as wanted. This is done for the drained models as well regarding the soil pressure, while the displacement is normalised to the diameter. Figure 5.1 shows the normalised p-y curve for Model 2 and 5. All the normalised models are shown in Appendix G.

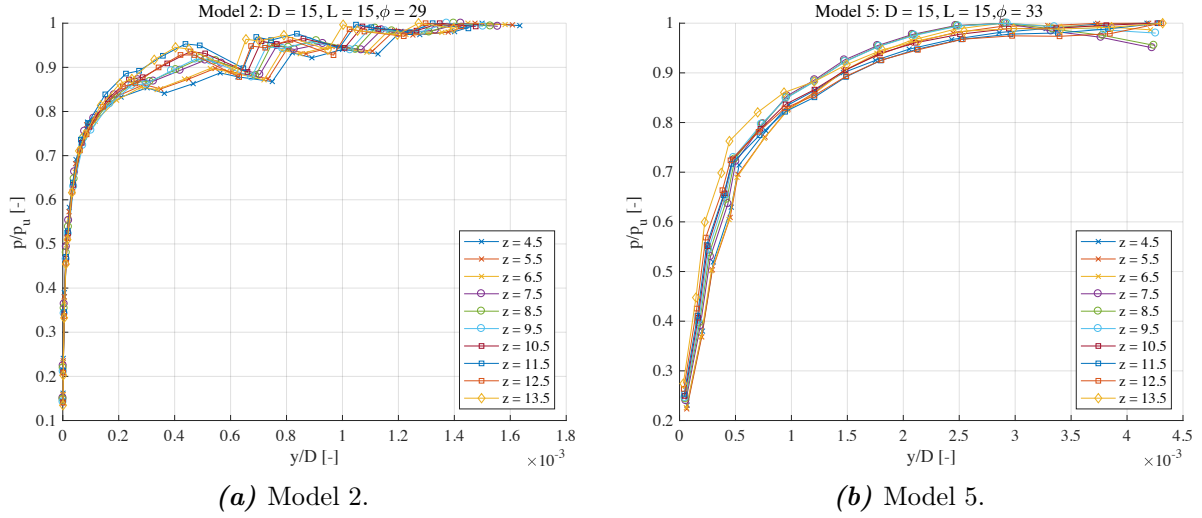


**Figure 5.1:** Normalised p-y curves. Displacement,  $y$ , normalised to bucket diameter,  $D$ , and soil pressure,  $p$ , to the ultimate soil pressure,  $p_u$ .

Since the ultimate soil pressure is not given by any formulation, it is necessary to analyse and define it as a function.

### Formulation of Ultimate Soil Pressure

As a simple and short expression of the p-y formulation is sought. A favourable formulation of the ultimate soil pressure would imply the most basic parameters known without the requirement of an extensive study of the soil. The basic parameters used as input parameters for the ultimate soil pressure are: the friction angle,  $\phi$ , bucket diameter,  $D$ , and effective vertical stress,  $\sigma'_{v0}$ . The parameters are combined as shown in Eq. (5.1).

$$\frac{\sigma'_{v0}}{\phi/D} \quad (5.1)$$

At first the data is not trimmed, thus all depths are included in the analysis. The results show a good linear correlation between the ultimate soil pressure and the parameters, which is shown in Figure 5.2. Furthermore the figure also shows, distinction between soft and stiff soil is needed.

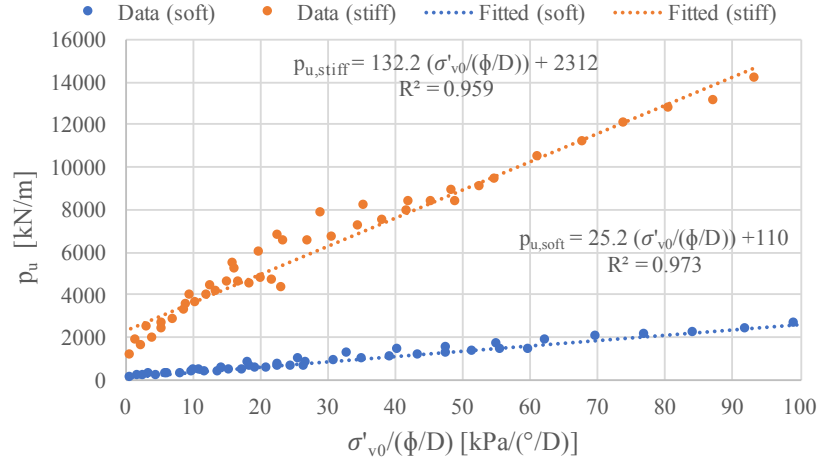


**Figure 5.2:** Correlation of  $p_u$  and  $\sigma'_{v0}/(\phi/D)$  for all models with non-trimmed data.

The fitted function is used to back-calculate the value of the ultimate soil pressure,  $p_u$ . Some of the values close to the top and bottom of the skirt are badly estimated with up to a 100 % deviation from the original value, as seen in Figure 5.5a. Because the correlation is influenced by the data from the top and bottom of the skirt, it seems to be caused by edge effects, which also occurred for the data from Østergaard et al. [2015]. Principle of the failure mechanism of the soil at the edges during horizontal loading, which causes the edge effects, is seen in Figure 5.3.

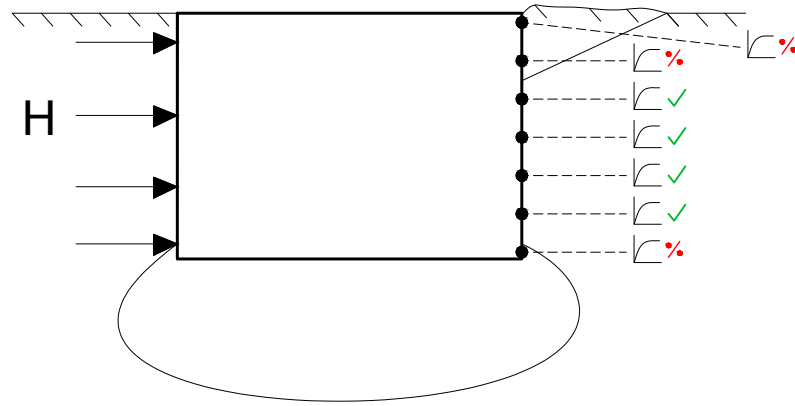


**Figure 5.3:** Outline of failure mechanism at the edges of the suction bucket, and which data points are accepted and disregarded.

In the vicinity at top of the skirt a wedge failure occurs, while a toe kick effect occurs at the skirt bottom. Due to the interference by the edge effects causing badly estimated results, the data sets are trimmed for certain depths at both edges. The process of trimming data is done by evaluating the strength of the correlation. The trimmed p-y curves as well as the non-trimmed p-y curves can be found in Appendix F.

The trimmed data shows a stronger correlation, cf. Figure 5.4, and the back-calculation shows a more precise estimation of the ultimate soil pressure, cf. Figure 5.5b.

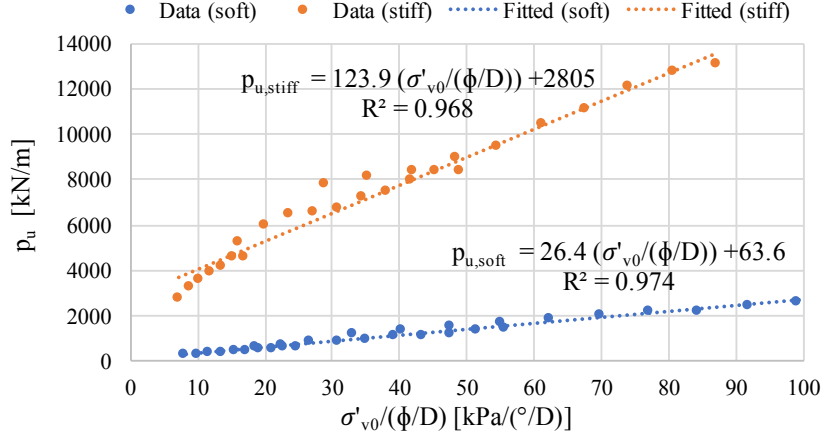


**Figure 5.4:** Correlation of  $p_u$  and  $\sigma'_{v0}/(\phi/D)$  for all models with trimmed data.

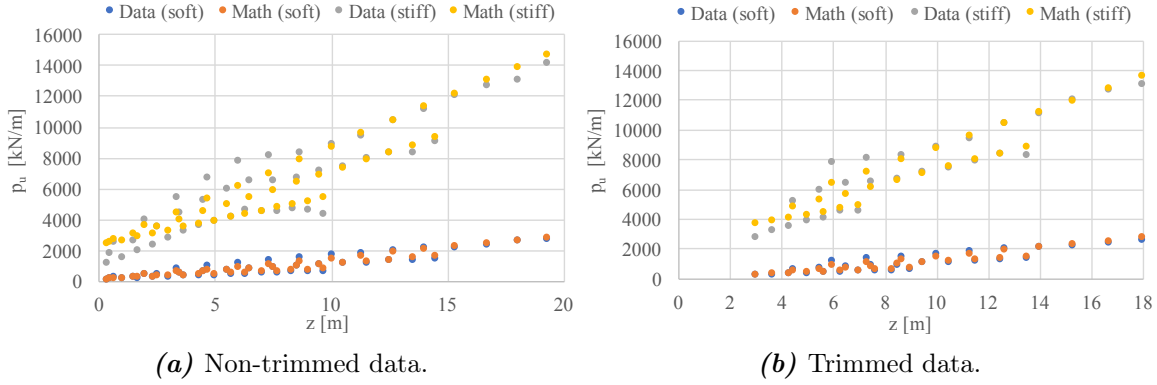


**Figure 5.5:** FE data vs. developed  $p_u$ -formulation.

The difference between the soft and stiff silt has to be addressed. Inspiration is found in Matlock [1970], where constants are used to differentiate between stiff and soft clays. Therefore, instead of having two different functions to calculate the ultimate soil pressure for the soft and stiff silt, only the fitted function for the stiff silt with a constant will be used, as shown in Eq. (5.2).

$$p_u = \left( 124 \cdot \frac{\sigma'_{v0}}{\phi/D} + 2805 \right) \cdot A \quad (5.2)$$

$A$  is the constant separating soft and stiff silt, and it is given in Eq. (5.3).

$$A = \begin{cases} 0.15 & \text{for soft silt} \\ 1 & \text{for stiff silt} \end{cases} \quad (5.3)$$

As the fitted function of the stiff silt, cf. Figure 5.4, is used as the main function to calculate the ultimate soil pressure,  $A = 1$  for stiff silt. To determine the value of  $A$  for the soft silt, the ratio between the two fitted functions of the soft and stiff silt is found, cf. Figure 5.6. From here constant  $A = 0.15$  is considered a representative value for the soft silt.



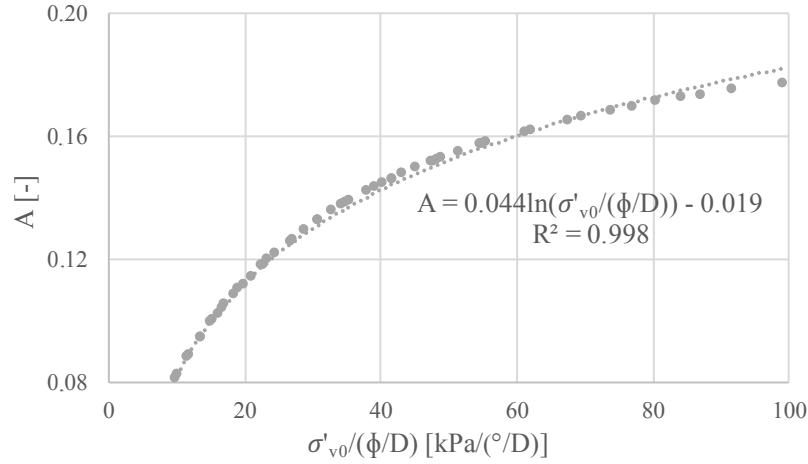


**Figure 5.6:** Constant  $A$  defined as the ratio of the soft and stiff silt.

The formulation of the ultimate soil pressure has been found and stated in Eq. (5.2), hence the next step is to determine a function and fit it to the normalised p-y curves for the drained models.

### 5.1.2 Mathematical Model

As mentioned initially, an approach similar to Østergaard et al. [2015] is sought, where four model parameters are used;  $\beta_1, \beta_2, \beta_3$  and  $\beta_4$ . Furthermore some inspiration is also gained from Matlock [1970], as the tanh-functions are powered by  $1/3$ , due to the steep initial stiffness for the p-y curves. The formulation is given in Eq. (5.4).

$$\frac{p}{p_u} = \beta_1 \cdot \tanh\left(\beta_2 \cdot \frac{y}{D}\right)^{1/3} + \beta_3 \cdot \tanh\left(\beta_4 \cdot \frac{y}{D}\right)^{1/3} \quad (5.4)$$

$\beta_{1-4}$  are not necessarily constant for the models, as they might depend on some parameters. Therefore, an analysis of the model parameters are carried out to find their value for each model, which would give the best fit of the FE data.

### Formulation of Model Parameters

To fit the data as well as possible, the model parameters have to be able to take any arbitrary value. All the models are well fitted with the best fit function with insignificant deviation from the FE data. The values of the four model parameters from the best fit analysis are extracted from each model and plotted against  $E_{50}D$ , cf. Figure 5.7.

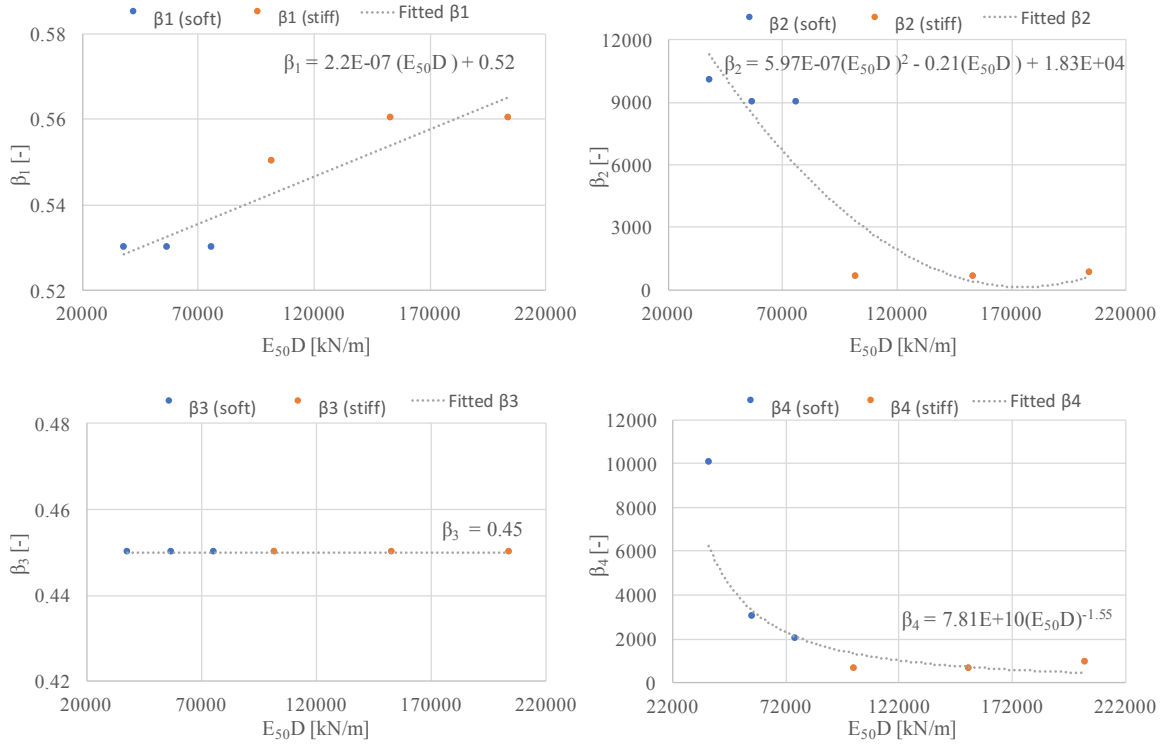


**Figure 5.7:** Best fit values of  $\beta_1 - \beta_4$  for drained models as functions of  $E_{50}D$ .

A common fit for both the stiff and soft silt is made for the four model parameters, which is shown by the grey dotted line with a mathematical expression in Figure 5.7. The mathematical expressions for the model parameters are given in Eq. (5.5). The result of the new p-y formulation for Model 2 and 5 is shown in Figure 5.8, while all drained models can be found in Appendix G.

$$\begin{aligned}
 \beta_1 &= 2.2 \cdot 10^{-7} \cdot (E_{50}D) + 0.52 \\
 \beta_2 &= 5.97 \cdot 10^{-7} \cdot (E_{50}D)^2 - 0.21E_{50}D + 1.83 \cdot 10^4 \\
 \beta_3 &= 0.45 \\
 \beta_4 &= 7.81 \cdot 10^{10} \cdot (E_{50}D)^{-1.55}
 \end{aligned} \tag{5.5}$$

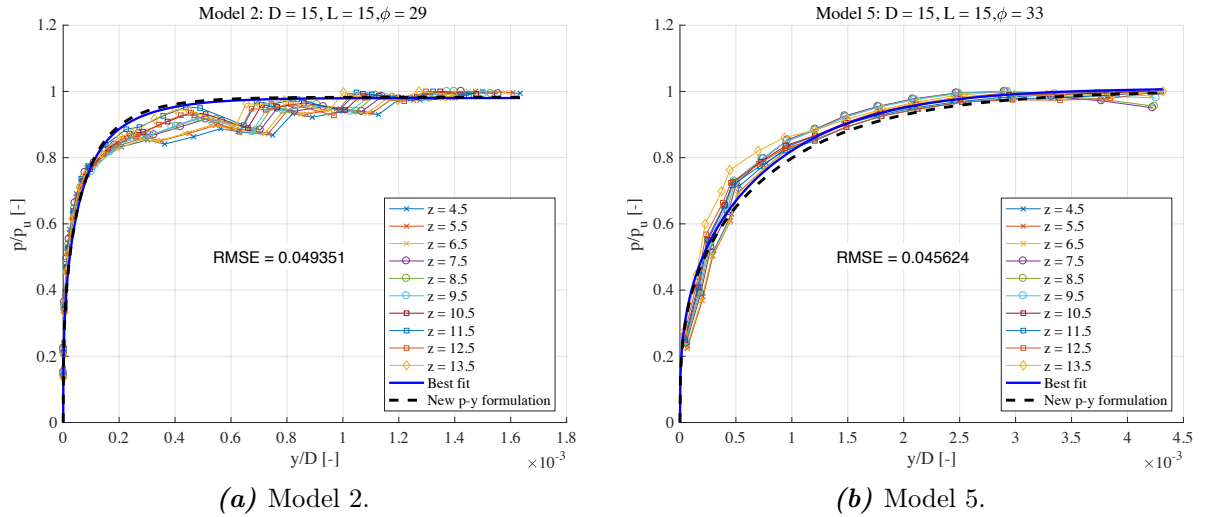


**Figure 5.8:** New p-y formulation, best fit and FE data. RMSE value is taken between the new p-y formulation and the FE data.

Remarks concerning the p-y formulation for drained models:

In the beginning the model parameters,  $\beta_{1-4}$ , were defined in relation to  $\phi/D$ . This was before realising, that the model parameters should be sought governed by the soil stiffness instead of the friction angle. As the aim of the formulations is to define them in a simple and logic way, the relation to the model parameters were changed to depend on  $E_{50}D$ . Nevertheless, vital experience were drawn from the examning of the data, which is briefly described in this paragraph.

In the best fit analysis, where the model parameters were analysed, the *lscurvefit* function in MATLAB was used at first. The function fits to non-linear data points by iterating one or more parameters to fit in sense of the least square method. The function resulted in significantly different values of the model parameters for the six drained models, as seen in Figure 5.9. For instance the difference in value between the soft and stiff silt for  $\beta_1$  is very different, as they take positive and negative values respectively.

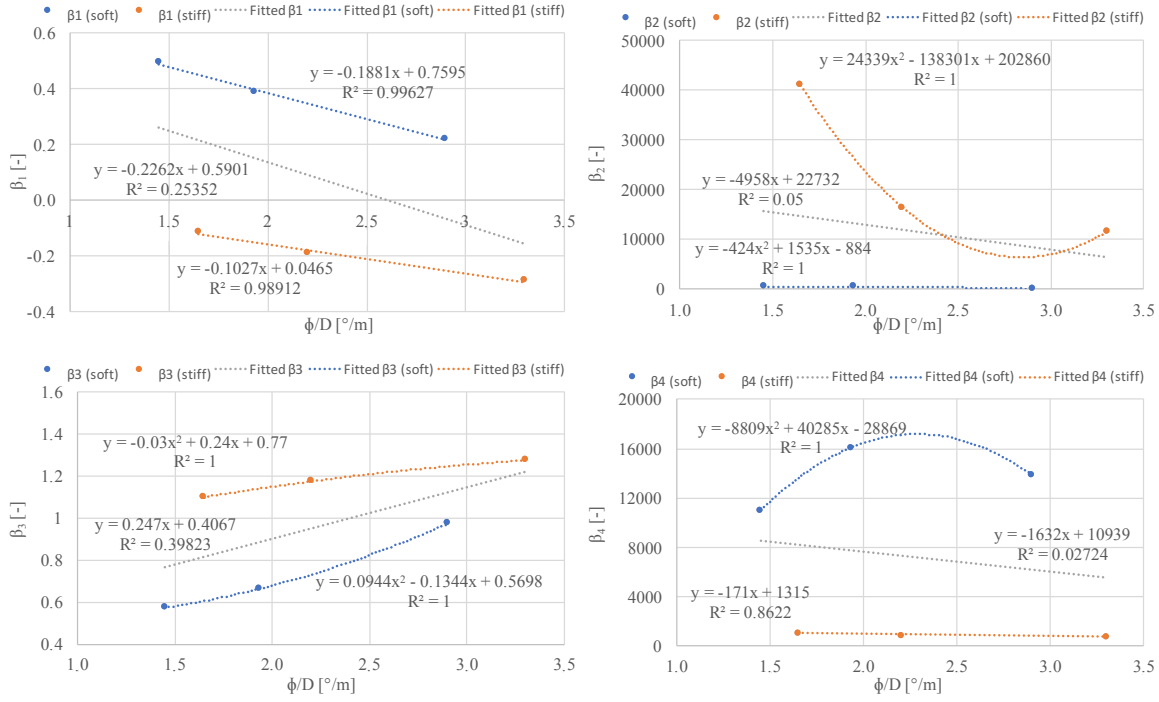


**Figure 5.9:** Best fit values of  $\beta_{1-4}$  for drained models with use of lscurvefit.

Fitting the data for both the soft and stiff silt, to obtain a linear function for each model parameter, resulted in an imprecise p-y formulation, as seen in Figure 5.10, where Model 1 is shown.

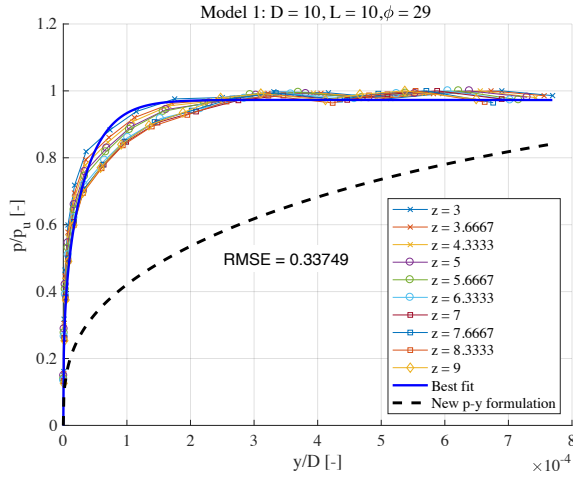


**Figure 5.10:** Model 1: p-y formulation based on lscurvefit.

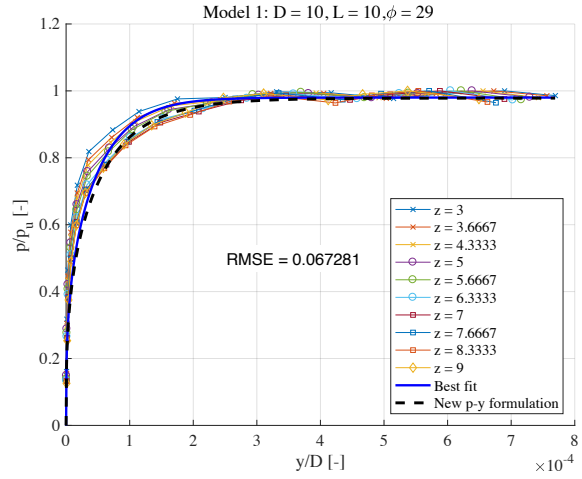


**Figure 5.11:** Model 1: p-y formulation based on semi-automatic iteration.

Before it was acknowledged that the problem was within the use of the lscurvefit function, different mathematical expression, cf. Eq. (5.6) and (5.7), were tried out.

$$\frac{p}{p_u} = \beta_1 \cdot \tanh\left(\beta_2 \cdot \frac{y}{D}\right)^{1/3} + \tanh\left(\beta_3 \cdot \frac{y}{D}\right)^{1/3} \quad (5.6)$$

$$\frac{p}{p_u} = \beta_1 \cdot p_u \cdot \tanh\left(\beta_2 \cdot z \cdot \frac{y}{D}\right)^{1/3} + \beta_3 \cdot \tanh\left(\beta_4 \cdot z \cdot \frac{y}{D}\right)^{1/3} \quad (5.7)$$

Both expression led to results of unacceptable character, as the model parameters once again showed significant differences in values and therefore also in the precision of the p-y formulation compared to the FE data.

Lastly the values of the obtained model parameters from the best fit analysis were analysed, and it was acknowledged that only  $\beta_2$  and  $\beta_4$  should give significant different values due to the initial stiffness of the p-y curves for the FE data. Therefore, a manual iteration of the four model parameters were performed, where  $\beta_1$  and  $\beta_3$  were kept as constant as possible, as the outcome of the mathematical expression is most sensitive to those two parameters. This iterative method gave better and more precise results, than the lscurvefit function, as seen in Figure 5.11. Thus, the method was adopted, and the model parameters were found in this manner and defined as in Eq. (5.5).

## 5.2 Undrained Silt

A similar form of the p-y formulation made for the drained silt is wanted for the undrained silt as well. The formulation will be based on the undrained shear strength,  $c_u$ , instead of the friction angle, as undrained cases depend on the total strength parameter.

The steps towards the new formulation, are basically the same. Therefore, less thorough description of the process is given. The data trimming and formulation of the model parameters can be found in [Appendix Folder, Data Processing, Fitting Undrained Silt.xlsx].

### 5.2.1 Normalisation

As for the drained models, the soil pressure,  $p$ , and displacement,  $y$ , are normalised to the ultimate soil pressure,  $p_u$ , and bucket diameter,  $D$ , respectively, as shown in Figure 5.12 for Model 8 and 11.

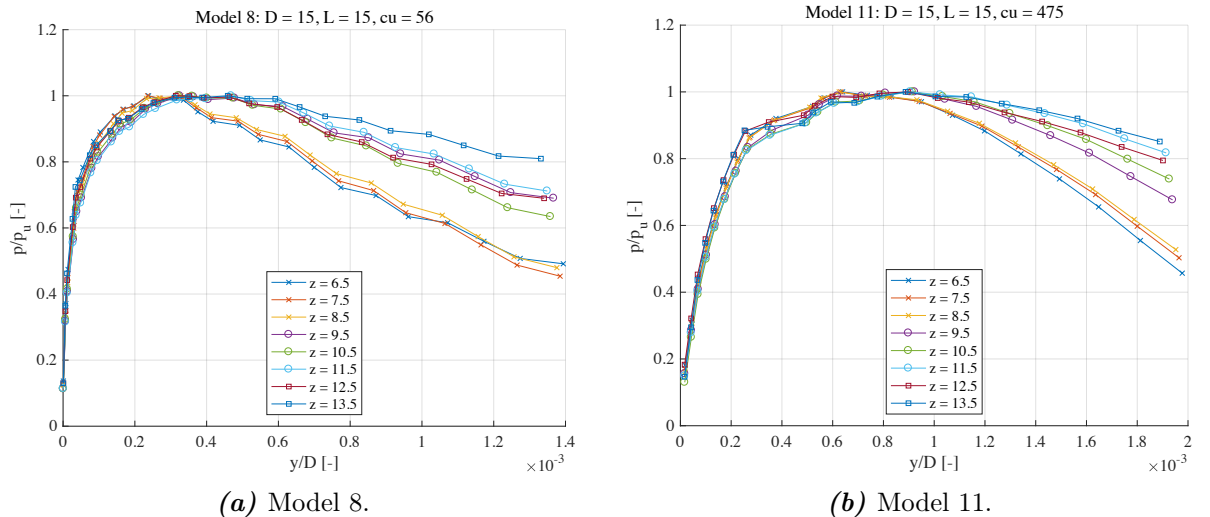


**Figure 5.12:** Normalising soil pressure and displacement with ultimate soil pressure,  $p_u$ , and bucket diameter,  $D$ .

It is evident, that only the part towards the peak is well normalised, since visible variation

occur between the layers from the peak towards the end. When looking at the relative variation between the layers, the problem is considered negligible, thus the normalisation is accepted.

### Formulation of Ultimate Soil Pressure

The method used to define the ultimate soil pressure will be the same as used for the drained models. The only difference will be the governing variable of the ultimate soil pressure. For the drained silt it was the friction angle, but for the undrained silt it is the undrained shear strength,  $c_u$ , as shown in Eq. (5.8).

$$\frac{\sigma'_{v0}}{c_u/D} \quad (5.8)$$

The non-trimmed data results in bad correlation, as shown in Figure 5.13. Thus, as for the drained cases, the data is trimmed until acceptable correlation is obtained. Again correlation gets stronger, when data points from the both skirt edges are excluded, cf. Figure 5.14. The edge effects can also be seen in Figure 5.16a, where back calculated values at the edges are significantly different from the non-trimmed data points.

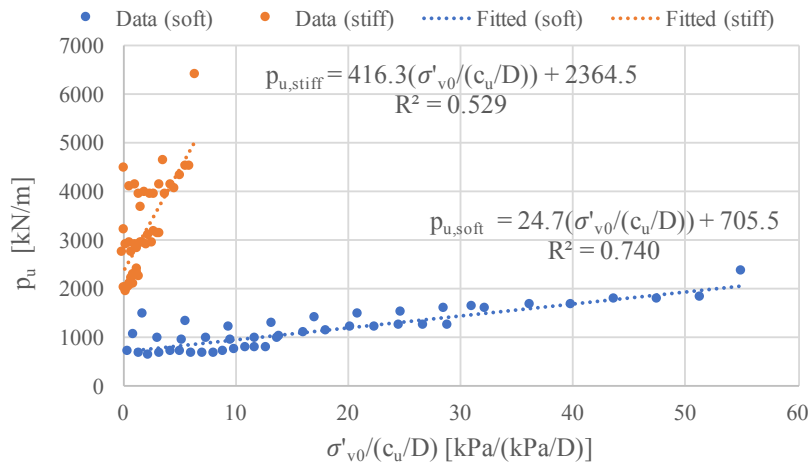


**Figure 5.13:** Correlation between  $p_u$  and  $\sigma'_{v0}/(c_u/D)$  for the undrained models with non-trimmed data.

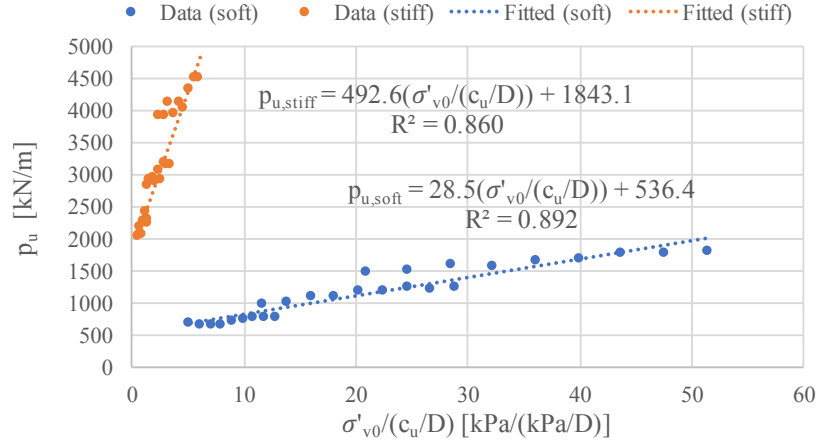


**Figure 5.14:** Correlation between  $p_u$  and  $\sigma'_{v0}/(c_u/D)$  for the undrained models with trimmed data.

Only one equation for defining the ultimate soil pressure is wanted, thus it is defined as in Eq. (5.9).

$$p_u = \left( 493 \cdot \frac{\sigma'_{v0}}{c_u/D} + 1843 \right) \cdot A \quad (5.9)$$

$A$ , which is given in Eq. (5.10), separates the soft and stiff silt from each other.

$$A = \begin{cases} 0.15 & \text{for soft silt} \\ 1 & \text{for stiff silt} \end{cases} \quad (5.10)$$

The constant  $A$  is based on the ratio between the fitted function for the soft and stiff silt, cf. Figure 5.15.

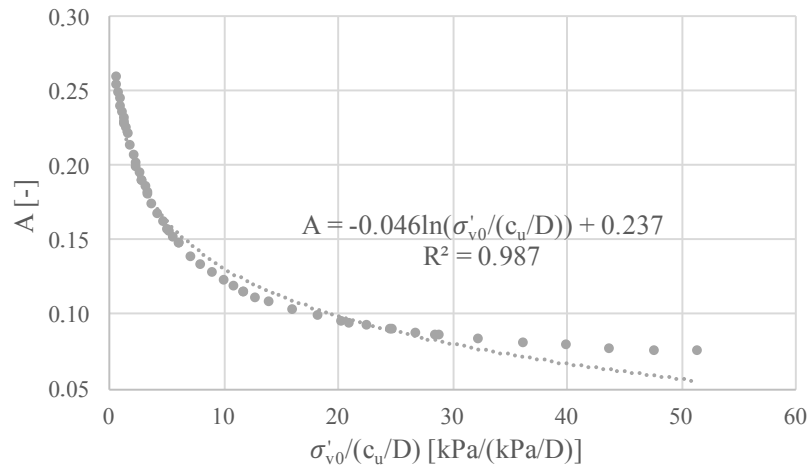


**Figure 5.15:** Constant  $A$  defined as the ratio of the soft and stiff silt.

The formulation of the ultimate soil pressure is defined. The precision of the estimation of the ultimate soil pressure compared to the trimmed data is visualised in Figure 5.16b.

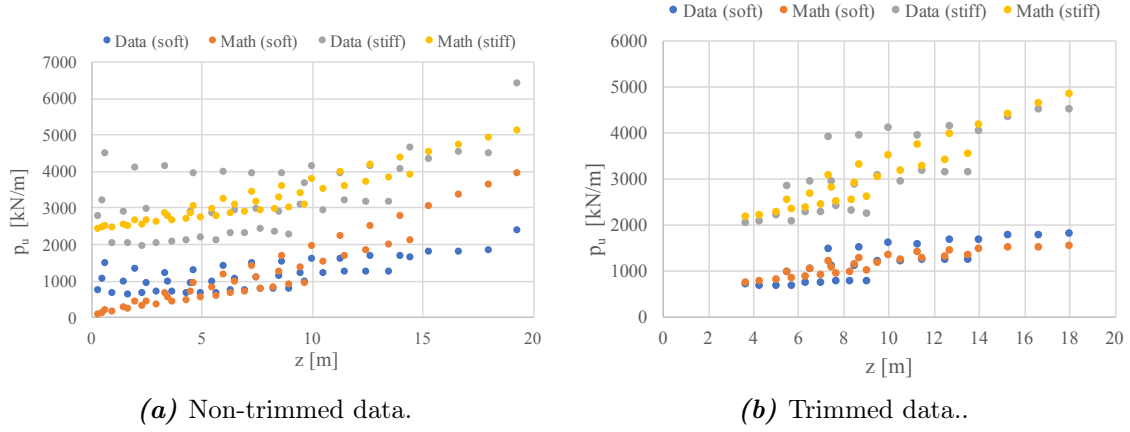


**Figure 5.16:** FE data vs. developed  $p_u$ -formulation.

### 5.2.2 Mathematical Model

The undrained models increase until the ultimate soil pressure is reached, from where it decreases to some value. This is significantly different from the behaviour seen from the drained models. Therefore, a more thorough look at the characteristics of the normalised p-y curves is needed to define a mathematical model.

#### Characteristics of p-y Curves

A pattern for all six undrained models are seen regarding the normalised displacement,  $y/D$ . The p-y curves for the soft undrained silt models peak at  $y/D \approx 0.00036$ , while the stiff undrained silt models peak at  $y/D \approx 0.0009$ . Furthermore the soil collapses at  $y/D \approx 0.0014$  and  $0.002$  for the soft and stiff silt respectively.

From the described characteristics of the normalised p-y curves, the soft silt models peak at normalised displacement approximately 0.4 of the value observed for the stiff silt models. While for the failure point, the soft silt is approximately 0.65 of the value observed for the stiff silt models. Based on those facts, definitions are made regarding the peak and failure point, cf. Eq. (5.12) and Figure 5.17.

$$0 \leq y/D < y_B = 0.0009B, \quad B = \begin{cases} 0.4 & \text{for soft silt} \\ 1 & \text{for stiff silt} \end{cases} \quad (5.11)$$

$$y_B \leq y/D < y_C = 0.002C, \quad C = \begin{cases} 0.65 & \text{for soft silt} \\ 1 & \text{for stiff silt} \end{cases} \quad (5.12)$$



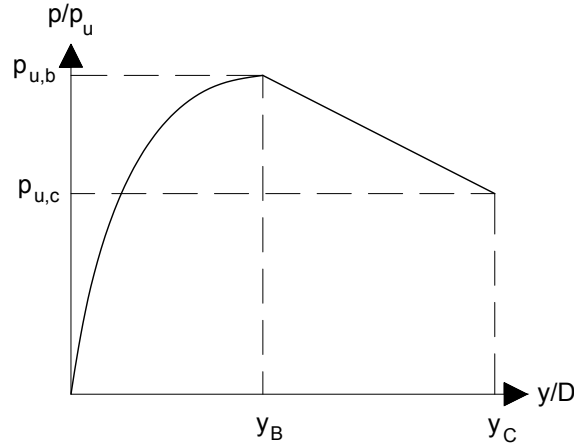


**Figure 5.17:** Principle division of undrained p-y curve.

Since the normalised displacement for the peak point,  $y_B$ , and failure point,  $y_C$ , is known and defined, the p-y formulation can be defined in the following intervals:

$$\frac{p}{p_u} \left( \frac{y}{D} < y_B \right) = \beta_1 \cdot \tanh \left( \beta_2 \cdot \frac{y}{D} \right)^{1/3} + \beta_3 \cdot \tanh \left( \beta_4 \cdot \frac{y}{D} \right)^{1/3} \quad (5.13)$$

$$\frac{p}{p_u} \left( \frac{y}{D} = y_B \right) = \beta_1 \cdot \tanh (\beta_2 \cdot y_B)^{1/3} + \beta_3 \cdot \tanh (\beta_4 \cdot y_B)^{1/3} \quad (5.14)$$

$$\frac{p}{p_u} \left( \frac{y}{D} = y_C \right) = 0.75G, \quad G = \begin{cases} 0.75 & \text{for soft silt} \\ 1 & \text{for stiff silt} \end{cases} \quad (5.15)$$

From Eq. (5.14) and (5.15) it is evident, that they define two points, which is also shown in Figure 5.17, where the soil pressure is considered to decrease linearly between  $y_B$  and  $y_C$ .

### Formulation of Model Parameters

$\beta_{1-4}$  are found, as they were for the drained models, cf. Figure 5.18.

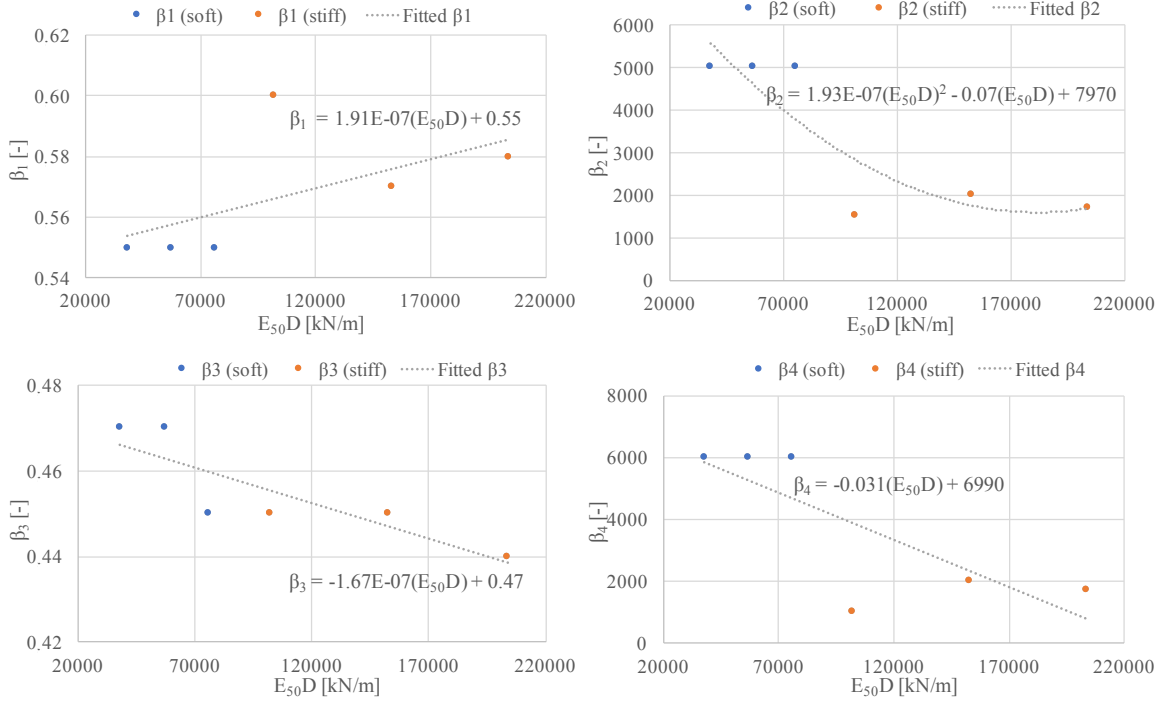


**Figure 5.18:** Best fit values of  $\beta_{1-4}$  for undrained models as functions of  $E_{50}D$ .

From Figure 5.18 the model parameters are defined in Eq. (5.16).

$$\begin{aligned}
 \beta_1 &= 1.91 \cdot 10^{-7} \cdot (E_{50}D) + 0.55 \\
 \beta_2 &= 1.93 \cdot 10^{-7} \cdot (E_{50}D)^2 - 0.07(E_{50}D) + 7970 \\
 \beta_3 &= -1.67 \cdot 10^{-7} \cdot (E_{50}D) + 0.47 \\
 \beta_4 &= -0.031(E_{50}D) + 6990
 \end{aligned} \tag{5.16}$$

The plots of the new p-y formulation for undrained models compared to the data and best fit for Model 8 and 11 are shown in Figure 5.19. Similar plots for all undrained models are found in Appendix G.

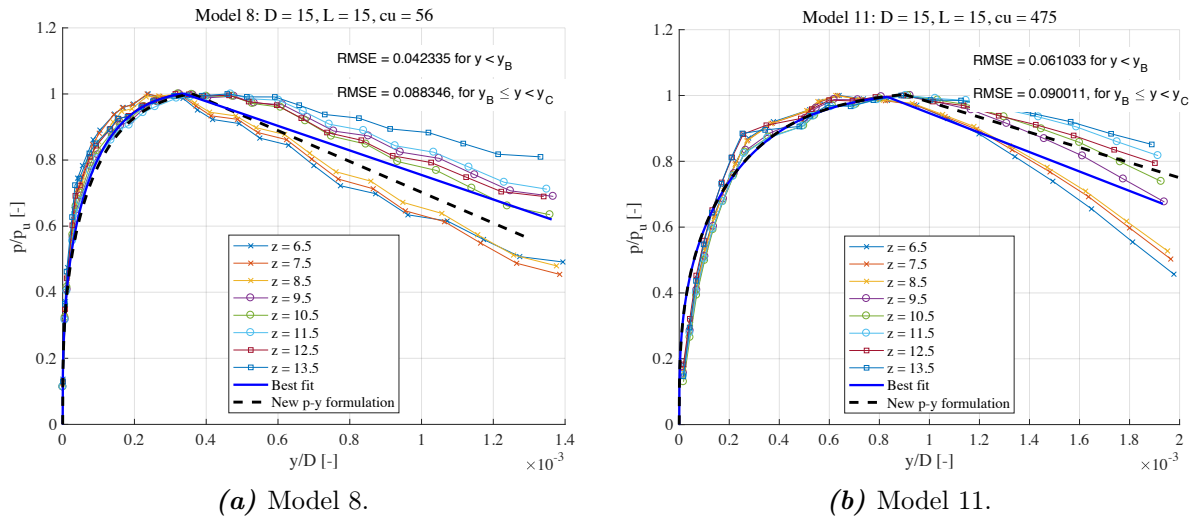


**Figure 5.19:** New p-y formulation, best fit and FE data. RMSE value is taken between the new p-y formulation and the FE data.

Remark concerning p-y formulation of undrained models:

At first an approach more identical to the drained models was carried out, where no division of the p-y formulation was made. Here the model parameters were sought, but no significant correlation of the model parameters across the models were obtainable, hence another approach was sought. Inspiration to divide the p-y formulation into parts came from Sullivan et al. [1980], as similar soil behaviour was observed. From here the characteristics of the p-y curves were analysed more thoroughly as described for the formulation of the undrained models.

The data of the silt have been processed, and separate p-y formulation for the drained and undrained models have been defined. As seen in the literature review in Chapter 2, many different formulations are given. Keeping the basics of the formulations the same, regardless of soil, would be favourable. Therefore, new p-y formulation for the drained sand studied in Østergaard et al. [2015] will be developed in a similar manner as developed for the drained silt.



# Formulation of p-y Curves

## for Sand

# 6

As mentioned in the literature review in Chapter 2, Østergaard et al. [2015] studied suction buckets in sand using FE as well. The p-y formulation, suggested by Østergaard et al. [2015], was not applicable for the silt, as shown in Chapter 4, thus new p-y formulations were sought and defined. Since the data of the 18 numerical models from Østergaard et al. [2015] is available, a new p-y formulation for the drained sand is sought developed similar to the drained silt. The 18 numerical models studied in Østergaard et al. [2015] and their input parameters for the HSsmall model are given in Table 6.1 and 6.2 respectively.

**Table 6.1:** Overview of the tested models in Østergaard et al. [2015].

Model no.	$D$ [m]	$L$ [m]	$\phi$ [°]	Model no.	$D$ [m]	$L$ [m]	$\phi$ [°]
1	10	5	30	10	15	15	30
2	10	5	35	11	15	15	35
3	10	5	40	12	15	15	40
4	10	10	30	13	20	10	30
5	10	10	35	14	20	10	35
6	10	10	40	15	20	10	40
7	15	7.5	30	16	20	20	30
8	15	7.5	35	17	20	20	35
9	15	7.5	40	18	20	20	40

**Table 6.2:** Strength and stiffness parameters for sand used for the numerical models in Østergaard et al. [2015].

$\phi$	[°]	30	35	40
$\psi$	[°]	0	5	10
$Q_{min}$	[-]	10.00	10.00	10.00
$\Delta\phi_1$	[°]	2.00	2.00	2.00
$I_D$	[%]	15.17	53.09	91.02
$\nu$	[-]	0.33	0.30	0.26
$E_{50}$	[MPa]	4.92	14.06	28.54
$E_{oed}$	[MPa]	7.39	18.87	35.15
$E_{ur}$	[MPa]	14.77	42.17	85.62
$e$	[-]	0.99	0.83	0.68
$G_0$	[MPa]	65.23	82.30	103.49
$\gamma_{0.7}$	[mm/m]	0.22	0.18	0.14
$K_0$	[-]	0.50	0.43	0.36
$c'$	[kPa]	0.10	0.10	0.10

## 6.1 Normalisation

The soil pressure and displacement are normalised to the ultimate soil pressure and bucket diameter respectively. The normalisation is accepted, since the curves for each model are

merged into one, which is seen in Figure 6.1 for Model 5 and 12.

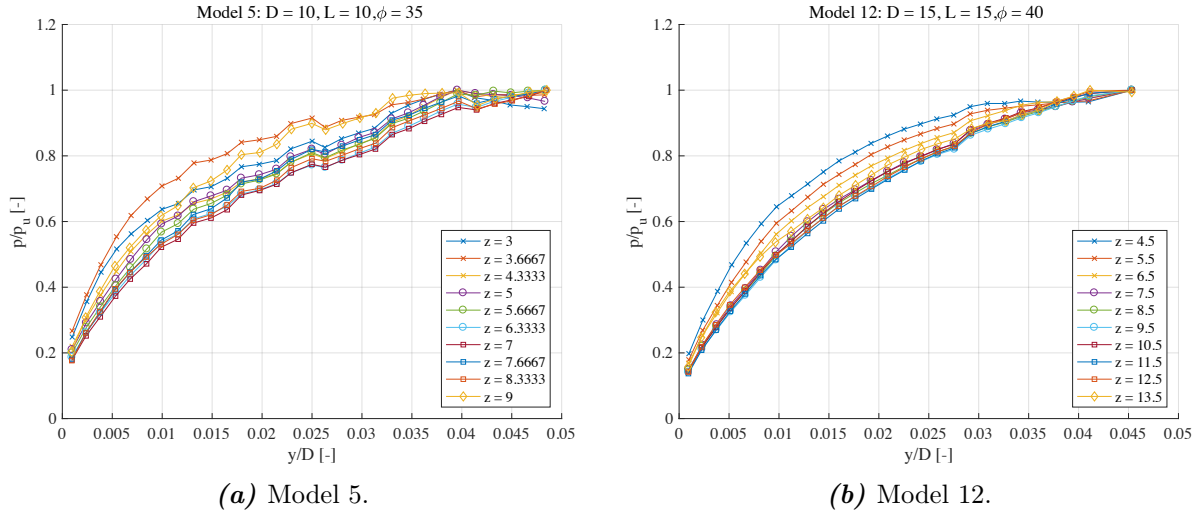


**Figure 6.1:** Normalised p-y curve for sand.

### 6.1.1 Formulation of Ultimate Soil Pressure

The data sets available from Østergaard et al. [2015] are trimmed for edge effects, hence the ultimate soil pressure correlates rather well with  $\sigma'_{v0}/(\phi/D)$  as seen in Figure 6.2. As for the silt, only one formulation is wanted for the ultimate soil pressure, where a constant is included, to take the different degree of soil stiffness into account. Thus, the formulation of the ultimate soil pressure from  $\phi = 40^\circ$  is used as the basic formulation.

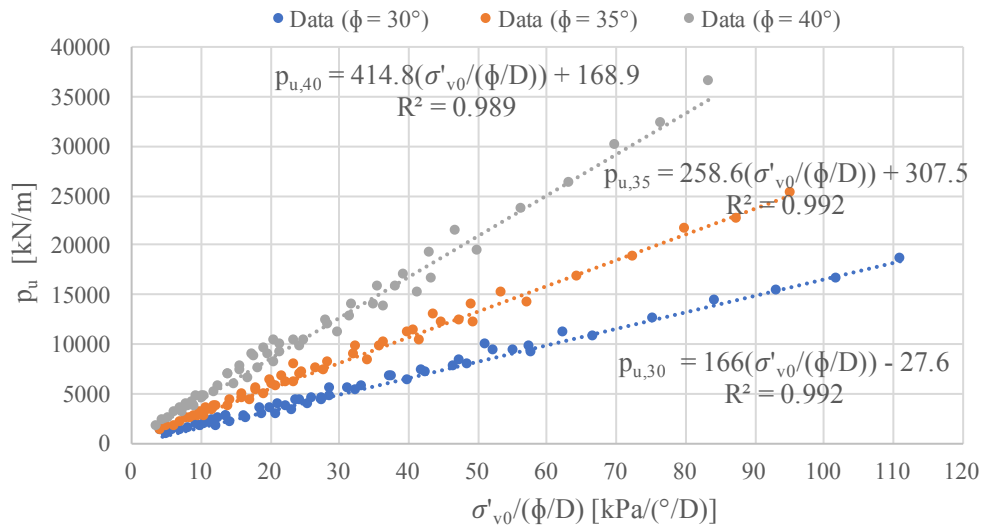


**Figure 6.2:** Correlation of  $p_u$  and  $\sigma'_{v0}/(\phi/D)$  for sand.

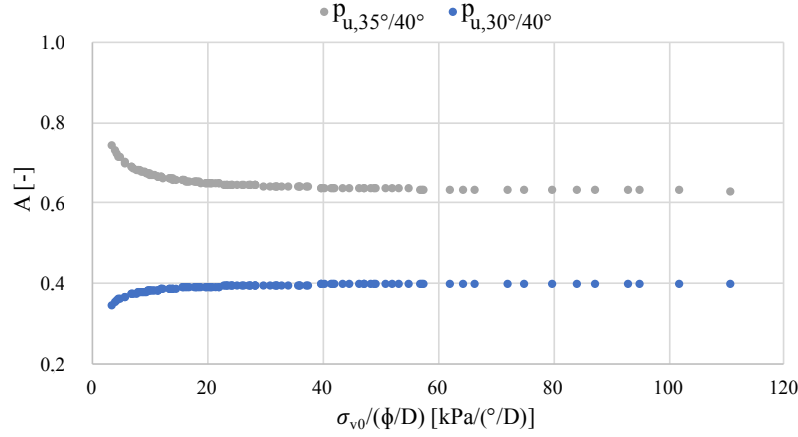


**Figure 6.3:** Constant  $A$  defined as the ratio between the three different sands.

The ratio of  $p_{u,30^\circ/40^\circ}$  and  $p_{u,35^\circ/40^\circ}$  is assumed to be constant, since the two ratios do not differ much from 0.4 and 0.65 respectively, as seen in Figure 6.3. Thus, the ultimate soil pressure is defined as in Eq. (6.1).

$$p_u = \left( 415 \frac{\sigma'_{v0}}{\phi/D} + 169 \right) \cdot A \quad (6.1)$$

where  $A$  is defined as:

$$A = \begin{cases} 0.4 & \text{for soft sand} \\ 0.65 & \text{for medium sand} \\ 1 & \text{for stiff sand} \end{cases}$$

## 6.2 Mathematical Model

The mathematical formulation for the sand is sought in manner of Eq. (6.2), which is the same, as the one used for both the drained and undrained silt.

$$\frac{p}{p_u} = \beta_1 \cdot \tanh \left( \beta_2 \cdot \frac{y}{D} \right)^{1/3} + \beta_3 \cdot \tanh \left( \beta_4 \cdot \frac{y}{D} \right)^{1/3} \quad (6.2)$$

### 6.2.1 Formulation of Model Parameters

The model parameters,  $\beta_{1-4}$ , are found by a best fit analysis in the exact same way as found for the silt. Figure 6.4 shows the model parameters from the best fit analysis, while the definition of the them is given in Eq. (6.3).

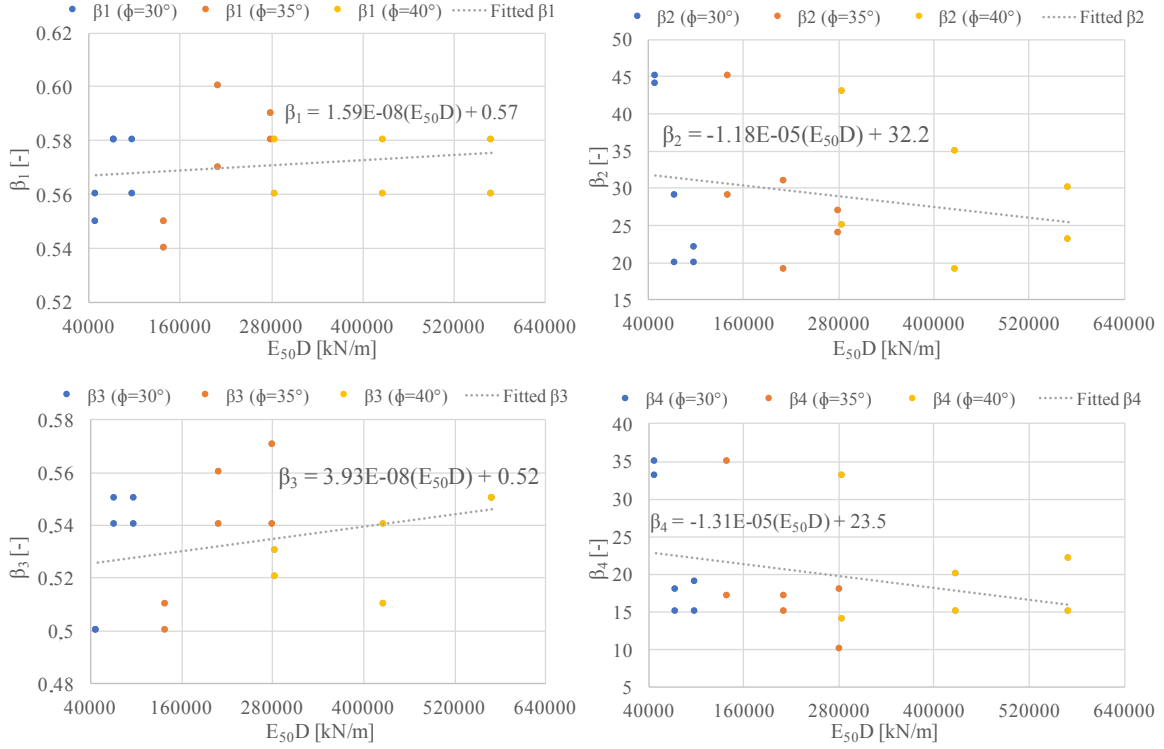
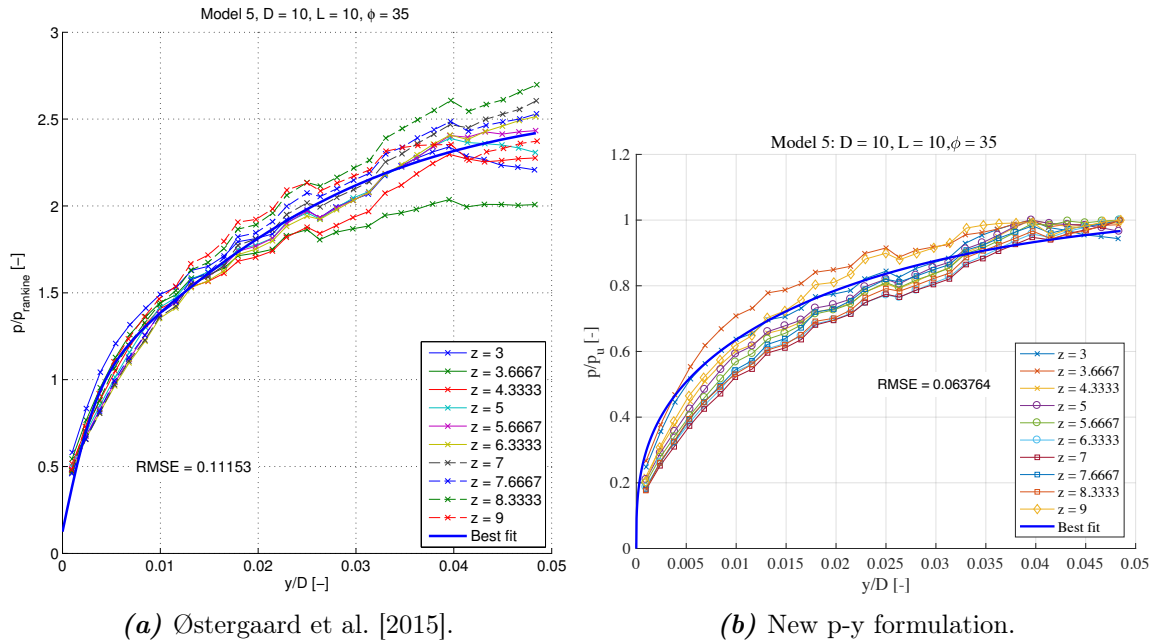


**Figure 6.4:** Best fit values of  $\beta_1 - \beta_4$  for sand as functions of  $E_{50}D$ .

$$\begin{aligned}
 \beta_1 &= 1.59 \cdot 10^{-8} \cdot (E_{50}D) + 0.57 \\
 \beta_2 &= -1.18 \cdot 10^{-5} \cdot (E_{50}D) + 32.2 \\
 \beta_3 &= 3.93 \cdot 10^{-8} \cdot (E_{50}D) + 0.52 \\
 \beta_4 &= -1.31 \cdot 10^{-5} \cdot (E_{50}D) + 23.5
 \end{aligned} \tag{6.3}$$

The analysis show less error in general for all models compared to the error from the best fit analysis in Østergaard et al. [2015], as for instance is shown in Figure 6.5 for Model 5.



**(a)** Østergaard et al. [2015].

**(b)** New p-y formulation.

**Figure 6.5:** Best fit of Model 5.



The plot of best fit function and the new p-y formulation for Model 5 and 12 are shown in Figure 6.6, while plots for all 18 models are found in Appendix H.

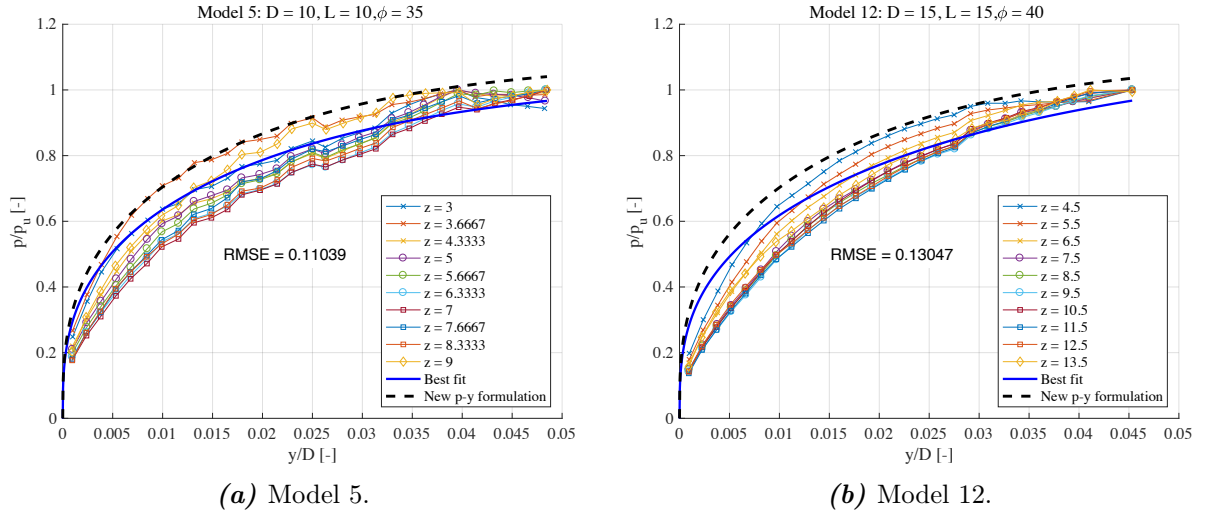


**Figure 6.6:** New p-y formulation, best fit and FE data for sand. RMSE value is taken between the new p-y formulation and the FE data.

It is proven, that the overall formulation is applicable for the sand as well as the silt. It is even shown, that the new formulation is more precise, since the model parameters and the p-y formulation fits better to the data compared to the formulation suggest by Østergaard et al. [2015].



# Conclusion 7

---

Since the p-y formulations, used to design offshore structures today, are based on slender piles, which behaves significantly different from the much less slender suction bucket, new p-y formulations are desirable. Therefore, the aim of this thesis has been to develop simple and practically usable p-y formulations for both drained and undrained silt with use of the FE program PLAXIS 3D AE. A total of 12 numerical models were simulated and analysed, where geometry of the bucket, soil strength and drainage type were combined.

The original plan was to perform a number of physical triaxial tests in the geotechnical laboratory to obtain the needed input parameters for the HSsmall material model, but due to the circumstances, this was not possible. The soil parameters used for the study were given by Lars Bo Ibsen, as a relation could not be found between the undrained shear strength and the other input parameters needed for HSsmall in PLAXIS. As the given parameters were only defined with effective strength parameters, the SHANSEP method was used to obtain the undrained shear strength for the silt by performing a number of undrained triaxial tests in PLAXIS.

Towards the final formulation, many different approaches were taken. At first the data was compared to the different existing p-y formulations from former studies, which were reviewed in the literature review. The analysis showed, that the soil response could not be described by the reviewed formulations. Furthermore, the data between the drained and undrained silt showed significant behavioural difference, thus separate definitions were needed to be sought.

With inspiration from Matlock [1970], the soil pressure,  $p$ , was normalised to the ultimate soil pressure,  $p_u$ , while the displacement,  $y$ , was normalised to the diameter of the bucket,  $D$ , with inspiration from Østergaard et al. [2015]. This was done for both the drained and undrained models, which gave acceptable results. Afterwards the ultimate soil pressure was defined, where it was shown to be governed by  $\sigma'_{v0}/(\phi/D)$  for the drained silt and by  $\sigma'_{v0}/(c_u/D)$  for the undrained silt.

With inspiration from Østergaard et al. [2015] and Matlock [1970] the mathematical expression, which describes the p-y curves, was defined. As the p-y curves for the drained silt rose to the ultimate soil pressure non-linearly and ending at a plateau, only one interval for the formulation was needed. The undrained silt on the other hand needed implementation of two intervals, due to its more complex p-y curves. The undrained silt also rose to the ultimate soil pressure non-linearly, but from the peak value it decreased in soil pressure. Therefore, until the peak the curve was formulated in the same manner as the drained silt, but from the peak until the end, the curve was formulated by a linear decreasing expression. The developed p-y curves and formulations are given graphically in Figure 7.1.

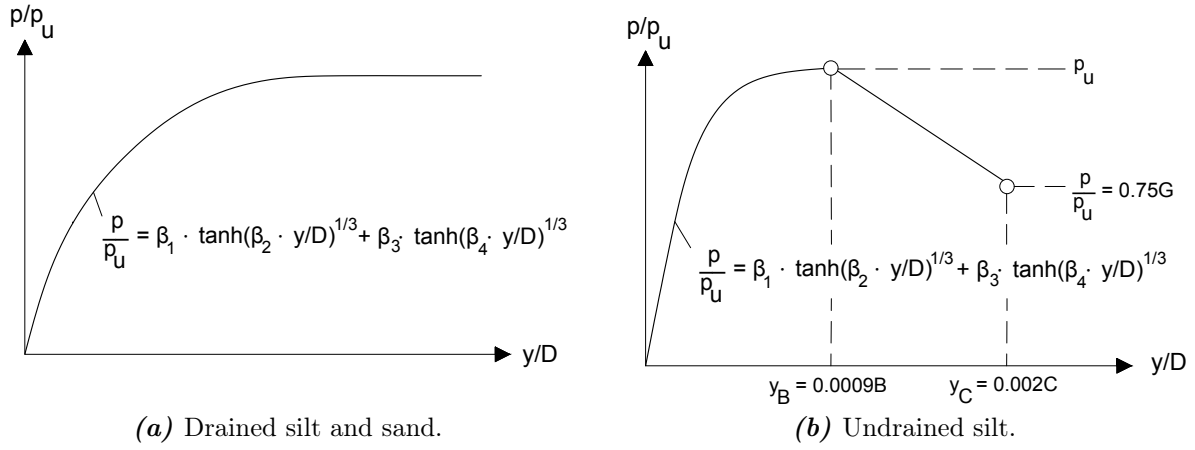


**Figure 7.1:** Principle of developed p-y curves for bucket foundations.

Since Østergaard et al. [2015] made a similar study of buckets in drained sand, and due to the availability of the data, a redefinition of the p-y curve for sand was sought in a similar expression as the silt. Compared to the original p-y formulation from Østergaard et al. [2015], the big difference in the redefined p-y formulation was found in the normalisation of the p-y curves and definition of model parameters. The soil pressure was normalised to the ultimate soil pressure instead of the Rankine pressure, which showed better results. Furthermore, the model parameters,  $\beta_1-4$ , for both the silt and sand were defined to be governed by soil stiffness instead of the friction angle, as Vahdatirad et al. [2016] concluded, the imprecise load-displacement estimations were due to the model parameters defined by Østergaard et al. [2015]. Hence the developed p-y formulations are more versatile, as they can capture soils, where the strength parameters are the same, but where the stiffnesses are different. This is also seen in Figure 7.2, where the p-y formulation developed by Østergaard et al. [2015] does not capture such cases.

The developed p-y formulations for silt and sand are governed by the diameter of the bucket, vertical effective in-situ stress, soil stiffness, and the friction angle (for drained silt and sand) or the undrained shear strength (for undrained silt). The objective was to define precise and practically applicable p-y formulations, which is considered successfully achieved, as the governing parameters are simple to derive, and the p-y formulations provide fairly precise estimations.

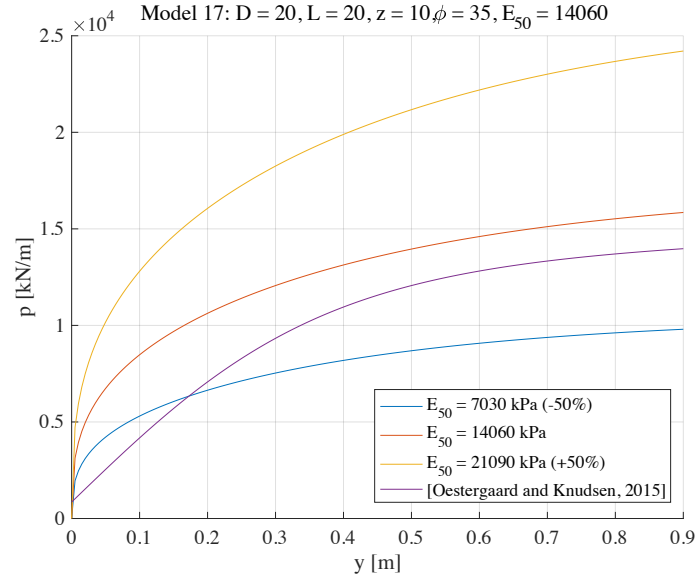


**Figure 7.2:** Changing only the soil stiffness  $\pm 50\%$  for the developed p-y formulation and the formulation developed by Østergaard et al. [2015] for Model 17.

### Further Work

Even though the aim of the study is met, an important acknowledgement is, that the new p-y formulations are only developed from a small number of models. The range of their validation has to be extensively studied with use of various combinations of the soil and bucket, before the formulation can be implemented in design tools. Therefore, if further work in continuation of this study is made, and the formulations in general are valid, a favourable element would be to decrease or express the constants in relation to one or a combination of basic parameters - similar to the constants  $C_{1-3}$  in Det Norske Veritas [2013]. Additionally, it would be interesting to study the validity of the formulation for clay, hence it might be possible to have the same formulation valid for silt, sand and clay.

The comparison between an analytical calculation and results obtained from a field test in Vahdatirad et al. [2016] can be made with the developed formulation for sand, to evaluate if the implementation of soil stiffness leads to more precise estimations of the soil pressure. Furthermore, it would be favourable to conduct a similar field test in silt and an analytical calculation to compare and evaluate the precision of the p-y formulation for silt.

It is not only universities, which tries to be on the forefront of the knowledge within the field. Some of the big industry market leaders are trying to reduce costs by examining the soil-structure interaction for big diameter piles by physical tests. In a joint industry project called PISA, a group of companies and universities have conducted several numbers of large scale tests of monopiles on onshore locations with different soil conditions. The test data should lead to vital knowledge about the soil-structure interaction and in more cost-efficient designs to benefit all partners in the project. It will be exciting to follow the outcome of the PISA project, and compare it to the results and conclusion obtained from this study and to any further work made in continuation of this thesis.



# Bibliography

---

- Achmus et al., 2016.** Martin Achmus, Mauricio Terceros and Klaus Thieken. *Evaluation of p-y Approaches for Large Diameter Monopiles in Soft Clay*. ISBN: 978-1-880653-88-3. International Society of Offshore and Polar Engineers, 2016.
- Andersen and Schjetne, 2013.** Knut H. Andersen and Knut Schjetne. *Database of Friction Angles of Sand and Consolidation Characteristics of Sand, Silt, and Clay*. American Society of Civil Engineers, 2013.
- Appendix Folder.** *Appendix Folder*. Main folder containing appendices.
- Brinkgreve et al., 2015.** R.B.J. Brinkgreve, S. Kumarswamy and W.M. Swolfs. *PLAXIS 3D Anniversary Edition*. ISBN-13: 978-90-76016-21-4. PLAXIS bv, 2015.
- Cox et al., 1974.** W. R. Cox, L. C. Reese and B. R. Grubbs. *Field Testing of Laterally Loaded Piles in Sand*. 1974. Proceedings of the Sixth Annual Offshore Technology Conference, Houston, Texas, paper no. OTC 2079.
- Det Norske Veritas, 2013.** Det Norske Veritas. *Design of Offshore Wind Turbines*. Det Norske Veritas AS, 2013.
- Det Norske Veritas, 1992.** Det Norske Veritas. *Foundations - Classification Notes No. 30.4*. Det Norske Veritas AS, 1992.
- DONG Energy, 2015.** DONG Energy. *Largest ever testing of wind turbine piles completed*, 2015. URL <http://www.dongenergy.com/en/media/newsroom/news/articles/largest-ever-testing-of-wind-turbine-piles-completed>. seen: 29.04.2017.
- DWIA and Offshoreenergy.dk, 2015.** DWIA and Offshoreenergy.dk. *Offshore Wind Denmark – A United Industry Thinking Big*, 2015. DWAI: Danish Wind Industry Association.
- Energistyrelsen, 2016.** Energistyrelsen. *Energistatistik 2015*, 2016. URL <https://ens.dk/sites/ens.dk/files/Statistik/energistatistik2015.pdf>. seen: 24.12.2016.
- Ibsen et al., 2005.** Lars Bo Ibsen, Morten Liingaard and Søren A. Nielsen. *Bucket Foundation, a status*, 2005. Copenhagen Offshore Wind Conference, Copenhagen, Denmark, 26-29 October 2005.
- Jensen et al., 2015.** Bjarne Chr. Jensen, Gunner Mohr, Asta Nicolajsen, Bo Mortensen, Henrik Bygbjerg, Lars Pilegaard Hansen, Hans Jørgen Larsen, Svend Ole Hansen, Dirch H. Bager, Eilif Svensson, Ejnar Søndergaard, Carsten Munk Plum, Hilmer Riberholt, Lars Zenke Hansen, Kaare K. B. Dahl, Henning Larsen, Per Goltermann, Jørgen S. Steenfelt, Carsten S. Sørensen and Werner Bai. *Teknisk Ståbi*. ISBN: 978-87-571-2844-4, 23rd edition. Praxis - Nyt Teknisk Forlag, 2015.
- Kramer, 1988.** Steven L. Kramer. *Development of p-y curves for analysis of laterally loaded piles in western Washington*. Washington State Department of Transportation, 1988.

- Matlock, 1970.** Hudson Matlock. *Correlation for Design of Laterally Loaded Piles in Soft Clays*. ISBN: 978-1-55563-709-5. Offshore Technology Conference, 1970.
- Recharge News, 2014.** Recharge News. *UK to test offshore 'suction bucket'*, 2014. URL <http://www.rechargenews.com/wind/article1365315.ece>. seen: 12.10.2016.
- Sullivan et al., 1980.** W. R. Sullivan, L. C. Reese and C. W. Fenske. *17. Unified method for analysis of laterally loaded piles in clay*. 1980. in Numerical methods in offshore piling, The Institution of Civil Engineers, pp. 135-146.
- Thieken et al., 2015.** Klaus Thieken, Martin Achmus and Katrin Lemke. *A new static p-y approach for piles with arbitrary dimensions in sand*. 2015. in Geotechnik, vol. 38, issue 4, Ernst and Sohn Verlag, pp. 267-288.
- Vahdatirad et al., 2016.** Mohammadjavad Vahdatirad, Alberto Troya Diaz, Lars Bo Ibsen, Lars Vabbersgaard Andersen, Sarah Firouzianbandpey and D. V. Griffiths. *A load-displacement based approach to assess the bearing capacity and deformations of mono-bucket foundations*. 2016. in A Zingoni (ed.), Insights and Innovations in Structural Engineering, Mechanics and Computation: proceedings of the sixth international conference on structural engineering, mechanics and computation, Cape Town, South Africa, 5-7 September 2016. C R C Press LLC, pp. 749-750.
- Wolf et al., 2013.** Torben Kirk Wolf, Kristian Lange Rasmussen, Mette Hansen, Hanne Ravn Roesen and Lars Bo Ibsen. *Assessment of p-y Curves from Numerical Methods for a Non-Slender Monopile in Cohesionless Soil*. 2013. in The Proceedings of the Twenty-third (2013) International Offshore and Polar Engineering Conference. vol. 2, International Society of Offshore and Polar Engineers, pp. 436-443. International Offshore and Polar Engineering Conference.
- Østergaard et al., 2015.** Martin Underlin Østergaard, Bjørn Stagthøj Knudsen and Lars Bo Ibsen. *P-y curves for bucket foundations in sand using finite element modeling*. 2015. in V. Meyer (ed.), Frontiers in Offshore Geotechnics III proceedings of the third international symposium on frontiers in offshore geotechnics (isfog 2015), Oslo, Norway, 10-12 June 2015. vol. 1, C R C Press LLC, London, pp. 343-348.



# **Determination of p-y Curves for Bucket Foundations in Silt and Sand Using Finite Element Modelling**

**Vinojan Vethanayagam  
Lars Bo Ibsen**



Aalborg University  
Department of Civil Engineering

**DCE Technical Memorandum No. 64**

# **Determination of p-y Curves for Bucket Foundations in Silt and Sand Using Finite Element Modelling**

by

Vinojan Vethanayagam  
Lars Bo Ibsen

June 2017

© Aalborg University

## Scientific Publications at the Department of Civil Engineering

**Technical Reports** are published for timely dissemination of research results and scientific work carried out at the Department of Civil Engineering (DCE) at Aalborg University. This medium allows publication of more detailed explanations and results than typically allowed in scientific journals.

**Technical Memoranda** are produced to enable the preliminary dissemination of scientific work by the personnel of the DCE where such release is deemed to be appropriate. Documents of this kind may be incomplete or temporary versions of papers—or part of continuing work. This should be kept in mind when references are given to publications of this kind.

**Contract Reports** are produced to report scientific work carried out under contract. Publications of this kind contain confidential matter and are reserved for the sponsors and the DCE. Therefore, Contract Reports are generally not available for public circulation.

**Lecture Notes** contain material produced by the lecturers at the DCE for educational purposes. This may be scientific notes, lecture books, example problems or manuals for laboratory work, or computer programs developed at the DCE.

**Theses** are monographs or collections of papers published to report the scientific work carried out at the DCE to obtain a degree as either PhD or Doctor of Technology. The thesis is publicly available after the defence of the degree.

**Latest News** is published to enable rapid communication of information about scientific work carried out at the DCE. This includes the status of research projects, developments in the laboratories, information about collaborative work and recent research results.

Published 2017 by  
Aalborg University  
Department of Civil Engineering  
Thomas Manns Vej 23,  
DK-9220 Aalborg SV, Denmark

Printed in Aalborg at Aalborg University

ISSN 1901-7278  
DCE Technical Memorandum No. 64

# Determination of p-y Curves for Bucket Foundations in Silt and Sand Using Finite Element Modelling

Vinojan Vethanayagam<sup>1</sup> Lars Bo Ibsen<sup>2</sup>

Department of Civil Engineering, Aalborg University

## Abstract

Design of offshore wind turbine foundations are today based on analytical formulas, which describes the link between a displacement,  $y$ , and the associated soil pressure,  $p$ . The formulas are empirically developed on slender piles with a slenderness ratio  $L/D > 30$ , but foundations of today are less slender than the tested piles. The suction bucket has a slenderness ratio of 0.5-1, thus its response is a rigid movement, where slender piles undergoes a flexible movement. Due to the importance of precise estimations, p-y formulations for suction buckets in drained and undrained silt are sought developed with use of finite element. In general the developed p-y formulations for the drained and undrained silt are fairly precise. Furthermore, the same method and basic formulation of the drained silt is applied to data of the drained sand from Østergaard et al. [2015]. The developed formulation herefore shows to be more versatile and precise than the formulation suggested by Østergaard et al. [2015]. The developed p-y formulations are functions of the effective vertical in-situ stress, soil stiffness, diameter of the bucket and the internal friction angle/the undrained shear strength.

## 1 Introduction

The empirically developed p-y curves are the analytical design tool for offshore foundations of today, which are recommended by the offshore design code, Det Norske Veritas [2013]. The piles used in the conducted field tests were small-diameter piles, which had slenderness ratios of  $L/D > 30$ . Matlock [1970] developed the suggested p-y curves for piles in clay by conducting tests in Lake Austin, USA with use of piles with  $L = 12.8$  m and  $D = 0.32$  m, while p-y curves for sand were formulated by Cox et al. [1974], where the tests were conducted at Mustang Island, USA with  $L = 21$  m and  $D = 0.61$  m piles.

Since the p-y curves were developed from small-diameter and slender piles, problems are introduced, when they are used to design foundations for wind turbines of today. Wind turbines gets bigger to cut the costs, thereby the foundations are also becoming bigger, hence the slenderness ratios are far less than piles from Matlock [1970] and Cox et al. [1974]. Monopiles and suction buckets are two foundations type, which are used offshore, and they behave significantly different from slender piles, as  $L/D \approx 5$  and 0.5-1 respectively. As seen in Figure 1, slender piles, such as the piles from Matlock [1970] and Cox et al. [1974], have a flexible response, while less slender piles, such as a monopile or suction bucket, have a more rigid response. Therefore, the p-y curves suggested in Det Norske Veritas [2013] are not precise, and it is possible to cut costs by introducing p-y curves valid for non-slender piles such as monopiles and

suction buckets.

Thieken et al. [2015] modelled monopiles in sand using finite element, from which the soil-structure interaction were simulated. Hence it was possible to develop p-y curves valid for monopiles in sand. Achmus et al. [2016] made a similar study for clay, where the p-y curves have not yet been developed, but are sought in a similar manner as in Thieken et al. [2015].

Even though monopiles and suction buckets both are considered non-slender piles, the slenderness ratio is significantly different. Thus, it would be favourable to develop p-y curves for suction buckets using finite element as well. Østergaard et al. [2015] studied suction buckets in drained sand with use of finite element, and developed a p-y formulation, which estimates the soil pressure fairly well.

In continuation of Østergaard et al. [2015], this article will develop p-y curves for suction buckets in drained and undrained silt using finite element by modelling a number of numerical models to simulate the soil-structure interaction. The formulation has to be simple and practically applicable without comprising on the precision. As it is in continuation of Østergaard et al. [2015], the formulation are sought to be similar in many senses. However, some elements of the formulation will be different, as Vahdatirad et al. [2016] used the formulation by Østergaard et al. [2015] in an analytical calculation, which were compared to data from a field test of a suction bucket. Here it was seen, that the small-strain response of the analytical model was softer than obtained in field test. Vahdatirad et al. [2016] concluded, it might be caused by the model parameters,  $\beta_{1-4}$ , which control the shape of the load-displacement response. Thus, this

<sup>1</sup>M.Sc. Student, Department of Civil Engineering, Aalborg University, Denmark

<sup>2</sup>Professor, Department of Civil Engineering, Aalborg University, Denmark

article will implement the soil stiffness as a governing parameter for the model parameters instead of the friction angle.

Since the data from Østergaard et al. [2015] is available, and it is assumed, that the model parameters cause imprecise predictions of the soil pressure, the p-y formulation for suction buckets in drained sand will be reconsidered in this article by developing a formulation similar to the silt.

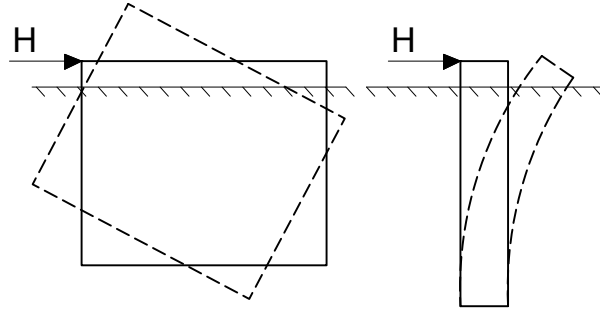


Figure 1: Response of non-slender and slender pile to a horizontal load.

## 2 Material Model

The numerical models will be defined with the use of the Hardening Soil Small Strain (HSsmall) material model. The HSsmall model is a sophisticated material model due to its interpretation capabilities of advanced soil behaviour. It takes hardening into account as the stiffness moduli are stress-dependent, thus value for each stiffness moduli are given at a reference pressure at  $p^{ref} = 100$  kPa. The stiffness moduli in the HSsmall model changes according to the current stress-state of the soil with use of a power law with the exponent  $m$ , and they are given in Eq. (1). Furthermore, the material model also take the additional stiffness at small strains into account, hence the model is capable of simulating real-life behaviour of the soil-structure interaction relatively well.

$$\begin{aligned} E_{oed} &= E_{oed}^{ref} \cdot \left( \frac{c \cdot \cos \phi + \sigma'_1 \cdot \sin \phi}{c \cdot \cos \phi + p^{ref} \cdot \sin \phi} \right)^m \\ E_{50} &= E_{50}^{ref} \cdot \left( \frac{c \cdot \cos \phi + \sigma'_3 \cdot \sin \phi}{c \cdot \cos \phi + p^{ref} \cdot \sin \phi} \right)^m \\ E_{ur} &= E_{ur}^{ref} \cdot \left( \frac{c \cdot \cos \phi + \sigma'_3 \cdot \sin \phi}{c \cdot \cos \phi + p^{ref} \cdot \sin \phi} \right)^m \\ G_0 &= G_0^{ref} \cdot \left( \frac{c \cdot \cos \phi + \sigma'_3 \cdot \sin \phi}{c \cdot \cos \phi + p^{ref} \cdot \sin \phi} \right)^m \end{aligned} \quad (1)$$

The calculation time is considered high, when using the HSsmall model, due to its advanced interpretation capabilities. Nevertheless, the material model allows to both take hardening of the soil and the small strain stiffness into account, which are considered utmost important to find the link between displacement,  $y$ , and the associated soil pressure,  $p$ . Thus the extra calculation time is well spend.

## 3 Determination of Input Parameters

As both drained and undrained silt are considered in the study, the modelling of the numerical models are different between these two types. The drained models are simply modelled as drained, where both strength and stiffness parameters are defined effective. On the other hand, the stiffness parameters are effective, while strength parameters are total for the undrained models, as they are modelled with use of Undrained (B) as in Achmus et al. [2016], which allows to define the undrained shear strength,  $c_u$ , as an input parameter.

The input parameters for the numerical models are given in Table 2, where two types of silts are used and denoted as soft and stiff silt. To model the silt with the HSsmall material model,  $G_0$  and  $\gamma_{0.7}$  have to be determined, furthermore the  $c_u$  for the soft and stiff silt has to be defined as well.

### 3.1 Determination of Shear Modulus and Threshold Shear Strain

$G_0$  and  $\gamma_{0.7}$  are found with use of Det Norske Veritas [1992], where a relation between the modulus no.,  $m$ , and the porosity,  $n$ , is given, where  $m$  is defined in intervals of:

Loose:	$m = 40 - 60$
Medium:	$m = 60 - 80$
Dense:	$m > 80$

With use of the above-mentioned intervals and the relation given in Figure 2,  $G_0$  and  $\gamma_{0.7}$  are obtained by Eq. (2) from Brinkgreve et al. [2015].

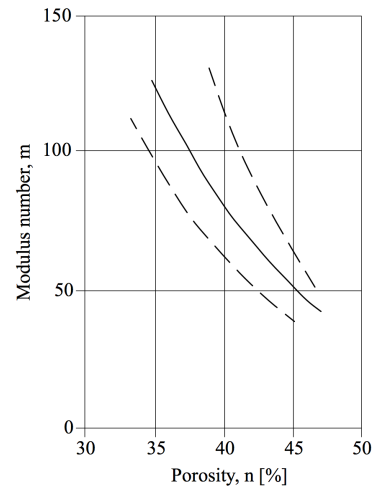


Figure 2: Relation between modulus no.,  $m$ , and porosity,  $n$ , [Det Norske Veritas, 1992, Fig. 5.9, Sec. 5.3.3.8].

$$\begin{aligned} G_0^{ref} &= 33 \cdot \frac{(2.97 - e)^2}{1 + e} \\ \gamma_{0.7} &= \frac{2c' (1 + \cos(2\phi')) - \sigma'_1 (1 + K_0) \sin(2\phi)}{9G_0} \end{aligned} \quad (2)$$

### 3.2 Determination of Undrained Shear Strength

In PLAXIS it is possible to perform undrained triaxial tests with a soil defined with effective strength and stiffness parameters. Thus, the SHANSEP method is used to determine  $c_u$ .

The SHANSEP formula is given in Eq. (3), where  $(c_u/\sigma'_1)_{nc}$  is the only unknown part of the equation. It is obtained by performing consolidated undrained (CU) triaxial tests at different values of OCR. Since the consolidation phase of the triaxial tests is performed with  $K_0$ -consolidation,  $\Lambda$  is set to 0.8, as recommended by Jensen et al. [2015]. Results from all the triaxial tests is shown in Table 1.

$$\left(\frac{c_u}{\sigma'_1}\right)_{oc} = \left(\frac{c_u}{\sigma'_1}\right)_{nc} \cdot OCR^\Lambda \quad (3)$$

The necessary input parameters, which are needed to define the soft and stiff silt as drained and undrained HSs-small materials, are given in Table 2.

Table 1: Triaxial test results.

Stiff silt			
OCR	$\sigma'_{1,nc}$	$\sigma'_{3,nc}$	$c_{u,nc}$
[-]	[kPa]	[kPa]	[kPa]
1.0	1080	497	448
1.4	1512	696	624
2.0	2160	994	885
4.0	4320	1987	1750
Average of $(c_u/\sigma'_1)_{nc} = 0.41$			
Soft silt			
1.0	80	42	31
1.4	112	58	43
2.0	160	83	60
4.0	320	166	120
Average of $(c_u/\sigma'_1)_{nc} = 0.38$			

Table 2: Strength and stiffness parameters for the soft and stiff soil.

Silt type		Soft	Stiff
$c_u$	[kPa]	56	475
$\phi'$	[°]	29	33
$\psi$	[°]	0	3
$c'$	[kPa]	1	15
$E_{50}$	[MPa]	3.8	10.2
$E_{oed}$	[MPa]	5	14
$E_{ur}$	[MPa]	11.4	30.6
$m$	[-]	0.5	0.5
$\gamma_{0.7}$	[mm/m]	0.19	0.19
$\nu$	[-]	0.29	0.26
$G_0$	[MPa]	77.8	102.4
$K_0$	[-]	0.52	0.46

## 4 Numerical Modelling

PLAXIS 3D AE is used to compute p-y curves for silt. In total three parameters are changed; drainage type, silt type and diameter of the bucket. The length of the bucket

is set to  $L/D = 1$ . Thereby a total of 12 numerical models are studied, cf. Table 3.

Table 3: Model overview.

Model no.	Drainage type	D and L [m]	Silt type
1	Drained	10	Soft
2	Drained	15	Soft
3	Drained	20	Soft
4	Drained	10	Stiff
5	Drained	15	Stiff
6	Drained	20	Stiff
7	Undrained	10	Soft
8	Undrained	15	Soft
9	Undrained	20	Soft
10	Undrained	10	Stiff
11	Undrained	15	Stiff
12	Undrained	20	Stiff

### 4.1 Mesh and Model Domain

Correct interpretation of the soil-structure interaction is important, thus interfaces are defined for the bucket, as suggested by both Wolf et al. [2013] and Brinkgreve et al. [2015]. Extended interfaces are needed to be defined for the bottom of the bucket skirt, as recommended by Brinkgreve et al. [2015], as stress concentrations can occur around corners.

A proximity volume, which encloses the bucket is defined, as Østergaard et al. [2015] did. The volume can be given a different mesh density than the rest of the model, as the most intensive shearing occurs closest to the bucket, thereby optimising the calculation time. The mesh density is determined from a convergence analysis, where it is concluded to set the overall coarseness to *medium* and the refinement factor of the proximity volume to *0.16*. From Figure 3 it is possible to see the significant difference in mesh density between the proximity volume and remaining soil volume.

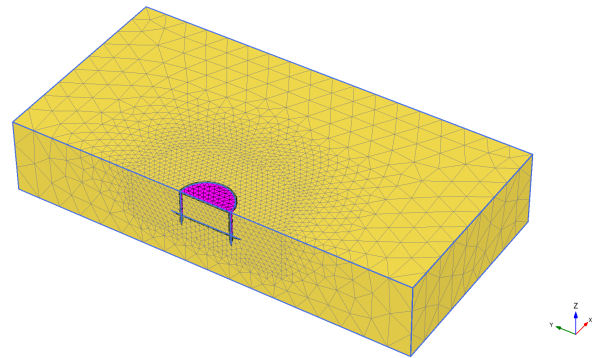


Figure 3: Meshed model.

The size of the model domain is determined from a model domain analysis, as the criteria is, that stresses cannot have a significant affect at the edges. The size of the model domain normalised to the geometry of the

bucket is shown in Figure 4, where the size of the bucket and extended interfaces are shown as well.

#### 4.2 Modelling of Suction Bucket

The thickness of the bucket and Young's modulus is set to 0.3 m and 600.000 MPa, which is considered enough to avoid deflection of the bucket, as only soil response is of interest.

The foundation of a wind turbine is in reality loaded with a horizontal and moment load, which results in rotation of the foundation. Wolf et al. [2013] showed, that calculation complexities arise due to rotation points, which differs from load case to load case. Instead Wolf et al. [2013] suggest the use of a total lateral loading, when examining p-y curves, as only lateral displacements and the associated soil pressure is of interest. Therefore, the models will only be applied with a horizontal displacement with the use of the prescribed displacement function in PLAXIS. Furthermore, only half of the bucket is modelled due to symmetry of geometrical and load conditions, thereby saving calculation time.

#### 4.3 Calculation Phases

The numerical models have five basic calculation phases: The first phase is the *initial phase* (Phase 0), where the initial stress-state of the soil is set with a  $K_0$ -procedure. Thereafter the structure is installed in the soil (Phase 1). As the installation can cause displacements, they are reset (Phase 3). Afterwards the bucket is displaced in the amount of the prescribed displacement (Phase 4). Lastly the bucket is unloaded (Phase 5). The two latter phases are repeated with increasing displacement for each load step, until the soil fails or the maximum prescribed displacement is reached.

#### 4.4 Data Extraction and Integration of Stresses

The displacements,  $y$ , are extracted from the unloading phases, as the plastic deformation is wanted. This can directly be extracted from PLAXIS, while it is not possible to directly extract the soil pressure,  $p$ . The data is instead given as stresses, thus they have to be integrated over an area to obtain the soil pressure. The stresses are extracted from the load phases.

The stresses can either be extracted from the soil elements, or the interface elements defined between the soil and skirt. The latter is used for extraction of stresses, as Wolf et al. [2013] analysed the precision of the different extraction methods, where stresses from the interface elements provided the most precise results.

When the bucket is laterally displaced, the soil moves laterally, thus occurrence of a normal stress,  $\sigma'_N$ , and a shearing stress,  $\tau_1$ , working around the pile, arise, cf. Figure 5. The figure also shows the occurrence of a second shear stress,  $\tau_2$ , which works vertically along the

skirt, but it is disregarded, as only the lateral soil pressure is of interest. Hence, the soil pressure is calculated by integration of  $\sigma'_N$  and  $\tau_1$ , as shown in Eq. (4).

$$\int_A = (\sigma'_N \sin \theta + \tau_1 \cos \theta) dA \quad (4)$$

The bucket skirt is divided into a number of horizontal slices, which describes a depth layer, and vertical slices, hence multiple areas are defined, cf. Figure 6. The stresses within each of the areas, e.g. the black marked area in Figure 6, are averaged and multiplied by the area. Lastly all areas within the same layer (horizontal slice) are summed and divided by the height of the layer to obtain the soil pressure,  $p$ .

### 5 Formulation of p-y Curves for Silt

To develop p-y curves for silt, four steps are taken:

1. Plot of p-y curves from the numerical models, where the data is trimmed for edge effects.
2. Normalise the soil pressure,  $p$ , and the displacement,  $y$ , with the ultimate soil pressure,  $p_u$  and diameter of the bucket,  $D$ , respectively.
3. Fitting of FE data to a mathematical function.
4. Define a p-y formulation based on the normalisation and fitted function.

#### 5.1 Step 1: Plot for p-y Curves

Figure 7 and 8 show the plot of the p-y curves for Model 5 and 11 respectively. Each curve refers to a depth,  $z$ , which is defined as the middle of each layer. Furthermore, there is significant difference between the drained and undrained behaviour. All the drained models reaches a plateau in the end, while all undrained models reaches a peak in soil pressure before it drops for further displacement. Due to the behavioural difference, the drained and undrained models will be processed separately.

#### 5.2 Step 2: Normalisation of p-y Curves

The displacement is normalised to the diameter of the bucket,  $D$ . As seen from Figure 7 and 8 the soil pressure increases with the depth, thus the normalisation should make the curves depth-independent. It is achieved by normalising the soil pressure to the ultimate soil pressure,  $p_u$ . As seen in Figure 9 and 10 the depth-dependency is eliminated, as the p-y curves more or less merge into one single curve.

##### 5.2.1 Formulation of Ultimate Soil Pressure

An analysis of the FE data is performed to determine a formulation for  $p_u$ . As the drained and undrained silt



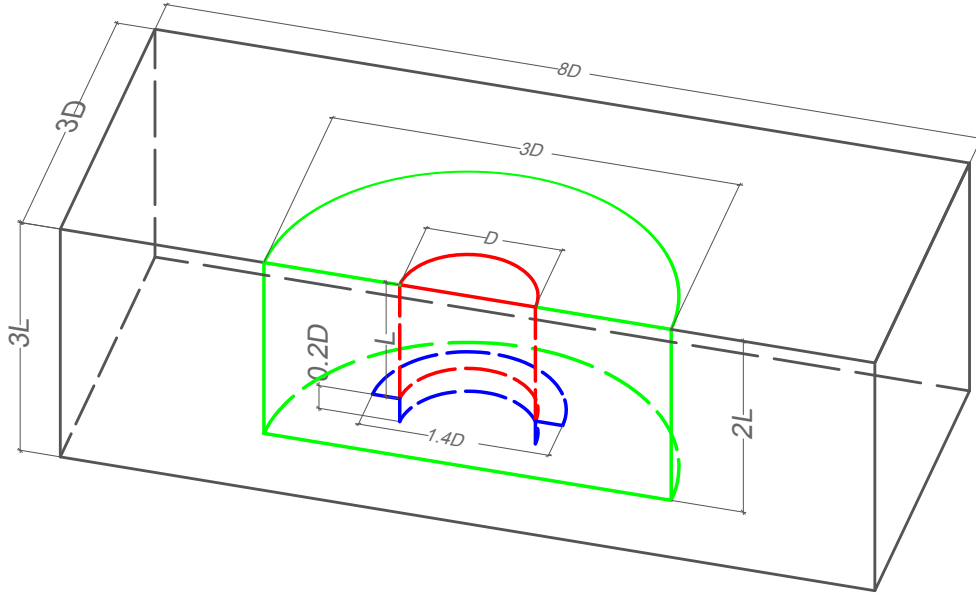


Figure 4: Overall model geometry normalised to the bucket diameter and length. Indication of line colors: black: soil contour/model domain, green: proximity volume with refined mesh, blue: interface extension and red: suction bucket [Østergaard et al., 2015].

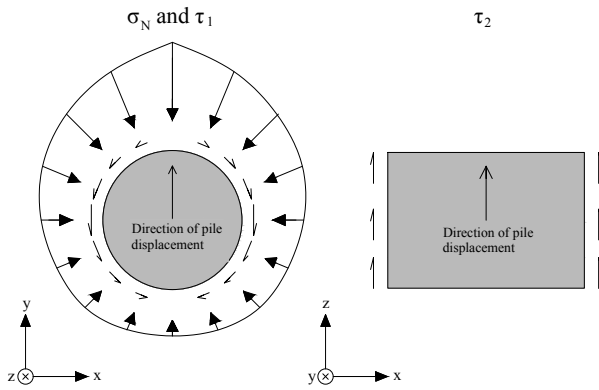


Figure 5: Displacement of pile in y- and z-direction with associating stresses working along the skirt of the suction bucket.

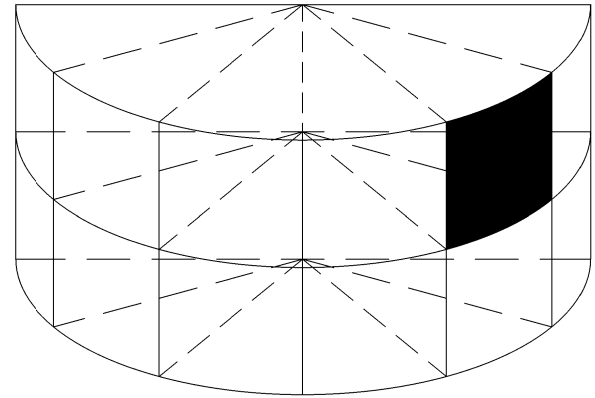


Figure 6: Principle of horizontal and vertical division of the bucket to define integration areas [Østergaard et al., 2015].

are separately processed, formulation will be different as well.

#### Drained Silt

From the analysis of the drained silt, a good correlation between the values of  $p_u$  and  $\sigma'_{v0}/(\phi/D)$  is obtained, as seen in Figure 11. The formulation of  $p_u$  is given in Eq. (5).

$$p_u = \left( 124 \cdot \frac{\sigma'_{v0}}{\phi/D} + 2805 \right) \cdot A \quad (5)$$

Where

$$A = \begin{cases} 0.15 & \text{for soft silt} \\ 1 & \text{for stiff silt} \end{cases}$$

#### Undrained Silt

The approach to define the  $p_u$  for the drained silt is used for the undrained silt as well. The only difference is the

correlation, as it is taken between  $p_u$  and  $\sigma'_{v0}/(c_u/D)$ . The analysis shows good correlation, hence the formulation of the ultimate soil pressure for the undrained silt is defined as in Eq. (6).

$$p_u = \left( 493 \cdot \frac{\sigma'_{v0}}{c_u/D} + 1843 \right) \cdot A \quad (6)$$

where  $A$  is equal to 0.15 and 1 for soft and stiff silt respectively, as for the drained silt.

#### 5.3 Step 3: Fitting of FE data to a Mathematical Formulation

The objective of the third step is to firstly define a mathematical formulation, which describes the normalised p-y curve. The formulation contains model parameters, which afterwards are iterated to fit the normalised p-y curve as well as possible (best fit). The model parameters are free to attain any value.

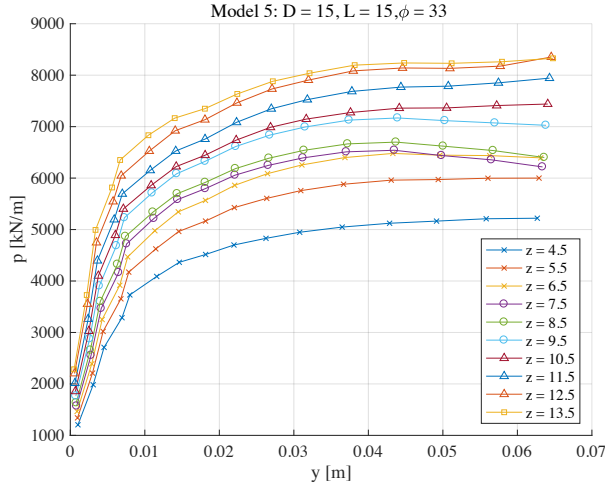


Figure 7: Step 1: Plot of p-y curve for Model 5 with trimmed data.

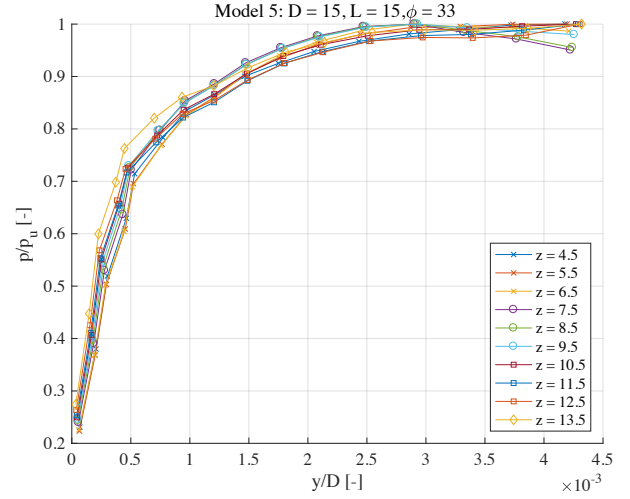


Figure 9: Step 2: Normalised Model 5.

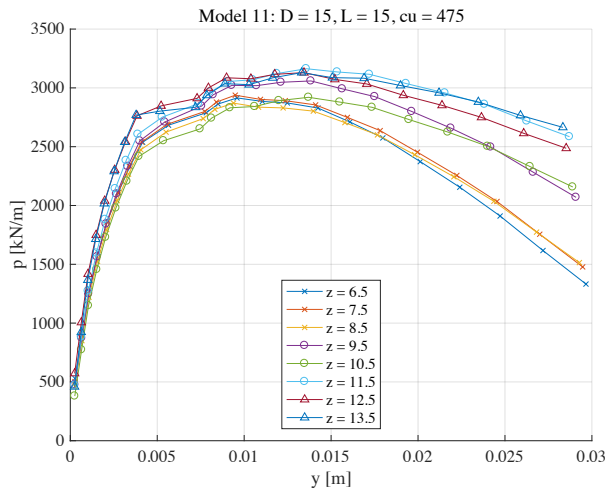


Figure 8: Step 1: Plot of p-y curve for Model 11 with trimmed data.

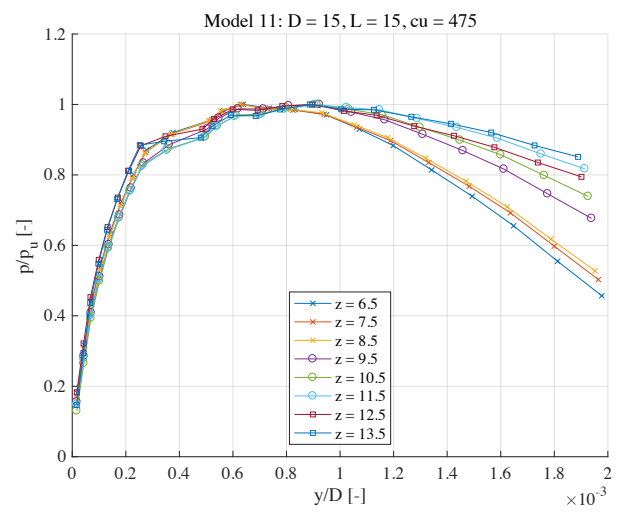


Figure 10: Step 2: Normalised Model 11.

### 5.3.1 Fitting of Drained Silt

The mathematical formulation used to describe the drained silt is given in Eq. (7).  $\beta_{1-4}$  are the model parameters, which are iterated to find the best fit of the normalised FE data. The plot of the best fit for Model 5 is seen in Figure 12.

$$\frac{p}{p_u} = \beta_1 \tanh\left(\beta_2 \frac{y}{D}\right)^{1/3} + \beta_3 \tanh\left(\beta_4 \frac{y}{D}\right)^{1/3} \quad (7)$$

### 5.3.2 Fitting of Undrained Silt

Due to the behaviour of the undrained silt, the p-y formulation is defined differently than for the drained silt, as it is defined in two parts; first part is defined similar to the drained silt, while the second part is defined as a linearly decreasing function, cf. Figure 13. The plot of the best fit for Model 11 is shown in Figure 14, while the intervals and mathematical formulation are defined as:

$$\begin{aligned} 0 \leq y/D < y_B = 0.0009B \\ y_B \leq y/D < y_C = 0.002C \end{aligned} \quad (8)$$

$$\begin{aligned} \frac{p}{p_u} \left( \frac{y}{D} < y_B \right) &= \beta_1 \tanh\left(\beta_2 \frac{y}{D}\right)^{1/3} \\ &+ \beta_3 \tanh\left(\beta_4 \frac{y}{D}\right)^{1/3} \end{aligned} \quad (9)$$

$$\begin{aligned} \frac{p}{p_u} \left( \frac{y}{D} = y_B \right) &= \beta_1 \tanh(\beta_2 y_B)^{1/3} \\ &+ \beta_3 \tanh(\beta_4 y_B)^{1/3} \end{aligned} \quad (10)$$

$$\frac{p}{p_u} \left( \frac{y}{D} = y_C \right) = 0.75G \quad (11)$$

where

$$\begin{aligned} B &= \begin{cases} 0.4 & \text{for soft soil} \\ 1 & \text{for stiff soil} \end{cases} \\ C &= \begin{cases} 0.65 & \text{for soft soil} \\ 1 & \text{for stiff soil} \end{cases} \\ G &= \begin{cases} 0.75 & \text{for soft soil} \\ 1 & \text{for stiff soil} \end{cases} \end{aligned}$$

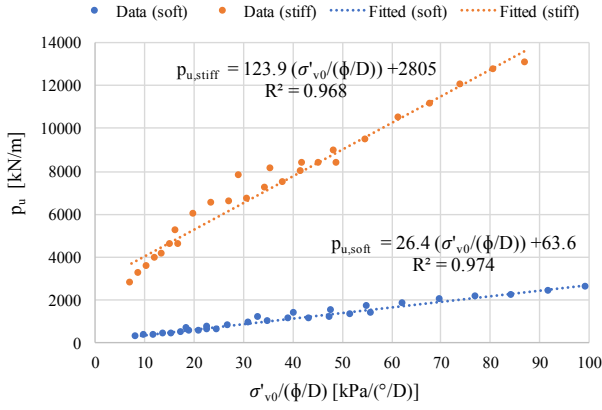
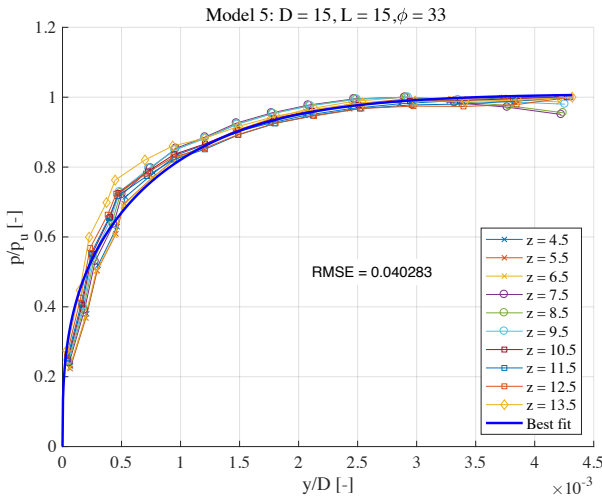
Figure 11: Correlation between  $p_u$  and  $\sigma'_{v0}/(\phi/D)$  for drained silt.

Figure 12: Step 3: Best fit of Model 5 compared to the normalised FE data.

#### 5.4 Step 4: Definition of New p-y Formulation

The only missing part is the formulations for the model parameters,  $\beta_{1-4}$ , as they for the best fit analysis could attain any value. They are sought defined in relation to the soil stiffness, as Vahdatirad et al. [2016] concluded the imprecision in load-displacement estimations were caused by the model parameters, which were defined in relation to the friction angle by Østergaard et al. [2015].

##### 5.4.1 Formulation of Model Parameters for Drained Silt

The value of the model parameters from the best fit analysis is plotted against  $E_{50}D$ , cf. Figure 15-18. In conclusion, the model parameters for the drained silt are defined in Eq. (12).

$$\begin{aligned}\beta_1 &= 2.2 \cdot 10^{-7} \cdot (E_{50}D) + 0.52 \\ \beta_2 &= 5.97 \cdot 10^{-7} \cdot (E_{50}D)^2 - 0.21E_{50}D + 1.83 \cdot 10^4 \\ \beta_3 &= 0.45 \\ \beta_4 &= 7.81 \cdot 10^{10} \cdot (E_{50}D)^{-1.55}\end{aligned}\quad (12)$$

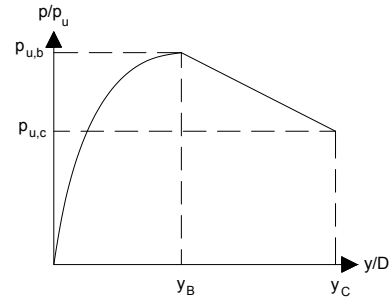


Figure 13: Principle division of p-y curve for undrained silt.

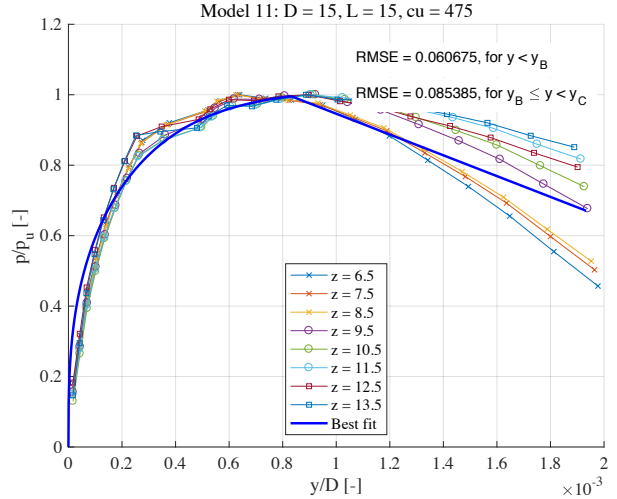


Figure 14: Step 3: Best fit of Model 11 compared to the normalised FE data.

#### 5.4.2 Formulation of Model Parameters for Undrained Silt

The model parameters for the undrained silt, given in Eq. (13), are obtained in the same way as for the drained silt.

$$\begin{aligned}\beta_1 &= 1.91 \cdot 10^{-7} \cdot (E_{50}D) + 0.55 \\ \beta_2 &= 1.93 \cdot 10^{-7} \cdot (E_{50}D)^2 - 0.07(E_{50}D) + 7970 \\ \beta_3 &= -1.67 \cdot 10^{-7} \cdot (E_{50}D) + 0.47 \\ \beta_4 &= -0.031(E_{50}D) + 6990\end{aligned}\quad (13)$$

In Figure 19 and 20 the developed p-y formulation is plotted for the drained and undrained silt for Model 5 and 11 respectively.

## 6 Formulation of p-y Curves for Sand

Østergaard et al. [2015] made a similar study for drained sand. As the data is available for the study, the same method used to define the p-y formulation for the drained silt is applied to the sand to obtain continuity and simple expressions regardless of soil.

### 6.1 Step 1-2: Plot and Normalisation of p-y Curves

As for the drained silt, the displacement,  $y$ , and soil pressure,  $p$ , are normalised to the diameter of the bucket,  $D$ , and the ultimate soil pressure,  $p_u$ . In Figure 21 and 22 the plot of the p-y curve and normalised p-y curve for

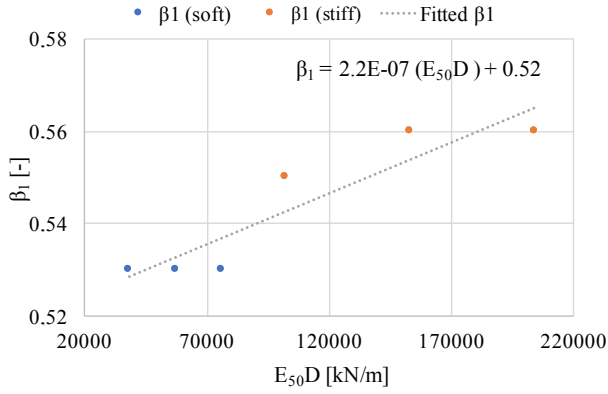


Figure 15: Step 4: Defining model parameter,  $\beta_1$ , in relation to  $E_{50}D$  for drained silt.

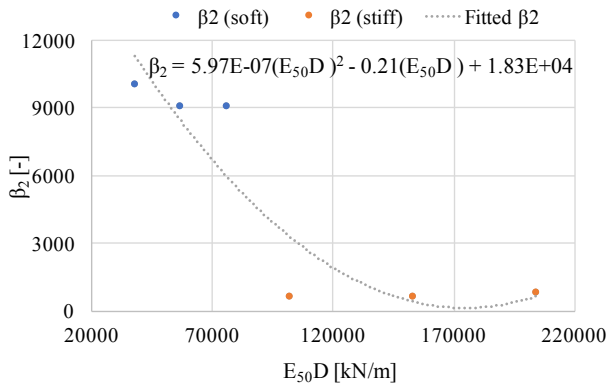


Figure 16: Step 4: Defining model parameter,  $\beta_2$ , in relation to  $E_{50}D$  for drained silt.

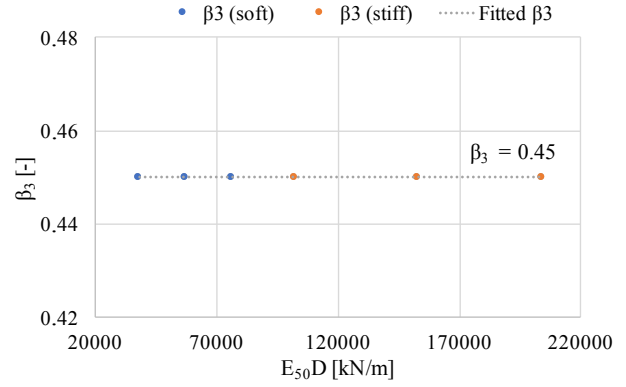


Figure 17: Step 4: Defining model parameter,  $\beta_3$ , in relation to  $E_{50}D$  for drained silt.

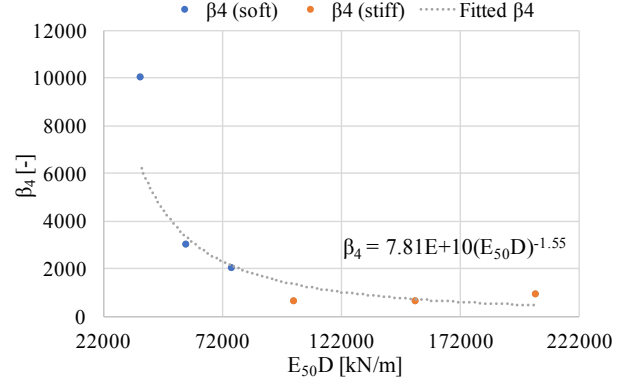


Figure 18: Step 4: Defining model parameter,  $\beta_4$ , in relation to  $E_{50}D$  for drained silt.

Model 8 is shown. The use of  $p_u$  for normalising  $p$  is better, since the p-y curves are more coinciding, compared to normalising with use of the Rankine pressure,  $p_R$ , as done in Østergaard et al. [2015].

### 6.1.1 Formulation of Ultimate Soil Pressure

The correlation between  $p_u$  and  $\sigma'_{v0}/(\phi/D)$  is analysed and shows good correlation for the sand, cf. Figure 23, from which the formulation of  $p_u$  is described, cf. Eq. (14).

$$p_u = \left( 415 \frac{\sigma'_{v0}}{\phi/D} + 169 \right) \cdot A \quad (14)$$

where A is defined as:

$$A = \begin{cases} 0.4 & \text{for soft sand} \\ 0.65 & \text{for medium sand} \\ 1 & \text{for stiff sand} \end{cases}$$

### 6.2 Step 3-4: Fitting of FE Data and Definition of New p-y Formulation

The mathematical expression used to describe the p-y curves for sand is given in Eq. (15), which is identical to the one used for the drained silt.

$$\frac{p}{p_u} = \beta_1 \tanh \left( \beta_2 \frac{y}{D} \right)^{1/3} + \beta_3 \tanh \left( \beta_4 \frac{y}{D} \right)^{1/3} \quad (15)$$

The FE data is fitted, where  $\beta_1$ – $\beta_4$  are free to attain any value to fit the data the best way possible. Afterwards the values are plotted against  $E_{50}D$ , as they are needed in a mathematical expression. The model parameters are defined in Eq. (16), while Figure 24 and 25 show the best fit and mathematical formulation compared to the FE data.

$$\begin{aligned} \beta_1 &= 1.59 \cdot 10^{-8} \cdot (E_{50}D) + 0.57 \\ \beta_2 &= -1.18 \cdot 10^{-5} \cdot (E_{50}D) + 32.2 \\ \beta_3 &= 3.93 \cdot 10^{-8} \cdot (E_{50}D) + 0.52 \\ \beta_4 &= -1.31 \cdot 10^{-5} \cdot (E_{50}D) + 23.5 \end{aligned} \quad (16)$$

## 7 Conclusion

It has been possible to develop p-y formulations by analysing numerical models of lateral displaced buckets in drained and undrained silt. Furthermore, the developed p-y formulation for drained sand showed to be more precise, than the formulation defined by Østergaard et al. [2015], by using the same basic formulation as the drained silt. The governing parameters for the soil pressure for a given displacement were determined to be: the diameter of the bucket, the vertical effective in-situ stress, the soil stiffness and either the friction angle or the undrained shear strength for the drained and undrained soil respectively.

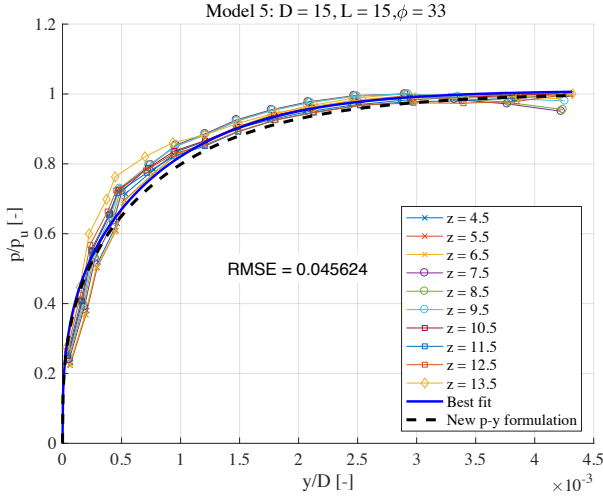


Figure 19: Step 4: New p-y formulation plotted against the best fit and FE data for Model 5.

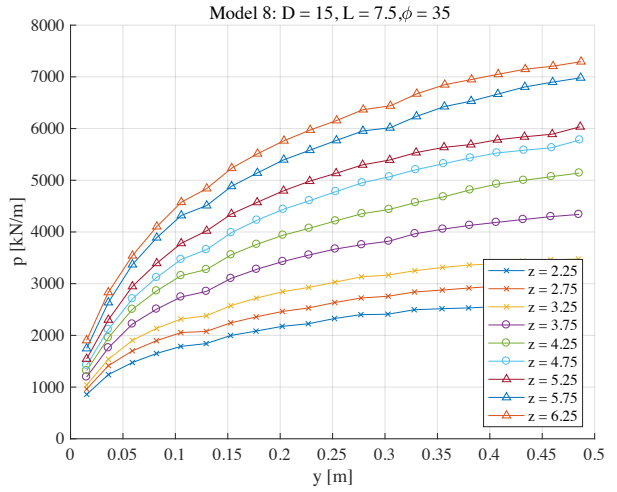


Figure 21: Step 1: Plot of p-y curve for Model 8.

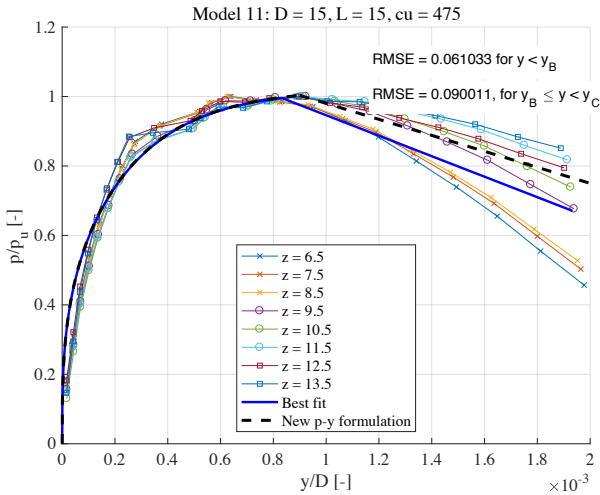


Figure 20: Step 4: New p-y formulation plotted against the best fit and FE data for Model 11.

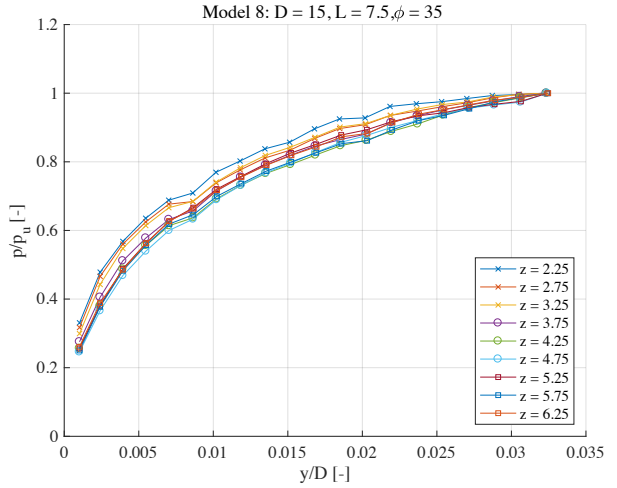


Figure 22: Step 2: Normalisation of p-y curve for Model 8.

The soil stiffness was successfully implemented in the formulations of the model parameters. This was an important objective, as the definition of the model parameters by Østergaard et al. [2015] were believed to cause the imprecision of the soil pressure estimation in Vahdatirad et al. [2016]. Another important outcome of the soil stiffness implementation, was the versatility of the developed p-y formulation, since soils can have different soil stiffnesses for the same friction angle or undrained shear strength, which affects the bearing capacity. These soils are captured by the developed p-y formulations, as the soil stiffness is a governing parameter, whereas the formulation by Østergaard et al. [2015] cannot capture such cases, cf. Figure 26. Thereby, the developed p-y formulations are more versatile, and since they are relative simple and practically applicable for both the silt and sand, it is possible to obtain fast computation of analytical models without compromising on the precision. It is a vital combination to reduce costs and time, hence the objective of the study is considered successfully achieved.

Only a small number of models has been studied, hence it is difficult to implement the formulation in design codes without further evidence of their validation. To validate the formulations, an extension of this study should be to evaluate more numerical models in a bigger spectrum with other strengths of the soil and bucket sizes. As the approach for defining p-y curves for drained silt has shown to be useful for sand as well, another interesting study would be to examine clays. If it is possible to streamline today's different p-y formulations to have the same basic p-y formulations for silts, sands and clays, it would be highly desirable for the sake of simplicity and continuity. If possible, the formulations for silt and sand could be used in a similar study as in Vahdatirad et al. [2016], to compare an analytical model to field tests conducted in similar soil conditions, as the p-y formulations are based on.

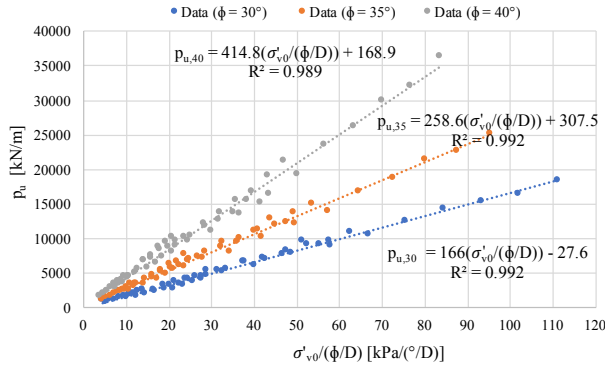
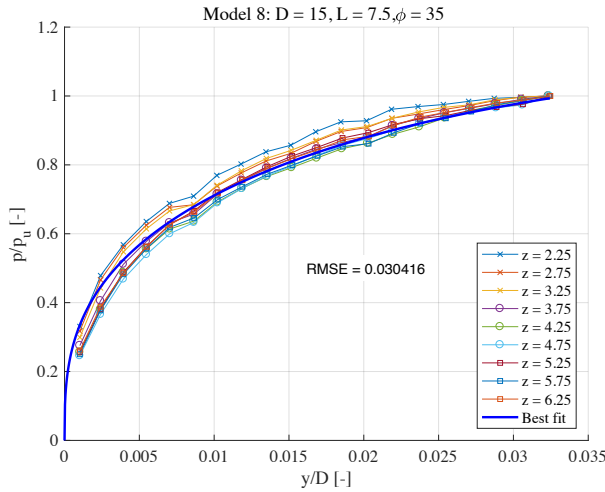
Figure 23: Correlation between  $p_u$  and  $\sigma'_{v0}/(\phi/D)$  for sand.

Figure 24: Step 3: Best fit of Model 8 compared to the normalised FE data.

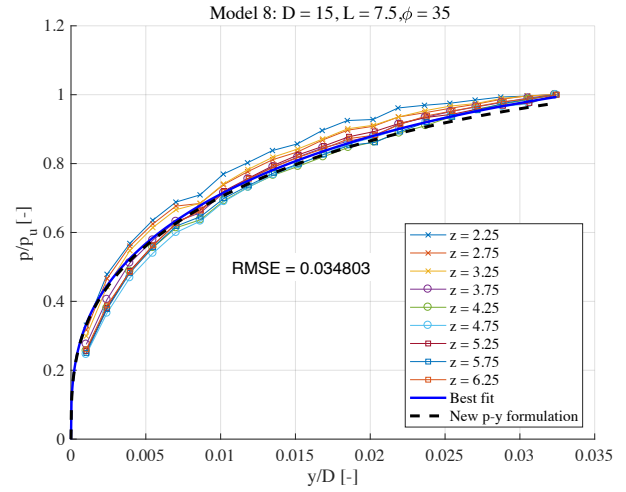
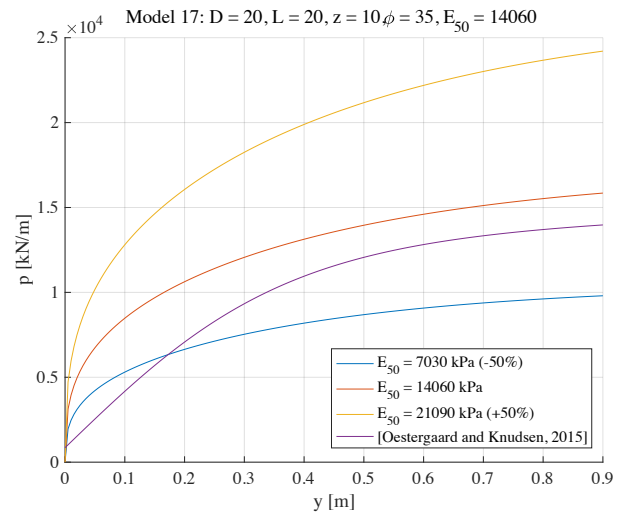


Figure 25: Step 4: New p-y formulation compared to the best fit and FE data for Model 8.

Figure 26: Changing only the soil stiffness  $\pm 50\%$  for the developed p-y formulation and the formulation developed by Østergaard et al. [2015].

## References

- Achmus, Terceros, and Thieken, 2016.** Martin Achmus, Mauricio Terceros, and Klaus Thieken. *Evaluation of p-y Approaches for Large Diameter Monopiles in Soft Clay*. ISBN: 978-1-880653-88-3. International Society of Offshore and Polar Engineers, 2016.
- Brinkgreve, Kumarswamy, and Swolfs, 2015.** R.B.J. Brinkgreve, S. Kumarswamy, and W.M. Swolfs. *PLAXIS 3D Anniversary Edition*. ISBN-13: 978-90-76016-21-4. PLAXIS bv, 2015.
- Cox, Reese, and Grubbs, 1974.** W. R. Cox, L. C. Reese, and B. R. Grubbs. *Field Testing of Laterally Loaded Piles in Sand*. 1974. Proceedings of the Sixth Annual Offshore Technology Conference, Houston, Texas, paper no. OTC 2079.
- Det Norske Veritas, 2013.** Det Norske Veritas. *Design of Offshore Wind Turbines*. Det Norske Veritas AS, 2013.
- Det Norske Veritas, 1992.** Det Norske Veritas. *Foundations - Classification Notes No. 30.4*. Det Norske Veritas AS, 1992.
- Jensen, Mohr, Nicolajsen, Mortensen, Bygbjerg, Hansen, Larsen, Hansen, Bager, Svensson, Søndergaard, Plum, Riberholt, Hansen, Dahl, Larsen, Goltermann, Steenfelt, Sørensen, and Bai, 2015.** Bjarne Chr. Jensen, Gunner Mohr, Asta Nicolajsen, Bo Mortensen, Henrik Bygbjerg, Lars Pilegaard Hansen, Hans Jørgen Larsen, Svend Ole Hansen, Dirch H. Bager, Eilif Svensson, Ejnar Søndergaard, Carsten Munk Plum, Hilmer Riberholt, Lars Zenke Hansen, Kaare K. B. Dahl, Henning Larsen, Per Goltermann, Jørgen S. Steenfelt, Carsten S. Sørensen, and
- Werner Bai. *Teknisk Ståbi*. ISBN: 978-87-571-2844-4, 23rd edition. Praxis - Nyt Teknisk Forlag, 2015.
- Matlock, 1970.** Hudson Matlock. *Correlation for Design of Laterally Loaded Piles in Soft Clays*. ISBN: 978-1-55563-709-5. Offshore Technology Conference, 1970.
- Thieken, Achmus, and Lemke, 2015.** Klaus Thieken, Martin Achmus, and Katrin Lemke. *A new static p-y approach for piles with arbitrary dimensions in sand*. 2015. in *Geotechnik*, vol. 38, issue 4, Ernst and Sohn Verlag, pp. 267-288.
- Vahdatirad, Diaz, Ibsen, Andersen, Firouziabandpey, and Griffiths, 2016.** Mohammadjavad Vahdatirad, Alberto Troya Diaz, Lars Bo Ibsen, Lars Vabbersgaard Andersen, Sarah Firouziabandpey, and D. V. Griffiths. *A load-displacement based approach to assess the bearing capacity and deformations of mono-bucket foundations*. 2016. in A Zingoni (ed.), *Insights and Innovations in Structural Engineering, Mechanics and Computation: proceedings of the sixth international conference on structural engineering, mechanics and computation*, Cape Town, South Africa, 5-7 September 2016. C R C Press LLC, pp. 749-750.
- Wolf, Rasmussen, Hansen, Roesen, and Ibsen, 2013.** Torben Kirk Wolf, Kristian Lange Rasmussen, Mette Hansen, Hanne Ravn

Roesen, and Lars Bo Ibsen. *Assessment of p-y Curves from Numerical Methods for a Non-Slender Monopile in Cohesionless Soil*. 2013. in The Proceedings of the Twenty-third (2013) International Offshore and Polar Engineering Conference. vol. 2, International Society of Offshore and Polar Engineers, pp. 436-443. International Offshore and Polar Engineering Conference.

**Østergaard, Knudsen, and Ibsen, 2015.** Martin Underlin Østergaard, Bjørn Staghøj Knudsen, and Lars Bo Ibsen. *P-y curves for bucket foundations in sand using finite element modeling*. 2015. in V. Meyer (ed.), *Frontiers in Offshore Geotechnics III* proceedings of the third international symposium on frontiers in offshore geotechnics (isfog 2015), Oslo, Norway, 10-12 June 2015. vol. 1, C R C Press LLC, London, pp. 343-348.





## **Recent publications in the DCE Technical Memorandum Series**



# Hardening Soil Small Strain B

---

There are different material models, which has their individual pros and cons. To establish new p-y formulations, the soil-structure behaviour has to be simulated well, i.a. by using an accurate material model.

Østergaard et al. [2015] studied bucket foundations in sand, where they made use of the HSsmall model due to its advanced material model and relatively real-life behaviour. Furthermore Achmus et al. [2016] used the HSsmall model as well, where monopiles in clay were studied, hence it is considered a suitable material model for this study as well. Therefore, this appendix contains a review of the HSsmall model to highlight its interpretation of soil behaviour and modelling features.

## HSsmall

The HSsmall model, compared to the well-known Mohr-Coloumb (MC) model, has considerable advantages, since it takes both shear and isotropic hardening into consideration by a shear locus and a yield cap respectively. The failure envelopes in effective principal stress space is seen in Figure B.1.

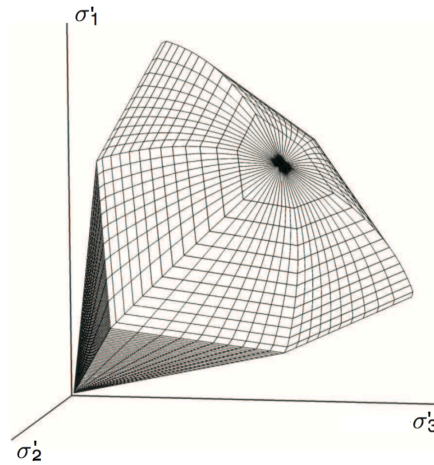


**Figure B.1:** Failure envelope of HSsmall model in effective principal stress space [Brinkgreve et al., 2015].

Even though Figure B.1 is similar to MC model regarding the hexagonal shaped shear locus, they have very different interpretation of the soil stiffness due to the hardening considered in the HSsmall model. In the MC model the strains are entirely elastic until reaching the failure envelope from where the material is perfectly plastic. The shear locus and yield cap of the HSsmall model can expand, where the locus at maximum shearing, with continued straining, will reach MC failure line as shown in Figure B.2. When this stage for the shear locus is reached, the material will undergo similar material behaviour as the MC model, namely perfectly plastic behaviour.

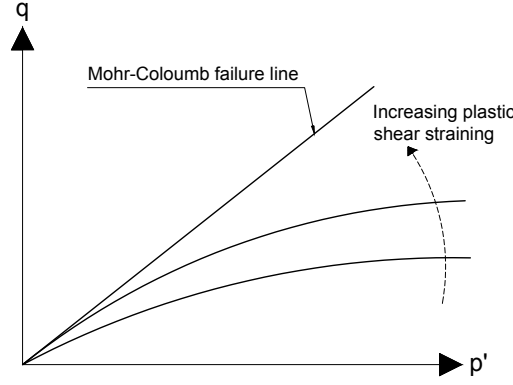


**Figure B.2:** Development of shear locus with increasing plastic shear straining [Brinkgreve et al., 2015].

The hardening of the material, as shown in Figure B.2, causes change in stiffness parameters, when the stress state changes. This is possible due to the use of a power law with the exponent  $m$ , which describes the amount of stress-dependency. Power  $m$  can be defined in an interval of 0.5-1, where 1 is used for soft soils indicated with a straight locus, and 0.5 for hard soils with a curved locus. Depending on the exponent,  $m$ , and at which stress state the soil is at, the model uses a certain stiffness modulus. Eq. (B.1) shows how the stiffness moduli used for the HSsmall model depends on the power  $m$  and reference pressure,  $p^{ref}$  ( $= 100$  kPa).

$$\begin{aligned}
 E_{oed} &= E_{oed}^{ref} \cdot \left( \frac{c \cdot \cos \phi + \sigma'_1 \cdot \sin \phi}{c \cdot \cos \phi + p^{ref} \cdot \sin \phi} \right)^m \\
 E_{50} &= E_{50}^{ref} \cdot \left( \frac{c \cdot \cos \phi + \sigma'_3 \cdot \sin \phi}{c \cdot \cos \phi + p^{ref} \cdot \sin \phi} \right)^m \\
 E_{ur} &= E_{ur}^{ref} \cdot \left( \frac{c \cdot \cos \phi + \sigma'_3 \cdot \sin \phi}{c \cdot \cos \phi + p^{ref} \cdot \sin \phi} \right)^m \\
 G_0 &= G_0^{ref} \cdot \left( \frac{c \cdot \cos \phi + \sigma'_3 \cdot \sin \phi}{c \cdot \cos \phi + p^{ref} \cdot \sin \phi} \right)^m
 \end{aligned} \tag{B.1}$$

The model also takes the effect of small strain stiffness into account. For larger strains the stiffness is affected by a decrease in stiffness with a non-linear progress. Thus the soil cannot fully recover from large strains, which is shown in Figure B.3 where e.g.  $E_{ur}$  is smaller than  $E_0$  or at the un- and reloading part, where hysteresis is observed. Figure B.3 furthermore shows another important aspect of the HSsmall model, which is the hyperbolic relationship between the strain,  $\epsilon_1$ , and deviatoric stress,  $q$ . HSsmall is significantly more precise than the MC model, which is defined by a bi-linear curve. [Brinkgreve et al., 2015]

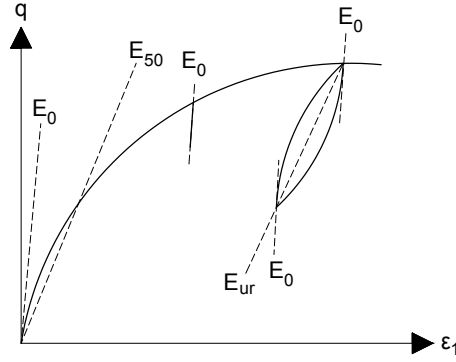


**Figure B.3:** Stress-strain curve for HSsmall model with the different effective stiffness moduli [Brinkgreve et al., 2015].

Figure B.4 shows decreasing stiffness with increased strain magnitude. It is seen that the stiffness decreases non-linearly and is dependent on the strain magnitudes. This is the small strain part of the HSsmall model, which differentiates it from the hardening soil model.

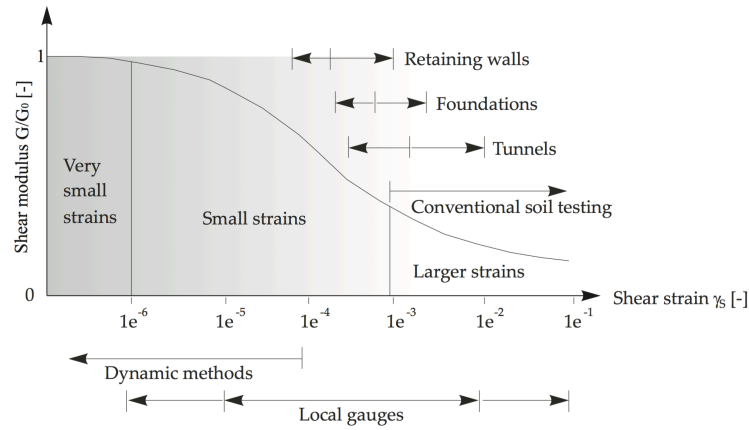


**Figure B.4:** Change of stiffness ratio of  $G/G_0$  as the magnitude of the strain changes [Brinkgreve et al., 2015].

### Input Parameters for Numerical Models

[Appendix Folder, Numerical Model, Soil Data.pdf] shows the parameters given by the supervisor is only enough for a HS model. As it is wanted to run the numerical models as the more refine HSsmall model, the to additional parameters; shear modulus,  $G_0$ , and threshold shear strain,  $\gamma_{0.7}$ , have to be defined.

The values for the parameters could be determined from other soils, which might seem to be similar, but as soil often is unique from soil to soil, a more theoretical approach is wanted.

From Brinkgreve et al. [2015]  $G_0$  and  $\gamma_{0.7}$  can be calculated as given in Eq. (B.2) and

(B.3).

$$G_0^{ref} = 33 \cdot \frac{(2.97 - e)^2}{1 + e} \quad (B.2)$$

$$\gamma_{0.7} = \frac{1}{9G_0} \cdot (2c' (1 + \cos(2\phi')) - \sigma'_1(1 + K_0) \sin(2\phi)) \quad (B.3)$$

To calculate the two parameters the only parameter needed is the void ratio,  $e$ . According to Det Norske Veritas [1992] the void ratio depends on the modulus number,  $m$ , which is defined in intervals:

Loose:  $m = 40 - 60$   
 Medium:  $m = 60 - 80$   
 Dense:  $m > 80$

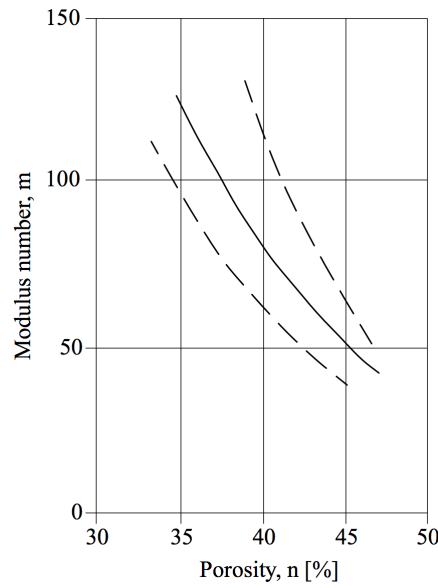


**Figure B.5:** Relation between modulus number,  $m$ , and porosity,  $n$  [Det Norske Veritas, 1992, Fig. 5.9, Sec. 5.3.3.8].

The relation between the void ratio and modulus number is given in Figure B.5. By knowing whether the soil is loose, medium or dense, the modulus number can be defined, thus the porosity and thereby the void ratio can be determined. The assumed modulus number and the related void ratio are given in Table B.1, where the calculated values for  $G_0$  and  $\gamma_{0.7}$  are given as well for the soft and stiff silt.

**Table B.1:** Values of  $G_0$  and  $\gamma_{0.7}$  for the soft and stiff soil studied.

Soil	$m$ [-]	$e$ [-]	$G_0$ [kPa]	$\gamma_{0.7}$ [mm/m]
Soft	40	0.88	76891	0.19
Stiff	70	0.70	102358	0.19

The stiffness moduli for the stiff silt are considered low even though it is classified as stiff in that context. Therefore, the modulus number for the stiff soil is assumed to be within the interval of a medium silt, to obtain a more realistic value.

# Undrained Shear Strength



As this thesis studies the deformation and bearing capacity for bucket foundations in silt, which can occur drained and undrained, both the total and effective strength parameters are needed as input parameters for the numerical models. This appendix will review the process to determine the undrained shear strengths used in the thesis, as there have been different approaches.

## C.1 From Undrained Shear Strength to Stiffness Parameters

In the beginning the focus was to determine the stiffness and deformation parameters from a given undrained shear strength, as this should be governing for the rest of the input parameters in the same way the friction angle was in Østergaard et al. [2015].

Østergaard et al. [2015] were able to determine all the necessary parameters for the material model from the friction angle alone. This was not possible for this case, as the formulas are only valid for sand, thus other studies were looked at.

Andersen and Schjetne [2013] was about consolidation characteristics of sand, clay and silt. Here research of the different deformation parameters was studied, but it was mostly valid for sand, and the silt was only considered in cases, where the soil was described as "silty sand". To determine the different parameters, the water content and  $D_{10}$  particle size was needed as well. Furthermore, it is mentioned lastly in the study, that the correlations should be used with caution, as they are only rough estimates.

Because the input parameters needed in the numerical model could not be calculated directly by assuming an undrained shear strength, and due to the uncertainties of the correlations, another approach was sought.

## C.2 From Stiffness Parameters to Undrained Shear Strength

Unfortunately no direct nor valid relation was to be found between undrained shear strengths and the sought stiffness parameters. Furthermore different people and companies with geotechnical expertise were contacted. One of the contacted was PLAXIS Support, who was not aware of any such parameter relation. Instead they recommended, if possible, that CPTs or triaxial test should be used to obtain the necessary parameters.

Lars Bo Ibsen gave the parameters needed for an drained numerical model, meaning that all the parameters (both stiffness and strength parameters) were effective. The parameters given can be found on [Appendix Folder, Numerical model, Soil Data.pdf]. Therefore, the undrained shear strength had to be found from the effective parameters, which was done by using SHANSEP.

### C.2.1 SHANSEP

The process of determining the undrained shear strength with use of SHANSEP is briefly described, but more detailed look at the calculations are found in [Appendix Folder, Numerical Models, Model and Parameters.xlsx].

The SHANSEP formula is presented by Eq. (C.1). As the only unknown part of the equation was  $(c_u/\sigma'_1)_{nc}$ , consolidated undrained (CU) triaxial tests were performed at different values of OCR. Notice the consolidation phase of the triaxial test was performed with  $K_0$ -consolidation, why  $\Lambda$  was set to 0.8, as recommended by Jensen et al. [2015].

$$\left(\frac{c_u}{\sigma'_1}\right)_{oc} = \left(\frac{c_u}{\sigma'_1}\right)_{nc} \cdot OCR^\Lambda \quad (C.1)$$

#### Undrained Triaxial Test

In PLAXIS triaxial tests can be modelled and performed both undrained and drained. Whether the soil is defined with only effective or total strength parameters does not matter, thus several CU triaxial tests for different OCR values are performed to determine  $(c_u/\sigma'_1)_{nc}$ .

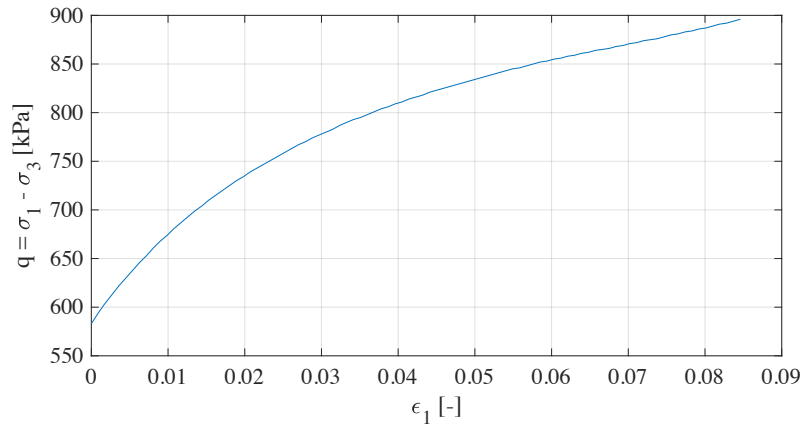


**Figure C.1:** Triaxial test result of stiff silt with OCR = 1.

The undrained shear strength obtained for each triaxial test is taken as:  $c_u = q/2$ , which from Figure C.1 results in  $c_u = 448$  kPa. This is also shown by Table C.1, where results for all the performed triaxial tests are shown.

**Table C.1:** Triaxial test results.

Stiff silt				Soft silt			
OCR [—]	$\sigma'_{1,nc}$ [kPa]	$\sigma'_{3,nc}$ [kPa]	$c_{u,nc}$ [kPa]	OCR [—]	$\sigma'_{1,nc}$ [kPa]	$\sigma'_{3,nc}$ [kPa]	$c_{u,nc}$ [kPa]
1.0	1080	497	448	1.0	80	42	31
1.4	1512	696	624	1.4	112	58	43
2.0	2160	994	885	2.0	160	83	60
4.0	4320	1987	1750	4.0	320	166	120
Average of $(c_u/\sigma'_1)_{nc} = 0.41$				Average of $(c_u/\sigma'_1)_{nc} = 0.38$			



In PLAXIS the input of the undrained shear strength has to be in relation to the reference pressure,  $p^{ref}=100$  kPa. Therefore, the undrained shear strength for the numerical models for the stiff and soft soil are 475 kPa and 56 kPa respectively.

Remark concerning the undrained shear strength:

The use of physical triaxial tests were the initial plan, but due to problems with the geotechnical laboratory, this was not possible. This would indeed have been the most favourable approach to obtain all the input parameters for the HSsmall material model, as suggested by PLAXIS Support.



# Guide for Numerical Modelling and Data Extraction



This appendix contains two step-by-step guides. This first guide explains, how a model is constructed in PLAXIS 3D AE manually by the use of the input program. The models can also be found in [Appendix Folder, Numerical Model, P-y Scripts], where they are given as command scripts, which can be loaded into PLAXIS. PLAXIS then automatically constructs the models by the commands given. This method is significantly faster, and the method allows for identical modelling every time.

The second guide explains the method to extract the data from PLAXIS 3D needed to run the programmed MATLAB scripts found in [Appendix Folder, MATLAB, masterloop.m].

## D.1 Step-by-Step Guide for Numerical Modelling

The geometry is normalised to the bucket dimensions;  $D$  and  $L$ . Note that only earlier versions of PLAXIS have predefined import structures, which are used in the numerical modelling. PLAXIS wants the users in newer versions to model the structure themselves either in PLAXIS manually or in AutoCad. Thus the used import structures cannot be found. A solution to this is to roll back to an older version of PLAXIS 3D, extract the import structure folder and update to a new version again.

1. Open PLAXIS and define the limits of the model domain/soil contour
  - a)  $x_{min} = -4D$ ,  $x_{max} = 4D$ ,  $y_{min} = -4D$  and  $y_{max} = 4D$
2. Create a borehole in (0,0) in the *Soil* mode tab
  - a) Add a layer with depth =  $3L$
  - b) Open the material dialogue and define the soil
3. Go to the *Structure* mode tab, where the bucket will be defined
  - a) Choose *import structure* → choose *vertical cylinder*
  - b) Set the scale for the bucket and place it in (0, 0,  $-L/2$ )
  - c) Select the bucket and right click → chose decompose into surfaces → select the bottom and inner volume of the bucket and delete it (only the skirt and top of the bucket should be present at this stage)
  - d) Select the bucket to right click and choose *create plate*
    - i. In the material dialogue, it is possible to define a plate material. The plate material (steel ) should here be defined
    - ii. Assign the plate material for the bucket as the steel defined for plate materials
4. Next step is to define extended interfaces at the end of the bucket skirt
  - a) Import a vertical cylinder through the *import structure* function (skirt)
    - i.  $h = 0.2D$  and  $D = D$  and insert in (0, 0,  $-(L+0.1D)$ )

- b) Import another vertical cylinder (bottom plate)
      - i.  $h = 1$ ,  $D = 1.4D$  and insert in  $(0, 0, -(L+0.5))$
      - ii. Select the structure and *decompose into surfaces*
      - iii. Delete everything except the bottom
5. Half of the structure at this point is outside the model domain. as only half the model is needed for the simulation due to symemtry, the part outside the model domain is deleted:
  - a) Choose *left view* and set  $x\text{-value} = 0$
  - b) Define a *surface* which covers all structures
  - c) Select all structure  $\rightarrow$  right click and choose *remove parametric* and thereafter *intersect and recluster*
  - d) Select all structures outside the model domain and delete them
6. Define interfaces
  - a) Through the material dialogue interfaces are defined as *Correct<sub>xx</sub>* and *Wrong<sub>xx</sub>*
    - i.  $xx$  indicates either the friction angle or undrained shear strength. In reality the user determines the indication totally by themselves. It is only used to easily extract data through MATLAB later in the data processing
  - b) Skirt is given following interfaces:
    - i. Positive and negative
  - c) Top (lid):
    - i. Negative
  - d) Extended interface bottom plate (lid):
    - i. Negative
  - e) Extended interface skirt
    - i. Positive and negative
  - f) Positive skirt interface is given *Correct<sub>xx</sub>* and negative interfaces of the skirt and bucket top is given *Wrong<sub>xx</sub>*
    - i. All other interfaces are correctly set by default by PLAXIS
  - g) Deifinition of proximity volume
    - i. Import *vertical cylinder*
    - ii.  $h = 2L$  and  $D = 3$  and insert in  $(0, 0, -L)$
    - iii. Cut the volume in half as done earlier
    - iv. Set the material of the proximity volume as the adjacent soil
7. Go to *Mesh* mode tab
  - a) Select everything within the proximity volume and set fineness factor to 0.16
  - b) Run the mesh with a coarseness of medium
8. Go to *Staged Construction* mode tab
  - a) Add an installation phase and select and activate interfaces
  - b) Add a loading phase with the wanted displacement

- c) Add an unloading phase by deselecting the predescribed displacement
- d) Add a load phase with increased displacement
- e) Add a unloading phase by deselecting the predescribed displacement
- f) The two abovementioned steps are continued until last load step

## D.2 Step-by-Step Guide for Data Extraction

The data, which is needed to establish the p-y curve for a model, has to be manually extracted in PLAXIS 3D. The extracting method for the displacement and stresses is slightly difference, thus they are given separately.

### Extracting the Displacement Data

1. Click on *View calculation results* (PLAXIS 3D Output will open).
2. Select a part of the bucket, right click and click *Select all*. Press enter (a new window opens).
3. Click on *Deformations* → *Total displacements* → *Table* (a new window opens with a table).
  - a) Select  $n^{\text{th}}$  unloading phase.
  - b) Press ctrl+A to select all numbers displayed in the table.
  - c) Press ctrl+E to export a text file of all the selected data.
    - i. Save the file as Disp(n).txt

### Extracting the Stress Data

1. Click on *View calculation results* (PLAXIS 3D Output will open).
2. Select a part of the interface, right click and click *Select all*. Press enter (a new window opens).
3. Click on *Interface stresses* → *Table of stress point values* (a new window opens with a table).
  - a) Select  $n^{\text{th}}$  load phase.
  - b) Press ctrl+A to select all numbers displayed in the table.
  - c) Press ctrl+E to export a text file of all the selected data.
    - i. Save the file as Stress(n).txt



# Convergence and Model Domain Analysis

# E

Getting reliable output from the numerical models, the mesh has to be fine, but this will also result in increased computation time. An optimal compromise is thereby needed, and a convergence analysis is the tool used to find the balance between calculation time and precision. Furthermore the size of the model domain has to be decided as well, which is done from a model domain analysis.

Before a convergence analysis is made, a short description of the elements used for meshing is given. This chapter is based on Brinkgreve et al. [2015].

## E.1 Mesh Elements

Meshing of the models in PLAXIS are not the same for the soil, plate (bucket) and interface, as they all have different types of elements.

### E.1.1 Soil Volume Elements

In PLAXIS soil volumes are discretised into 10-noded tetrahedral elements, as shown in Figure E.1.

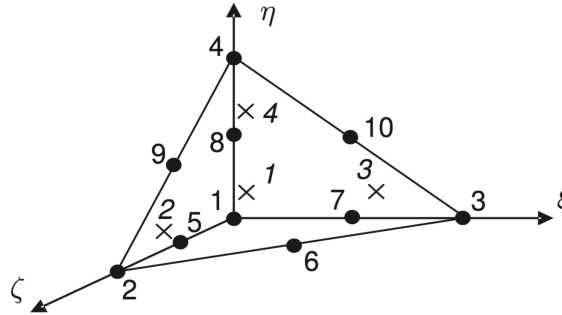


**Figure E.1:** 10-noded tetrahedral element used for soil volumes in PLAXIS [Brinkgreve et al., 2015].

The black dots seen in Figure E.1 are the nodes of the element. These nodes have three degrees of freedom (d.o.f.) per node in  $u_x$ ,  $u_y$  and  $u_z$ . The crosses illustrated in the figure are the Gauss integration points. [Brinkgreve et al., 2015]

### E.1.2 Plate Elements

The suction bucket is defined as a plate, hence it is discretised into 6-noded triangular plate elements, cf. Figure E.2. The element has six d.o.f. per node;  $u_x, u_y, u_z, \phi_x, \phi_y$  and  $\phi_z$ , where the three last ones are rotational d.o.f. [Brinkgreve et al., 2015]

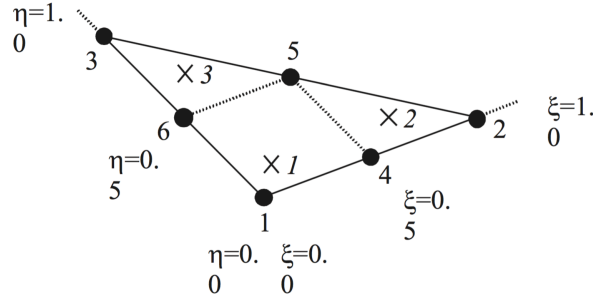


**Figure E.2:** 6-noded triangular plate element [Brinkgreve et al., 2015].

### E.1.3 Interface Elements

The interfaces are discretized into 12-noded interface elements. Instead of having single nodes as the elements for the soil volume or the plate, the interface element nodes consist of a pair of nodes. This allows it to be compatible with the 6-noded triangular side of the soil volume element or the plate element. [Brinkgreve et al., 2015]

## E.2 Convergence Analysis

To obtain fast computation and precise results, a convergence analysis is needed. It is decided not to give the whole model the same fineness factor, but only some part of the model. Since the most intensive stresses and displacements are near the bucket, a proximity volume is defined, where this volume will be given a finer refinement factor. Thereby calculation time is kept low without lacking on precision significantly. The proximity volume and overall volume is seen in Figure E.3. [Wolf et al., 2013]

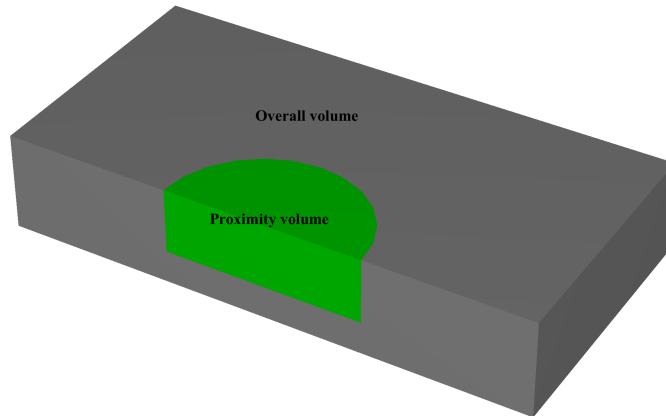


**Figure E.3:** Soil divided into an overall volume (grey) and proximity volume (green).

PLAXIS has an automatic mesh generator, where only a few inputs regarding the overall fineness and the refined fineness factor can be chosen by the user. It has been decided, that the overall fineness of the mesh is set to *medium*, thus only the refined mesh for the proximity volume is left for the further analysis.

The models run are equal to *Model 5* regarding the geometry and input parameters. Only the refinement factor of the proximity volume is changed compared to Model 5.



Determining the size of the model domain and the fineness factor is an iterative process. Hence the size of the model domain used in the convergence analysis, is the size concluded from the model domain analysis.

In total 8 simulations have been made with the following refinement factor of the proximity volume: 0.5, 0.35, 0.28, 0.23, 0.18, 0.17, 0.16 and 0.14.

To determine what the refinement factor should be to get both precise and fast computation, the data is analysed with regard to no. of elements and time as shown in Figure E.4 and E.5, where the data labels indicate the refinement factor of the proximity volume. In Table E.1 the results from the analysis are summarized.

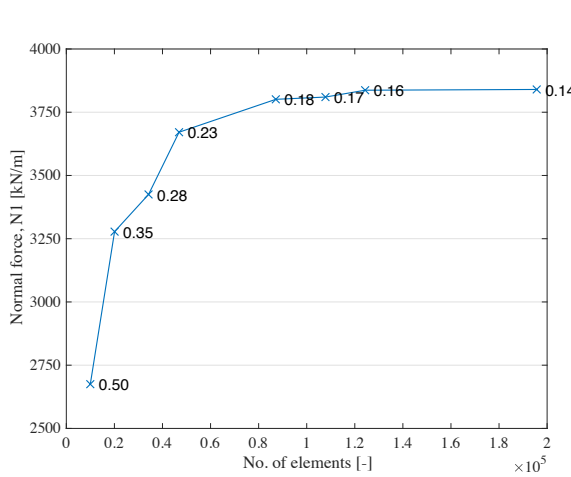


**Figure E.4:** Normal force in relation to no. of elements.

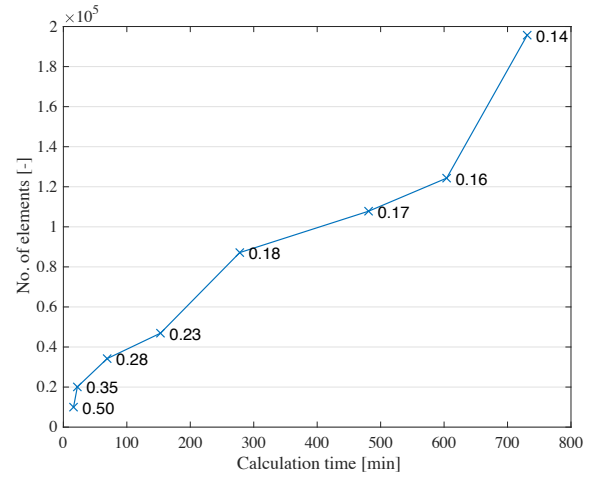


**Figure E.5:** Calculation time in relation to no. of elements.

**Figure E.6:** Results of convergence analysis.

**Table E.1:** Convergence results.

Refinement factor [-]	Elements [-]	Normal force [kN/m]	Deviation [%]	Calc. time [min]
0.50	9973	2675		16
0.35	20074	3278	22.54	22
0.28	34205	3425	4.48	69
0.20	68373	3671	7.18	153
0.18	87145	3801	3.54	278
0.17	107800	3810	0.23	481
0.16	124307	3837	0.71	604
0.14	195673	3840	0.08	731

The force in the convergence analysis was taken as the maximum force of a loading phase from PLAXIS 3D Output. As seen by Table E.1 the model starts to converge at a refinement factor of 0.18, and the calculation time is considered fast, as the calculation time is significantly increased for the remaining models run.

Undrained models were also simulated to see if any requirement to the mesh density is different from the drained models. At the point these models were simulated, the

undrained soil parameters were not determined. Therefore the analysis was performed with parameters given by Lars Bo Ibsen. The parameters were determined from an undrained silt sample, thus the conclusion of the analysis was assumed to be valid for the silt studied in the thesis as well. Plotting of the undrained models revealed, that depths were not clearly separated. It is known that the pressure should increase with depth, but it was seen that the curves overlapped each other as seen in figure E.7. As this was considered a significant problem, since this project is dependent on reliable data, troubleshooting the problem was needed.

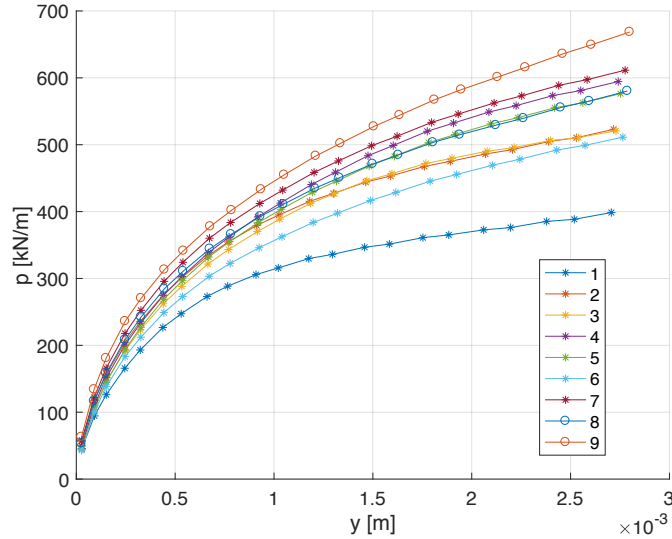


**Figure E.7:** P-y curve with a refined mesh factor of 0.18. 1 in the legend indicates the layer closest to the mudline, while 9 is closest to the base of the bucket.

### E.2.1 Troubleshooting

To figure out why this happened, only a parameter at each troubleshooting model could be changed, hence around 30 models were simulated. The changed parameters for the troubleshooting were:

- Model setup
- Soil
- Displacement
- Refined mesh factor

Regarding the model setup; since the guide and PLAXIS files from Østergaard et al. [2015] were available, these were simulated with the silt soils used for this project. Furthermore, the developed numerical model for this project was used to simulate the sand studied in Østergaard et al. [2015] as well. Here it was seen, that the model setup did not have an impact on the issue. But it was seen, as Østergaard et al. [2015] studied sand, hence drained behaviour, this had an impact on the p-y plot, since the force in the p-y curves increased with increasing depth. Thus the focus went more specific to the drained and undrained behaviour in PLAXIS.

Different silt, with all the input parameters needed for HSsmall, were made available by the Lars Bo Ibsen with both effective and total strength parameters to find a solution to the

issue, both Undrained (A) and (B) were simulated. The conclusion from these simulations were, that they did not seem to have any relation to the problem, and neither did it help, when displacements were regulated.

Lastly the number of elements in the proximity volume were increased by making the mesh finer, as a more detailed look at the outcome stresses revealed an inefficient amount of stress points for certain areas. Wolf et al. [2013] also describes the problems concerning inefficient number of stress points at each considered integration area. Here it is mentioned, that the affect of stress concentrations is reduced, when an efficient amount of stress points are represented at each area considered. Therefore, a model with an increased refinement factor was run. The result for this model is seen in Figure E.8. Here it is seen, that the force increases with depth significantly better than before.

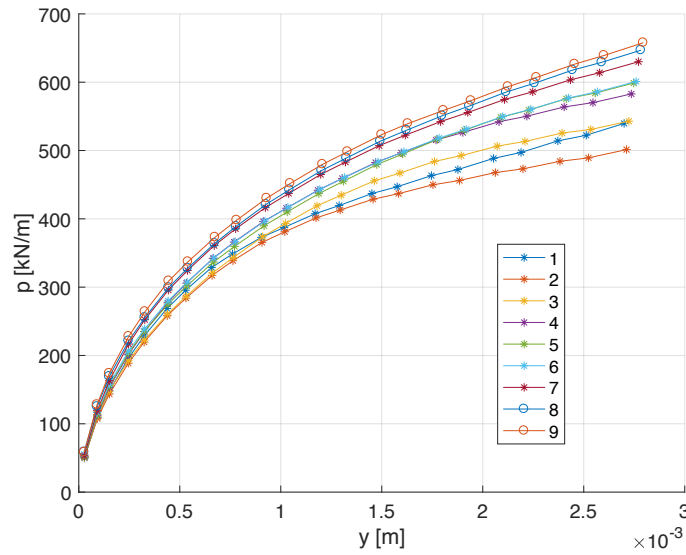


**Figure E.8:** P-y curve with a refined mesh factor of 0.16. 1 in the legend indicates the layer closest to the mudline, while 9 is closest to the base of the bucket.

When comparing Figure E.7 and E.8 it is clearly seen, that there are significant differences, as curves are not overlapping with denser mesh, and thus pressure increases with depth as expected. An even more dense mesh might have given even better results, but due to the significant increase in calculation time, it cannot be done. Furthermore, the computers used for the project only had 3 GB RAM, which is not enough, when very dense meshes demand more computational power.

From a time and precision perspective it is concluded to go with a minimum of 0.16 for the refined mesh factor in the proximity volume to make sure, that enough elements are represented at each area to get reliable results, even though it increases the calculation time significantly.

### E.3 Analysis of Model Domain

When running the models, stresses should not affect the edges of the model domain, as this would imply that the model domain is not big enough. Choosing too big of a model

domain, the calculation time will increase without having any advantageous. Thus stresses are looked at for a loading and unloading phase, and if the edges are not significantly affected, the model domain size is accepted.



*Figure E.9:*  $\sigma'_{yy}$  for a loading phase.

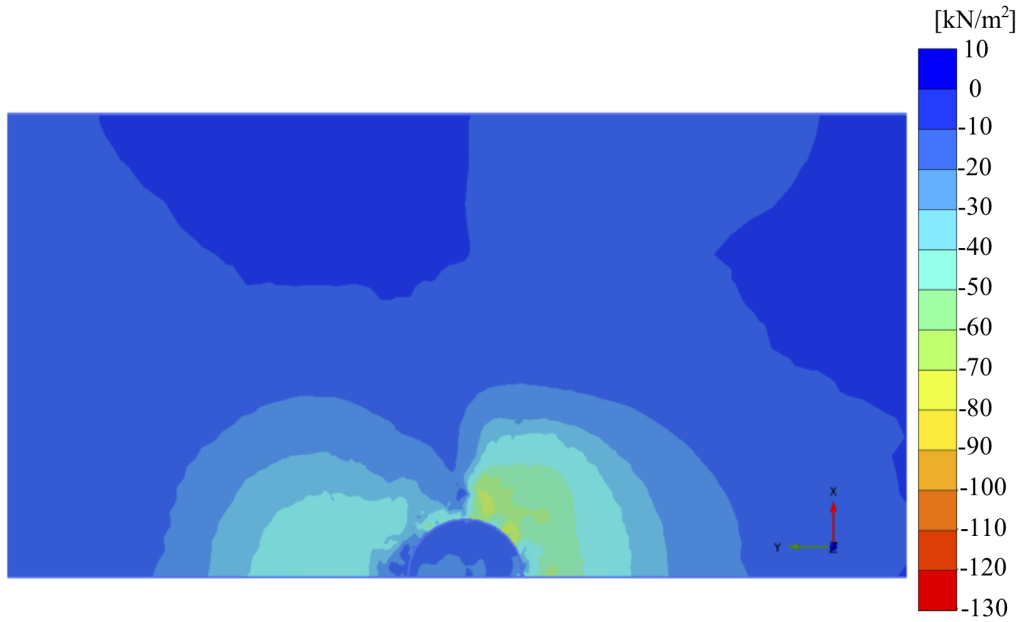


*Figure E.10:*  $\sigma'_{yy}$  for an unloading phase.

As seen in Figure E.9 and E.10, the edges of the model domain are not affected in a significant matter, why the size of the model domain is accepted. The domain size corresponds almost to the size used in Østergaard et al. [2015]. The size of the model domain and other geometries are shown in Figure E.11, where the dimensions are normalised to the length and diameter of the bucket.

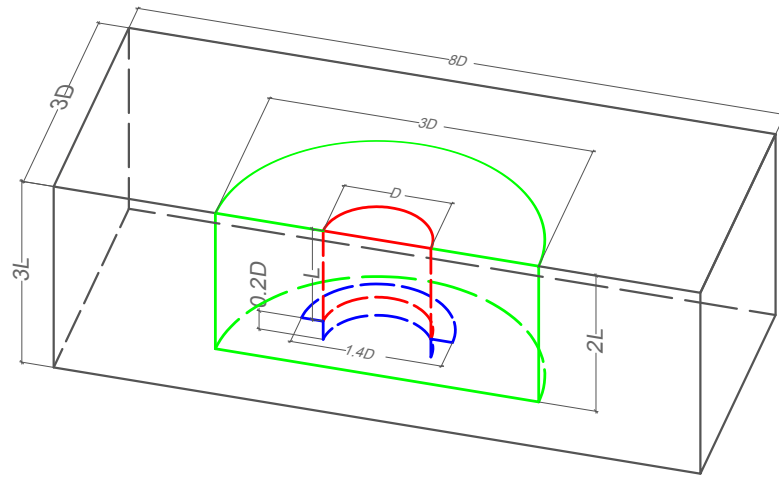


**Figure E.11:** Model geometry normalised to bucket length and diameter.



# P-y curves of Numerical Models

F

The results for all the numerical models are presented as p-y curves in this appendix. Each model is presented with two p-y curves; non-trimmed and trimmed curves. The non-trimmed p-y curves present all 15 subdivided depths, while the trimmed p-y curves only represent depths, which are not affected by edge effects.

## Model 1

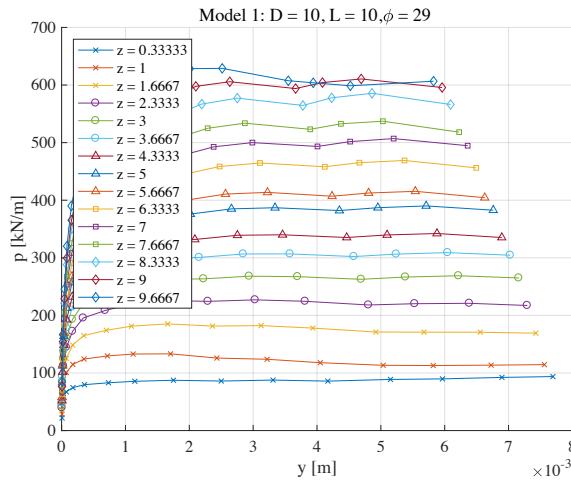


**Figure F.1:** Model 1: non-trimmed p-y curve.

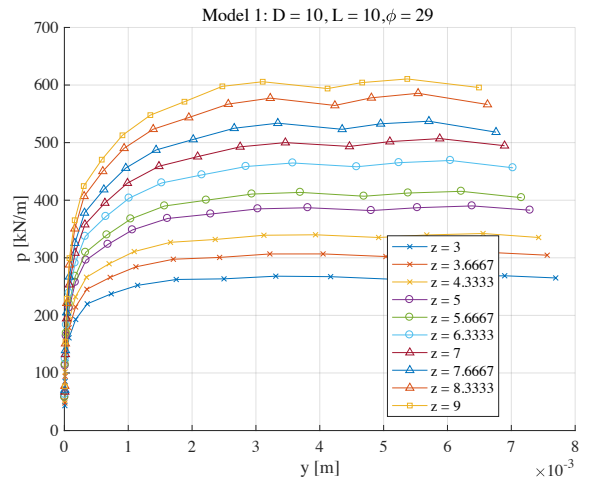


**Figure F.2:** Model 1: trimmed p-y curve.

## Model 2

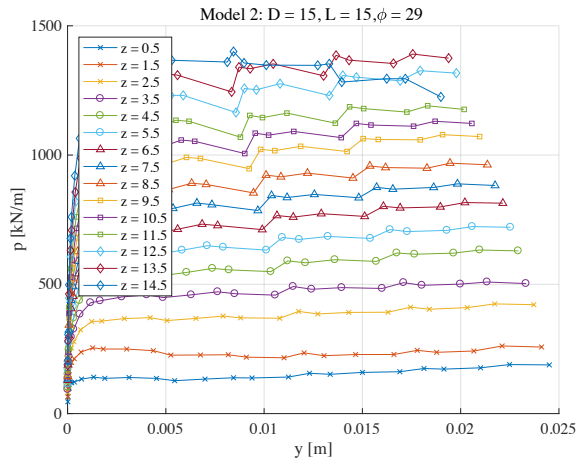


**Figure F.3:** Model 2: non-trimmed p-y curve.

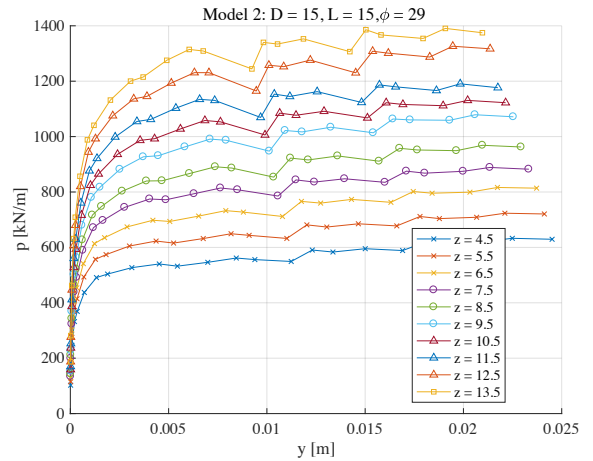


**Figure F.4:** Model 2: trimmed p-y curve.

## Model 3

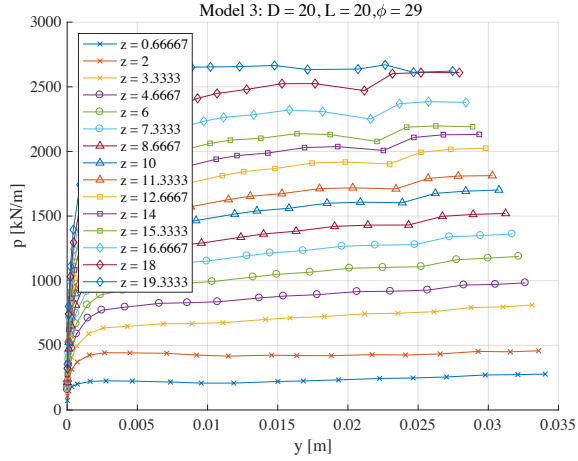


**Figure F.5:** Model 3: non-trimmed p-y curve.

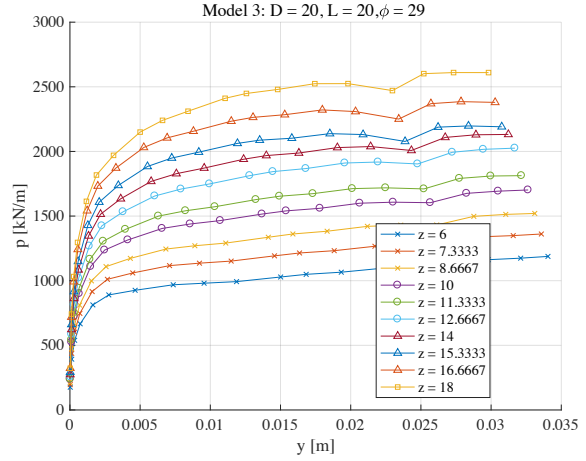


**Figure F.6:** Model 3: trimmed p-y curve.

## Model 4

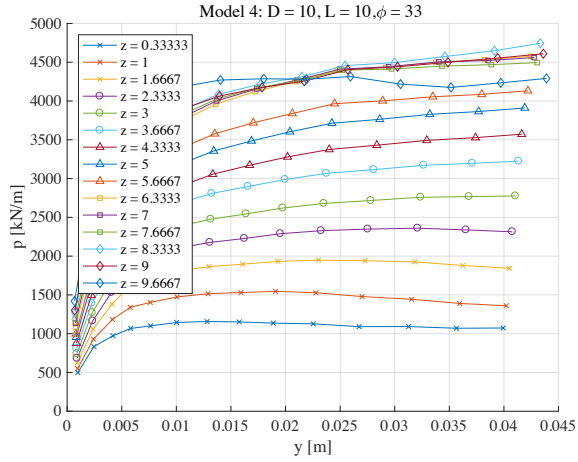


**Figure F.7:** Model 4: non-trimmed p-y curve.

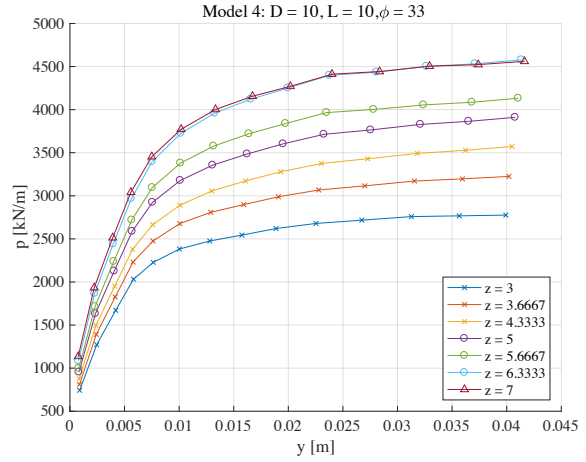


**Figure F.8:** Model 4: trimmed p-y curve.

## Model 5

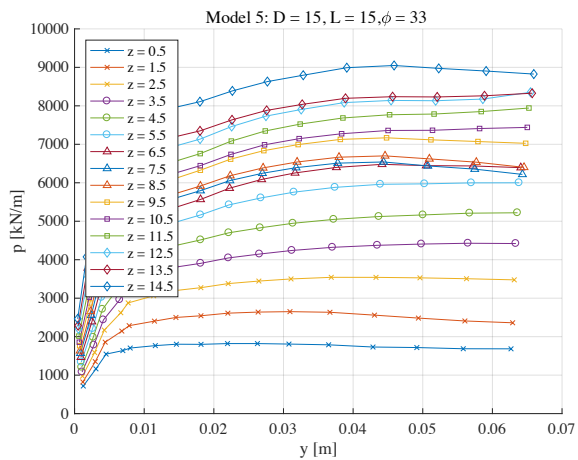


**Figure F.9:** Model 5: non-trimmed p-y curve.

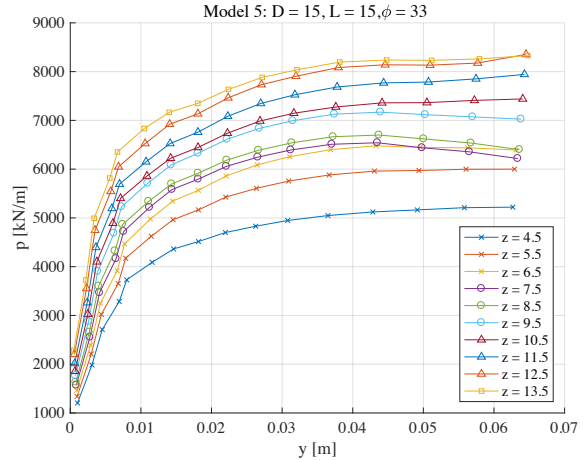


**Figure F.10:** Model 5: trimmed p-y curve.



## Model 6

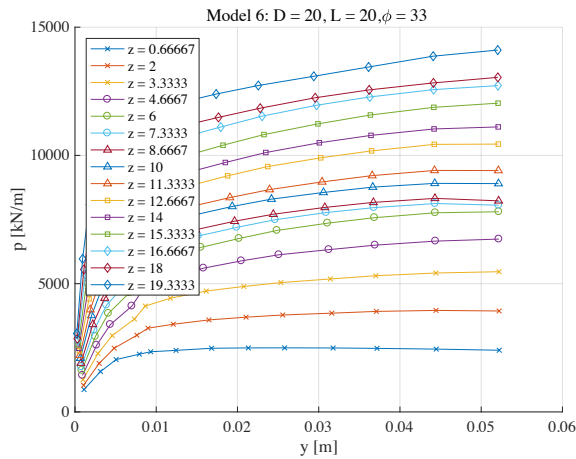


**Figure F.11:** Model 6: non-trimmed p-y curve.

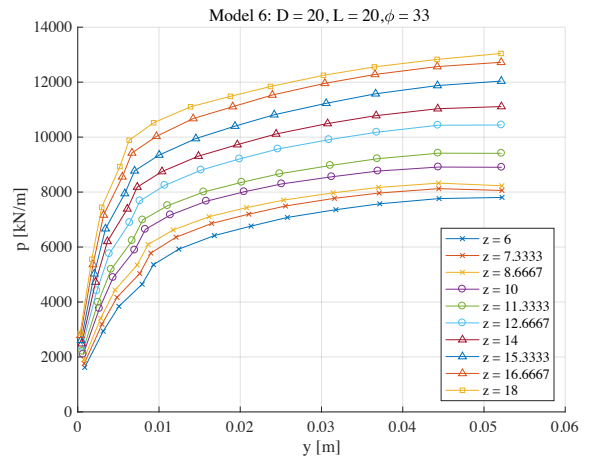


**Figure F.12:** Model 6: trimmed p-y curve.

## Model 7

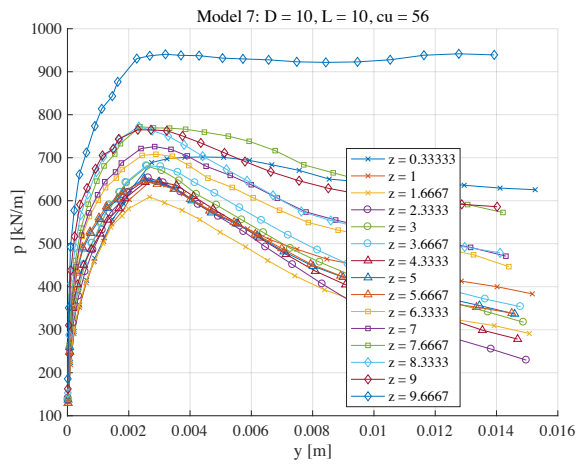


**Figure F.13:** Model 7: non-trimmed p-y curve.

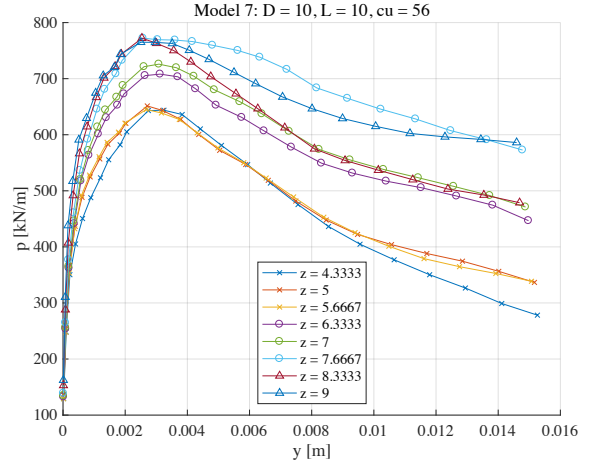


**Figure F.14:** Model 7: trimmed p-y curve.

## Model 8

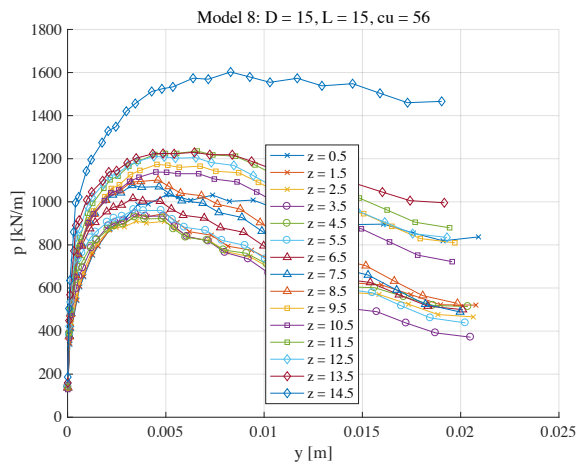


**Figure F.15:** Model 8: non-trimmed p-y curve.

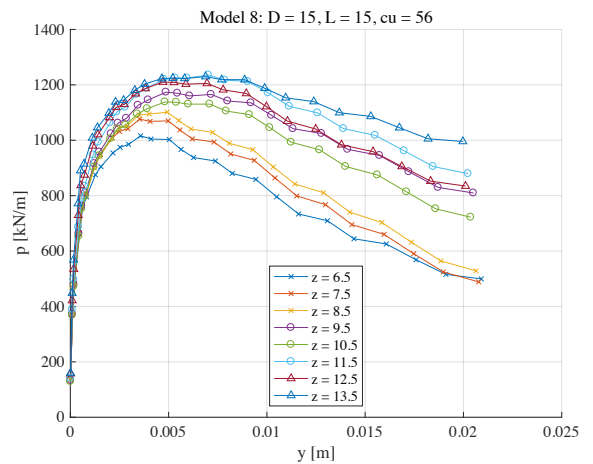


**Figure F.16:** Model 8: trimmed p-y curve.

## Model 9

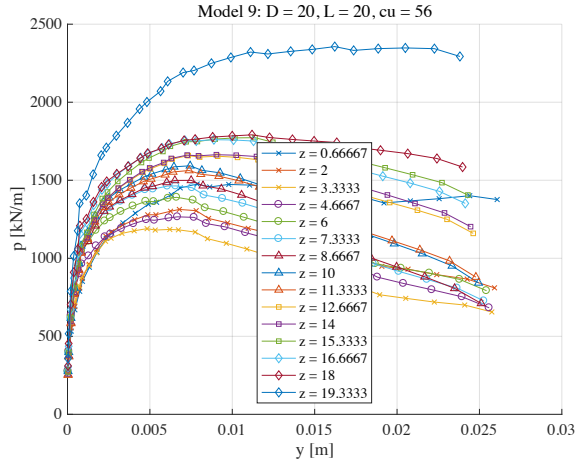


**Figure F.17:** Model 9: non-trimmed p-y curve.

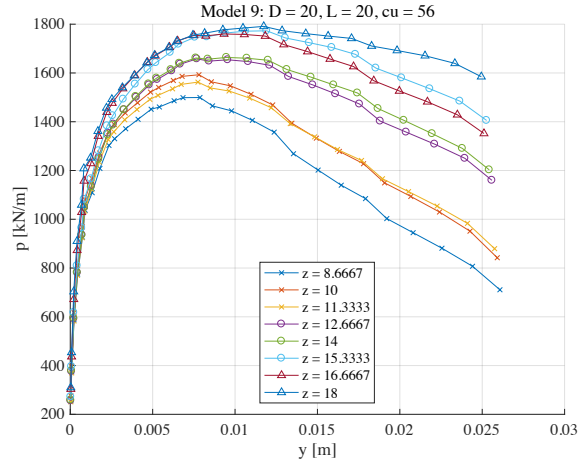


**Figure F.18:** Model 9: trimmed p-y curve.

## Model 10

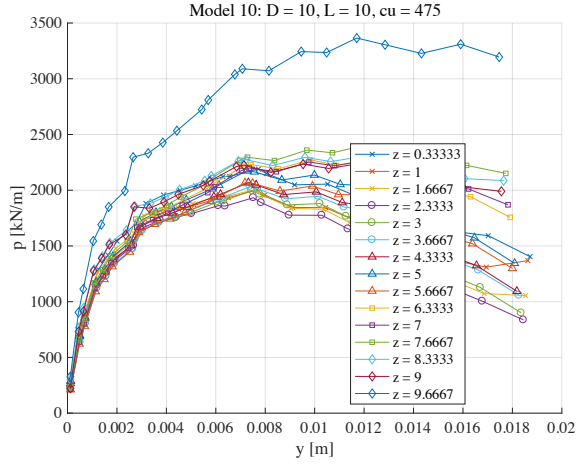


**Figure F.19:** Model 10: non-trimmed p-y curve.

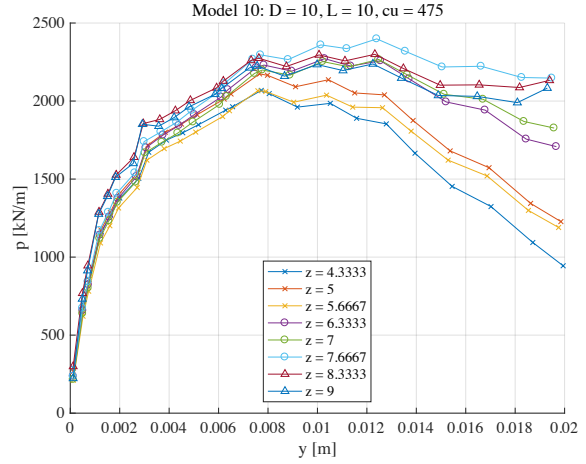


**Figure F.20:** Model 10: trimmed p-y curve.

## Model 11

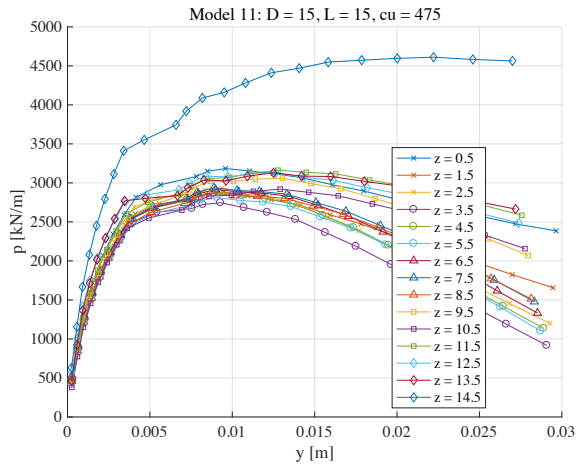


**Figure F.21:** Model 6: non-trimmed p-y curve.

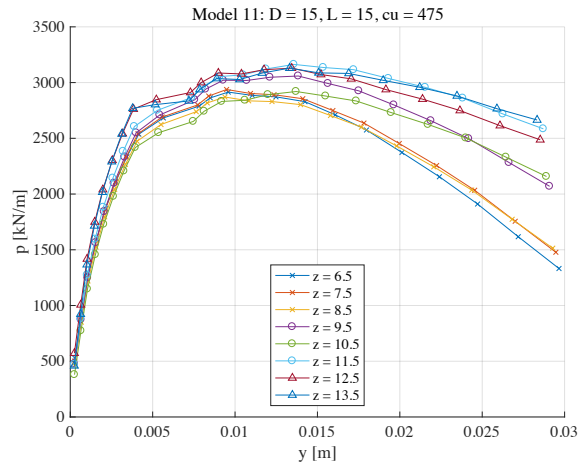


**Figure F.22:** Model 11: trimmed p-y curve.

## Model 12

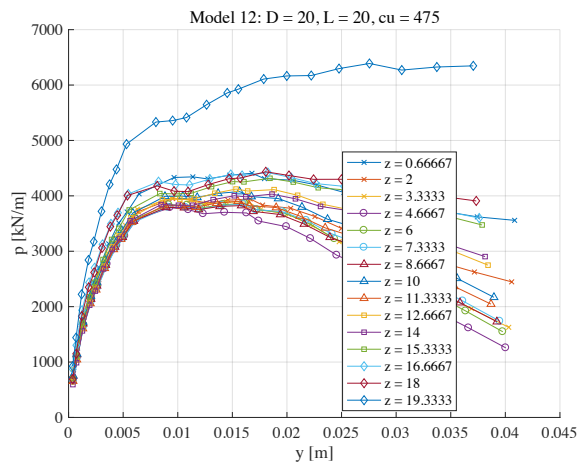


**Figure F.23:** Model 12: non-trimmed p-y curve.

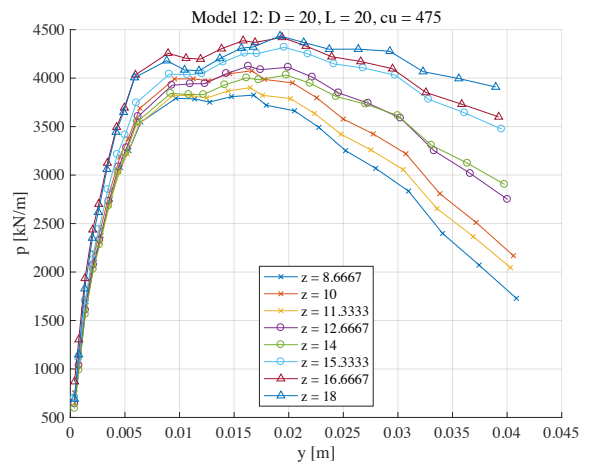


**Figure F.24:** Model 12: trimmed p-y curve.

## Conclusion

As seen by the p-y curves, there is a significant difference between the drained and undrained models. Thus in the further work for the thesis, distinction between drained and undrained models are made, as the data processing will be approached differently for those two categories.

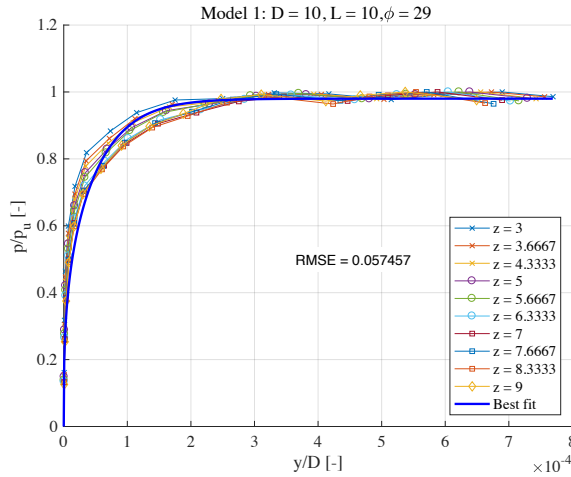


# Plot of p-y Curves for Silt

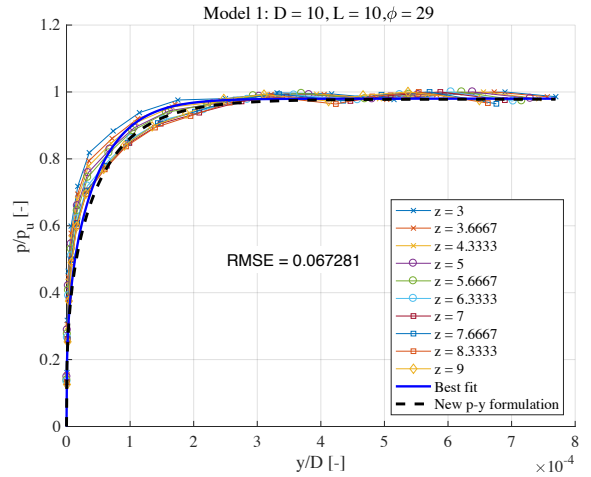


Plots of best fit and the developed p-y formulation for the silt are shown by the figures below. The figures also show the normalised p-y curves, as both the soil pressure,  $p$ , and displacement,  $y$ , are shown normalised to the ultimate soil pressure,  $p_u$ , and bucket diameter,  $D$ , respectively.

## Model 1

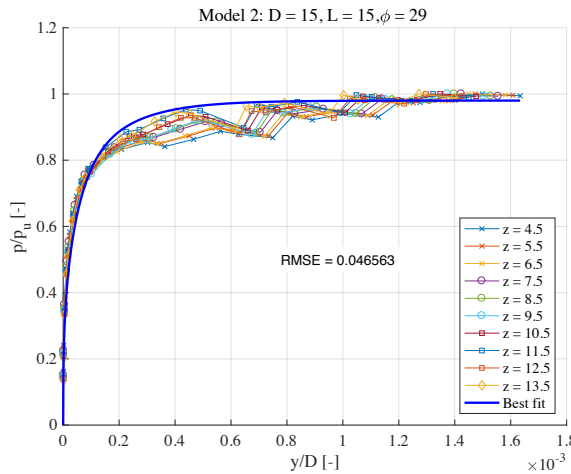


**Figure G.1:** Model 1: Best fit function vs. FE data.

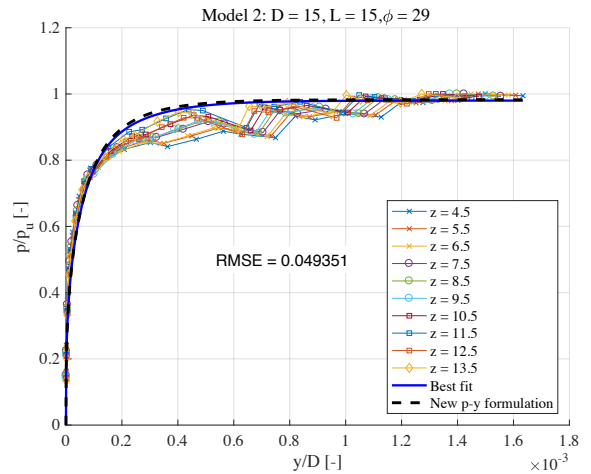


**Figure G.2:** Model 1: New p-y formulation vs. FE data.

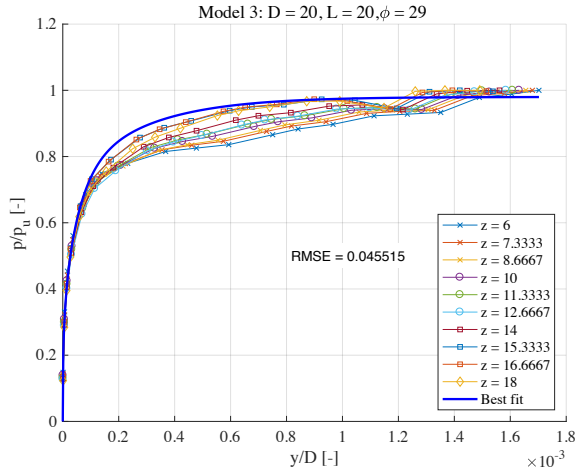
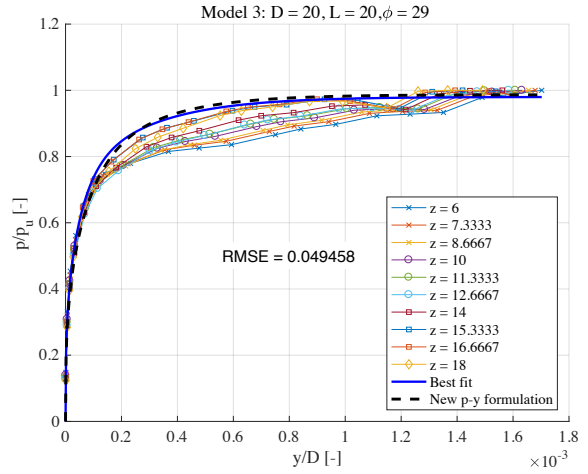
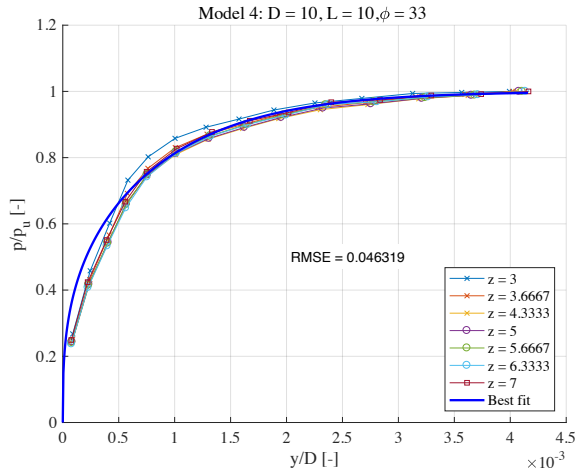
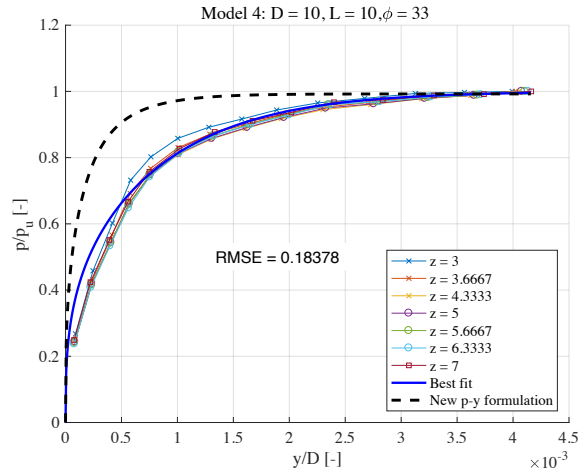
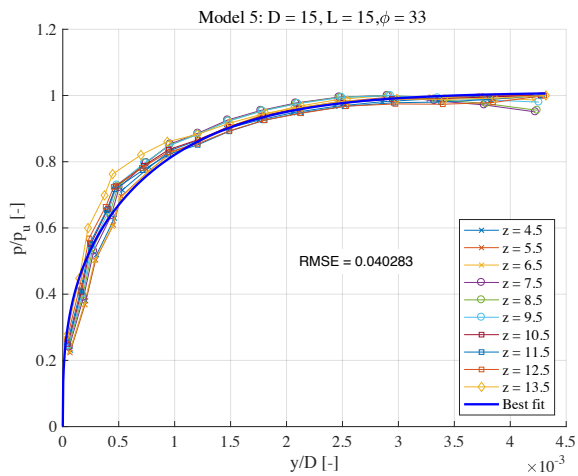
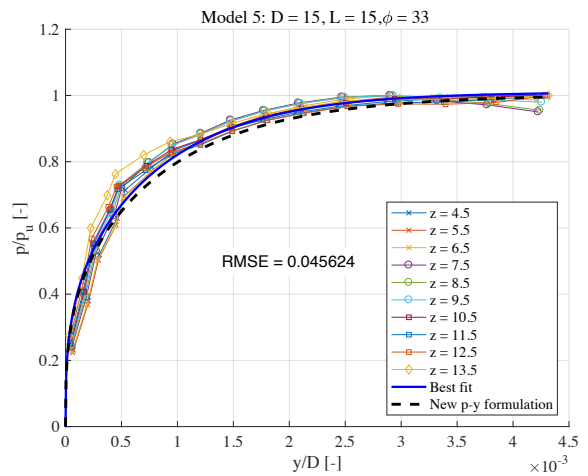
## Model 2



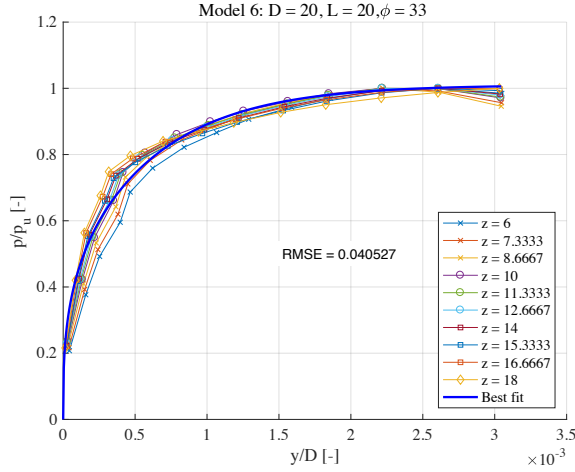
**Figure G.3:** Model 2: Best fit function vs. FE data.



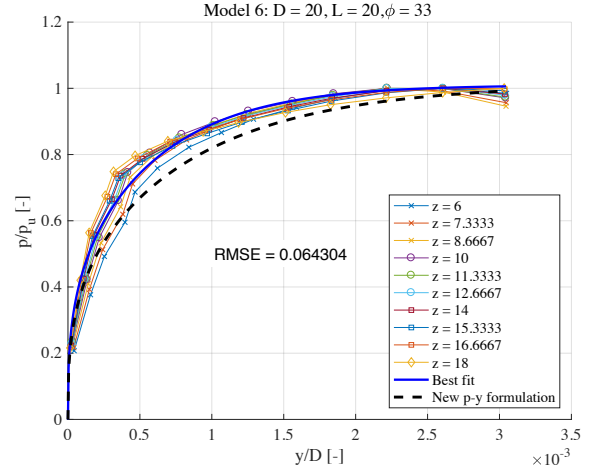
**Figure G.4:** Model 2: New p-y formulation vs. FE data.

**Model 3****Figure G.5:** Model 3: Best fit function vs. FE data.**Figure G.6:** Model 3: New p-y formulation vs. FE data.**Model 4****Figure G.7:** Model 4: Best fit function vs. FE data.**Figure G.8:** Model 4: New p-y formulation vs. FE data.**Model 5****Figure G.9:** Model 5: Best fit function vs. FE data.**Figure G.10:** Model 5: New p-y formulation vs. FE data.

## Model 6

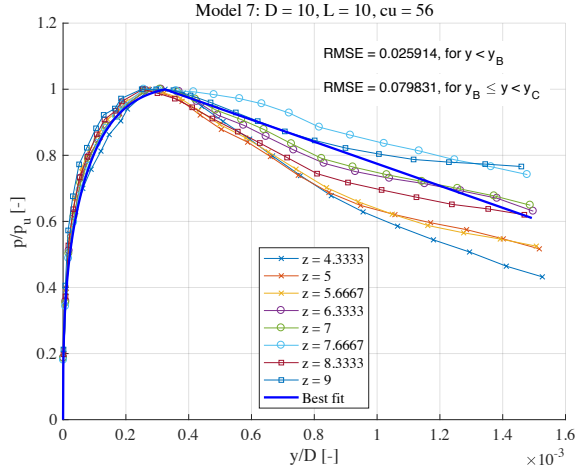


**Figure G.11:** Model 6: Best fit function vs. FE data.

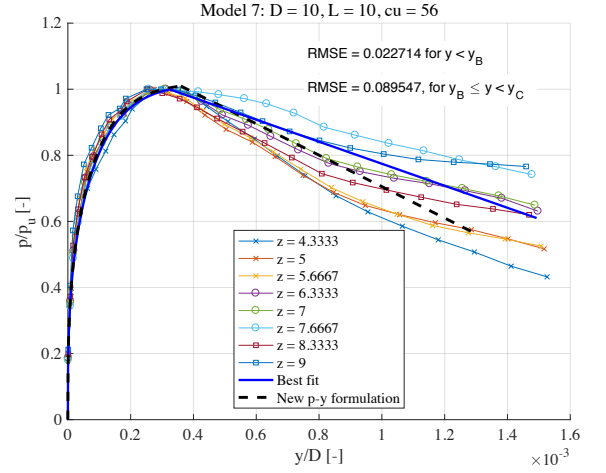


**Figure G.12:** Model 6: New p-y formulation vs. FE data.

## Model 7

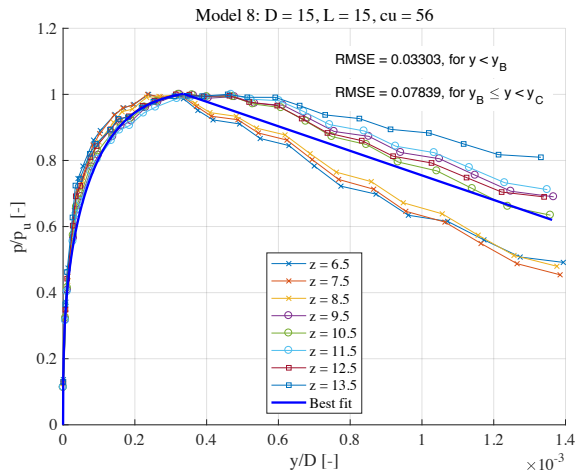


**Figure G.13:** Model 7: Best fit function vs. FE data.

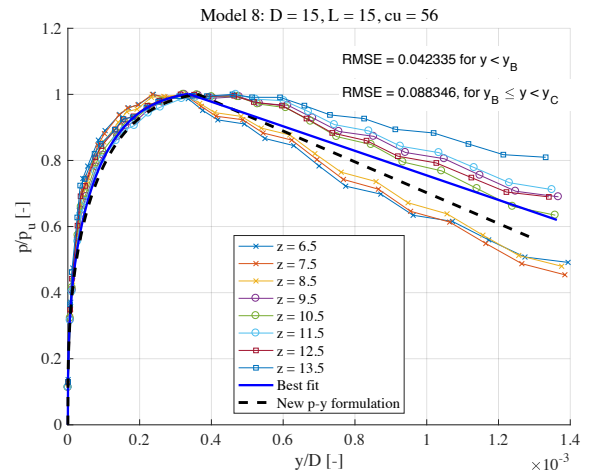


**Figure G.14:** Model 7: New p-y formulation vs. FE data.

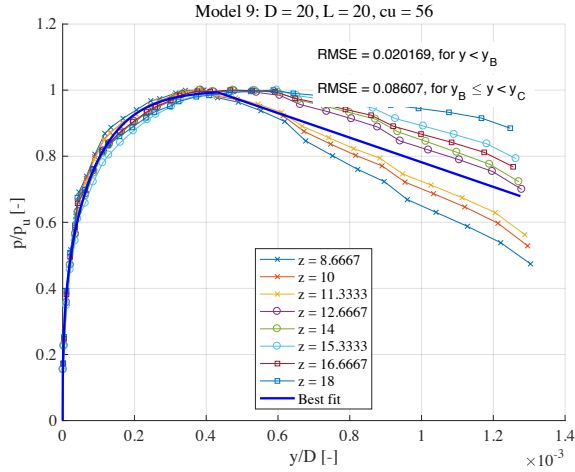
## Model 8



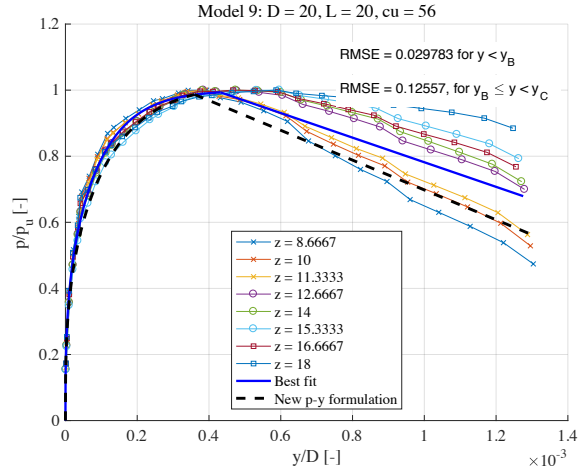
**Figure G.15:** Model 8: Best fit function vs. FE data.



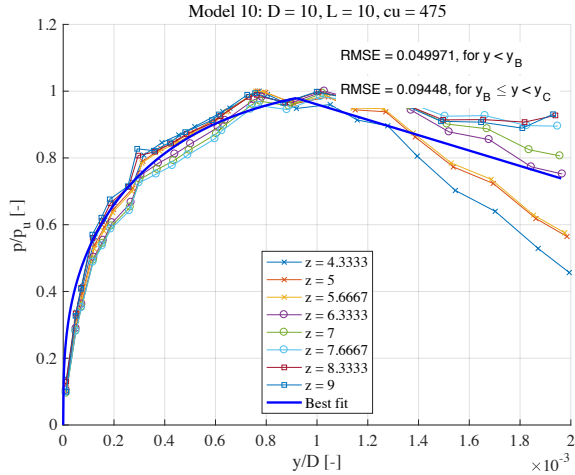
**Figure G.16:** Model 8: New p-y formulation vs. FE data.

**Model 9**

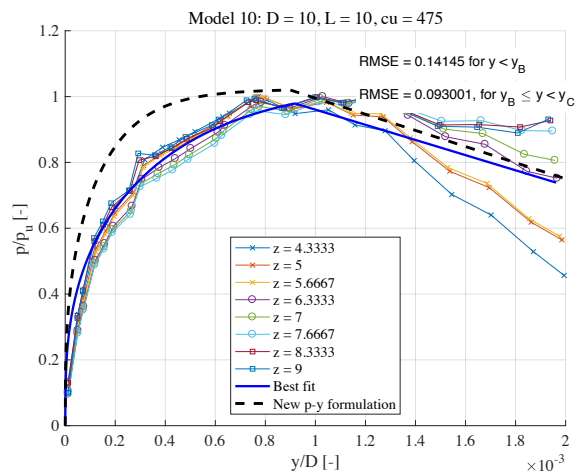
**Figure G.17:** Model 9: Best fit function vs. FE data.



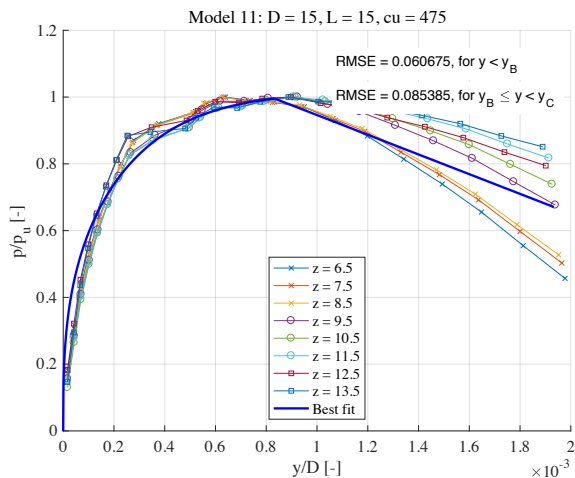
**Figure G.18:** Model 9: New p-y formulation vs. FE data.

**Model 10**

**Figure G.19:** Model 10: Best fit function vs. FE data.



**Figure G.20:** Model 10: New p-y formulation vs. FE data.

**Model 11**

**Figure G.21:** Model 11: Best fit function vs. FE data.

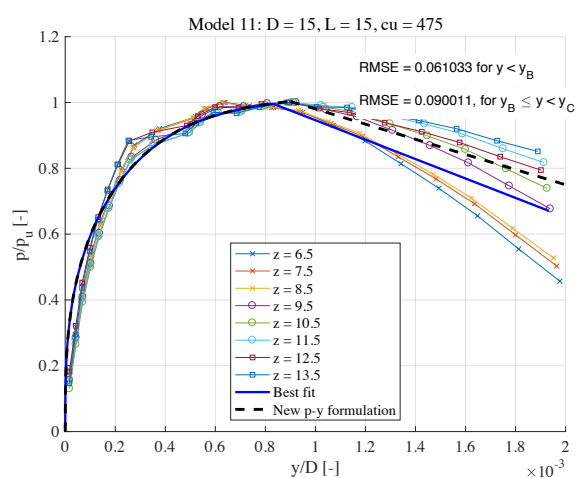


**Figure G.22:** Model 11: New p-y formulation vs. FE data.



## Model 12

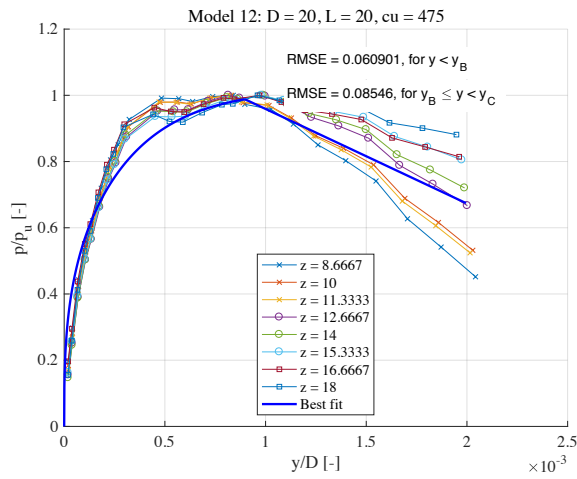


**Figure G.23:** Model 12: Best fit function vs. FE data.

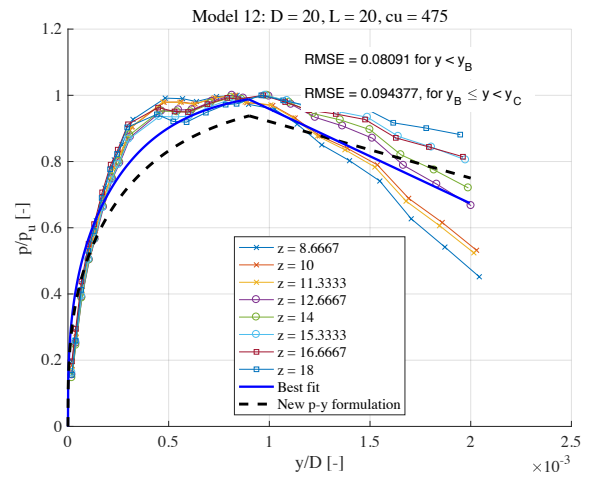


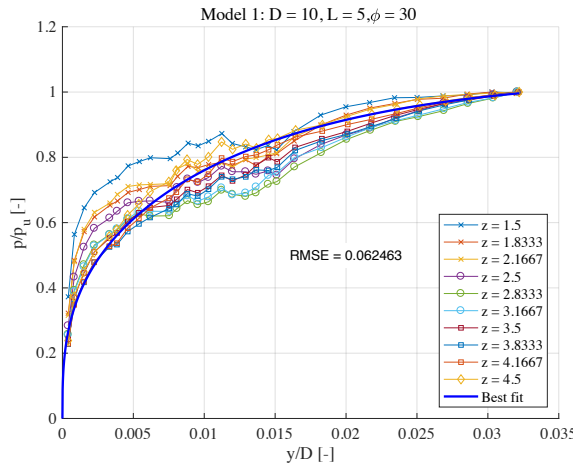
**Figure G.24:** Model 12: New p-y formulation vs. FE data.



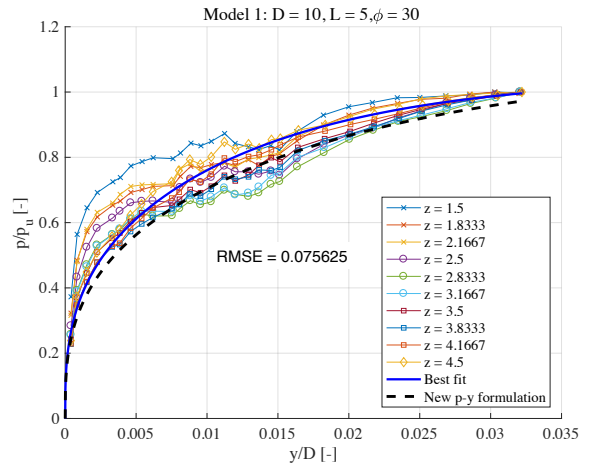
# Plot of p-y Curves for Sand H

Plots of best fit and the developed p-y formulation for the sand are shown in this appendix. The figures also show the normalised p-y curves, as both the soil pressure,  $p$ , and displacement,  $y$ , are shown normalised to the ultimate soil pressure,  $p_u$ , and bucket diameter,  $D$ , respectively.

## Model 1

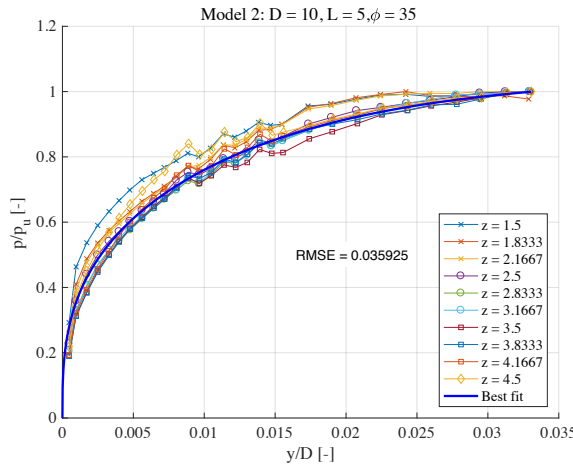


**Figure H.1:** Model 1: Best fit function vs. FE data.

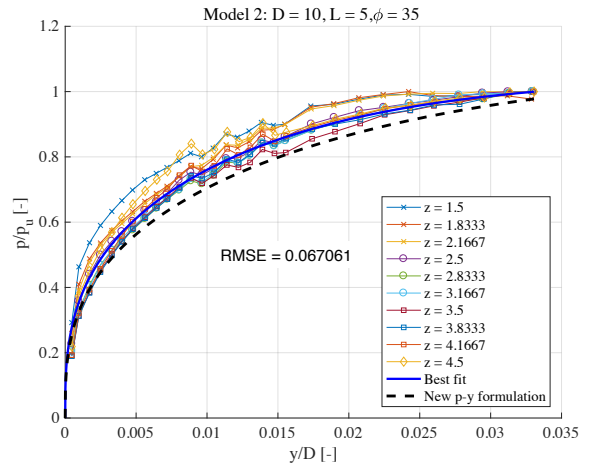


**Figure H.2:** Model 1: New p-y formulation vs. FE data.

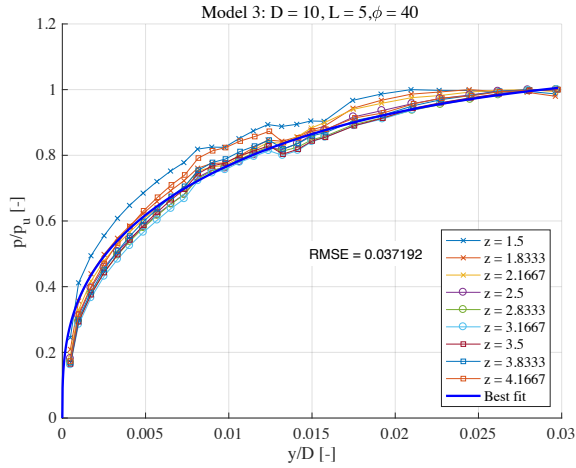
## Model 2



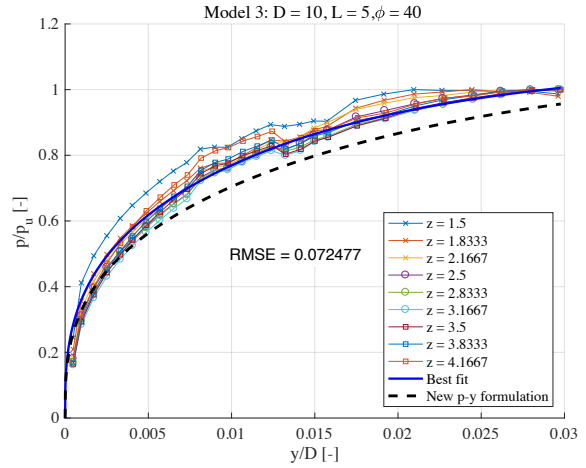
**Figure H.3:** Model 2: Best fit function vs. FE data.



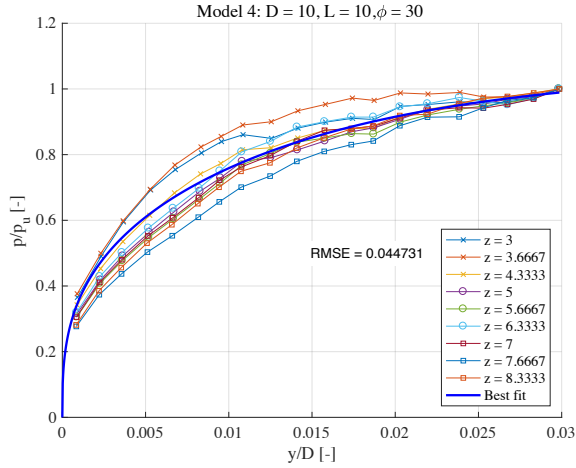
**Figure H.4:** Model 2: New p-y formulation vs. FE data.

**Model 3**

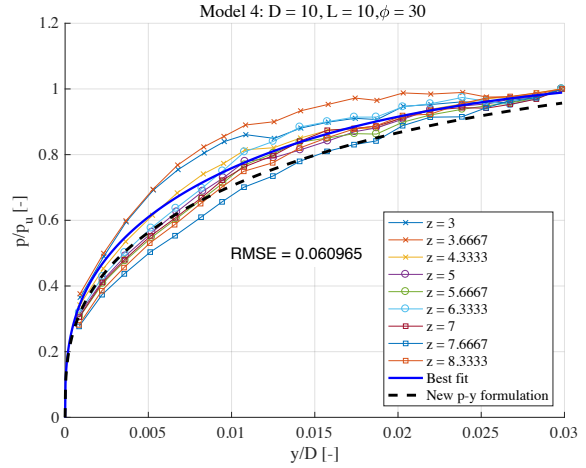
**Figure H.5:** Model 3: Best fit function vs. FE data.



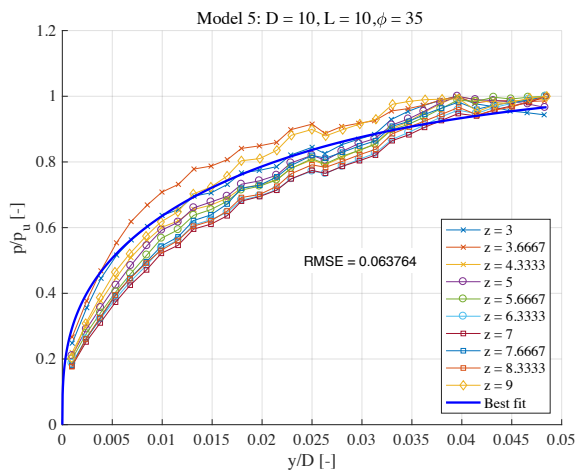
**Figure H.6:** Model 3: New p-y formulation vs. FE data.

**Model 4**

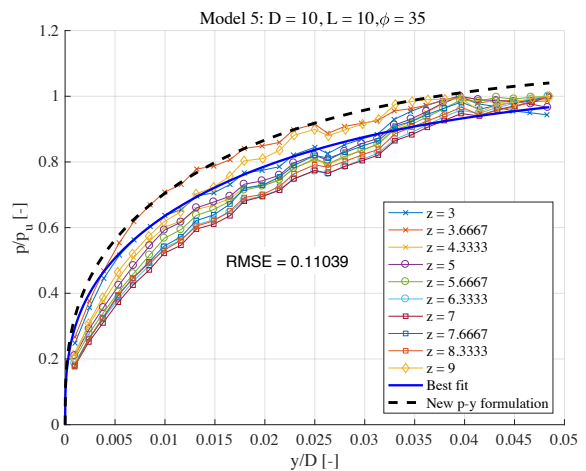
**Figure H.7:** Model 4: Best fit function vs. FE data.



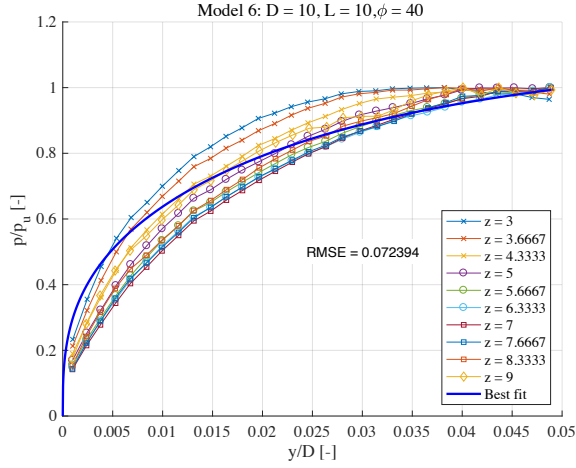
**Figure H.8:** Model 4: New p-y formulation vs. FE data.

**Model 5**

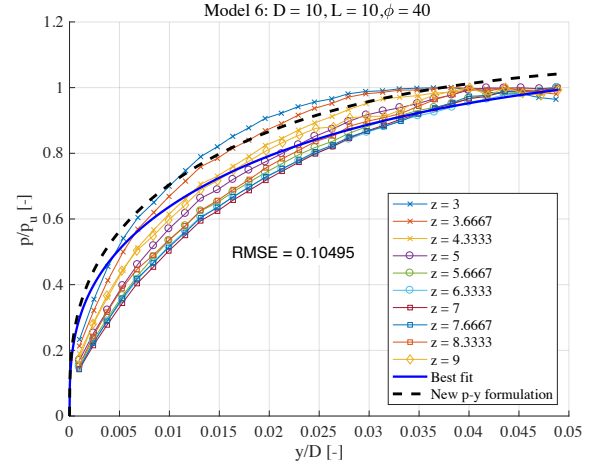
**Figure H.9:** Model 5: Best fit function vs. FE data.



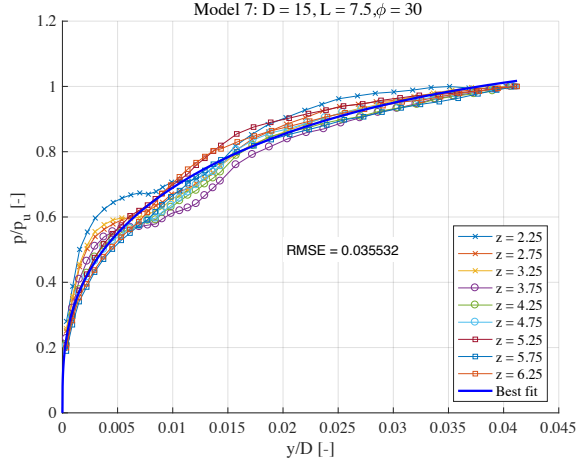
**Figure H.10:** Model 5: New p-y formulation vs. FE data.

**Model 6**

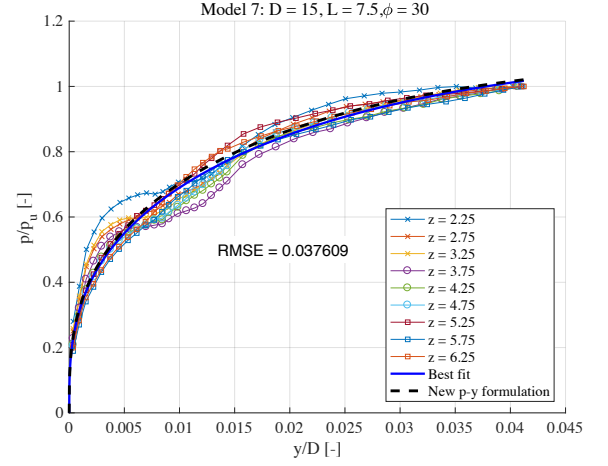
**Figure H.11:** Model 6: Best fit function vs. FE data.



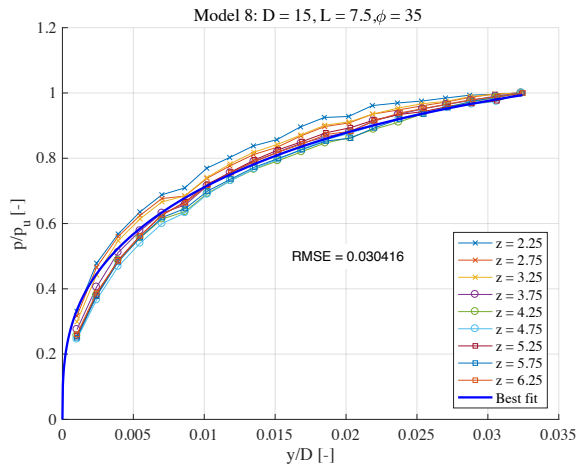
**Figure H.12:** Model 6: New p-y formulation vs. FE data.

**Model 7**

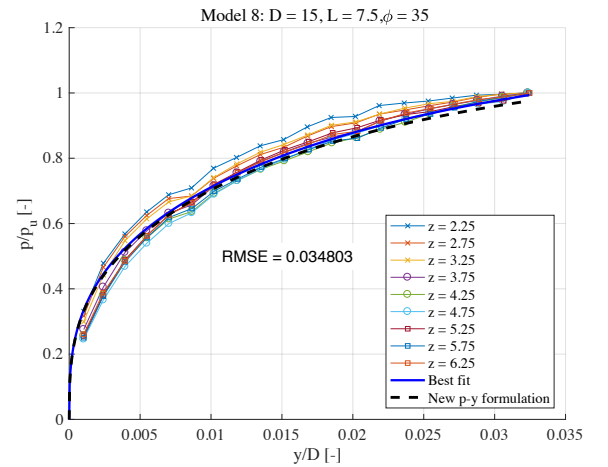
**Figure H.13:** Model 7: Best fit function vs. FE data.



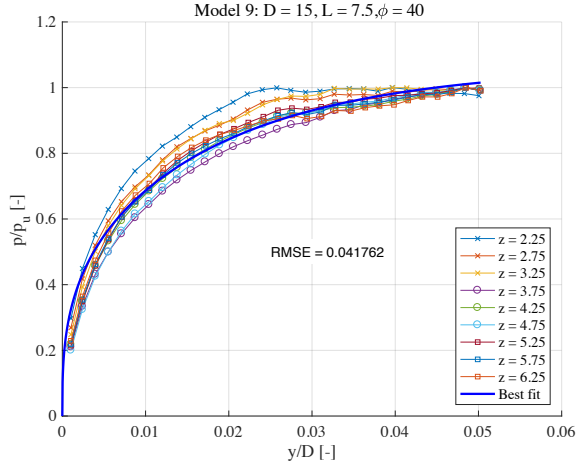
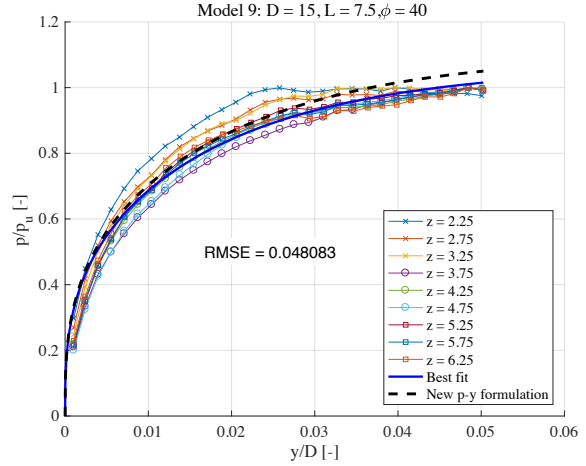
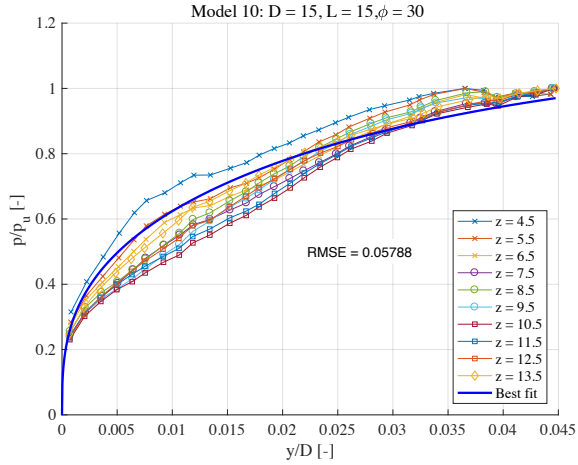
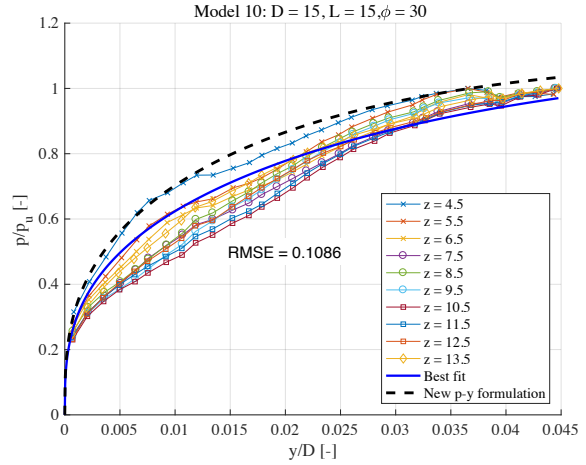
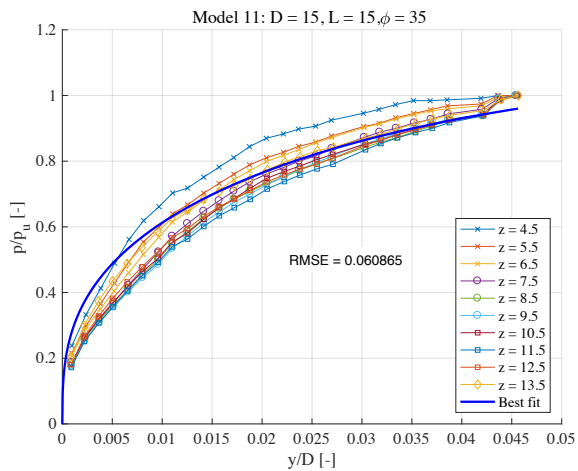
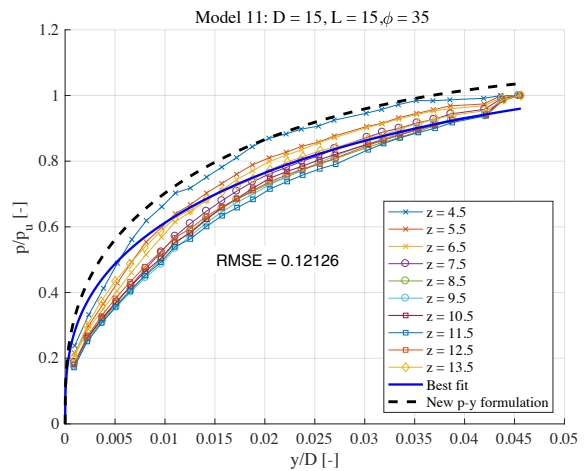
**Figure H.14:** Model 7: New p-y formulation vs. FE data.

**Model 8**

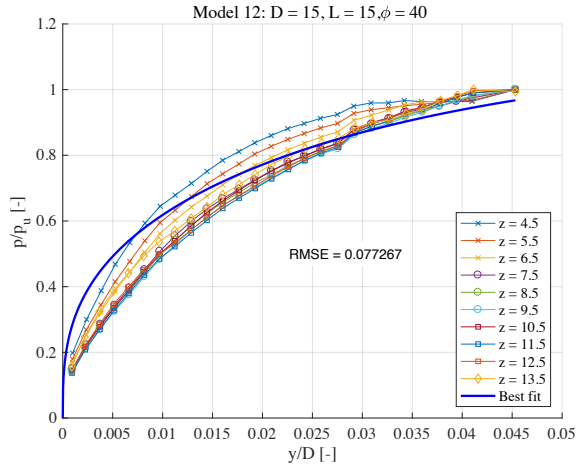
**Figure H.15:** Model 8: Best fit function vs. FE data.



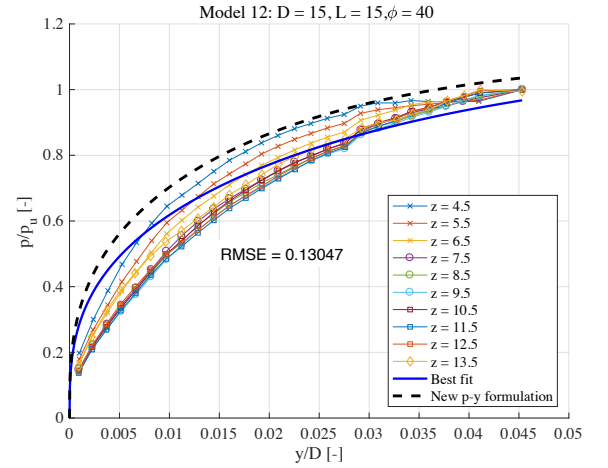
**Figure H.16:** Model 8: New p-y formulation vs. FE data.

**Model 9****Figure H.17:** Model 9: Best fit function vs. FE data.**Figure H.18:** Model 9: New p-y formulation vs. FE data.**Model 10****Figure H.19:** Model 10: Best fit function vs. FE data.**Figure H.20:** Model 10: New p-y formulation vs. FE data.**Model 11****Figure H.21:** Model 11: Best fit function vs. FE data.**Figure H.22:** Model 11: New p-y formulation vs. FE data.

## Model 12

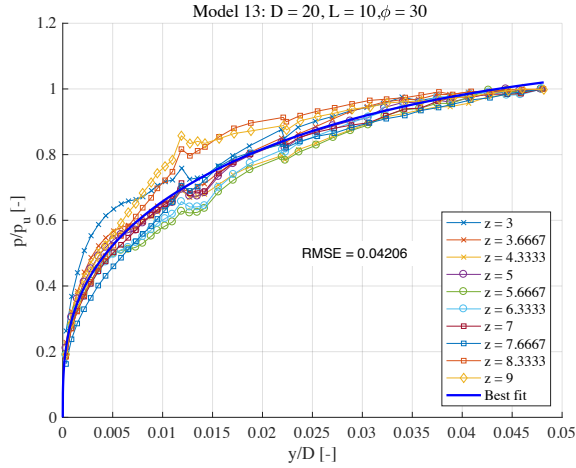


**Figure H.23:** Model 12: Best fit function vs. FE data.

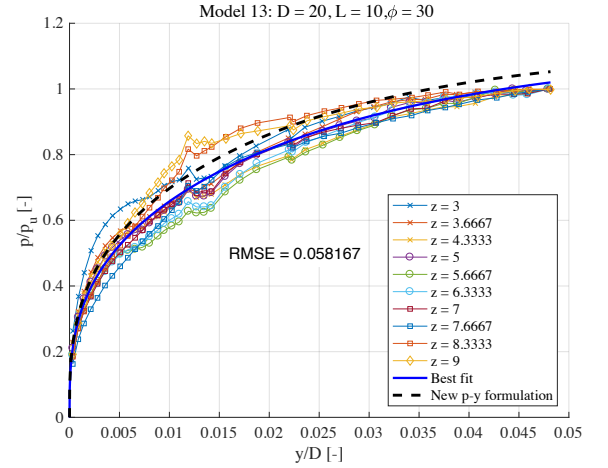


**Figure H.24:** Model 12: New p-y formulation vs. FE data.

## Model 13

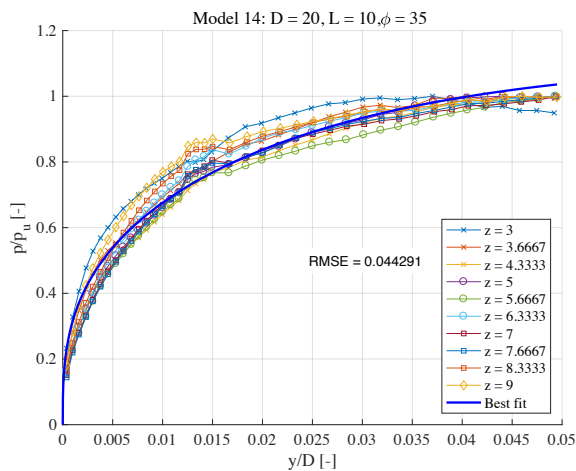


**Figure H.25:** Model 13: Best fit function vs. FE data.

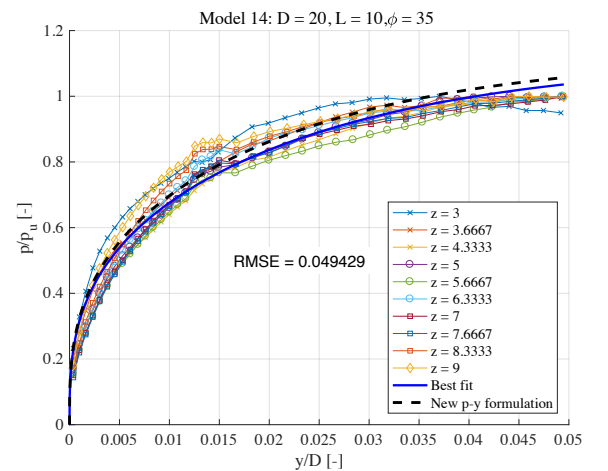


**Figure H.26:** Model 13: New p-y formulation vs. FE data.

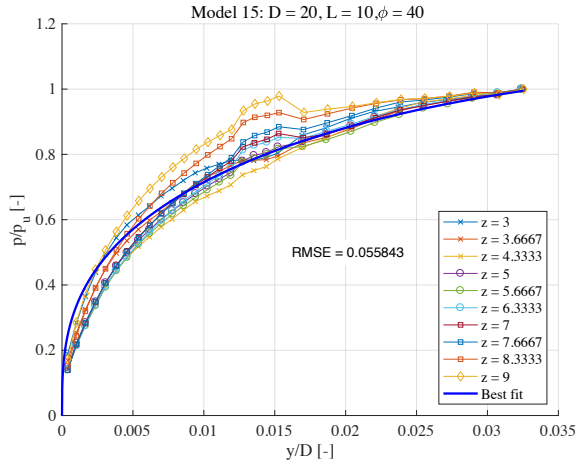
## Model 14



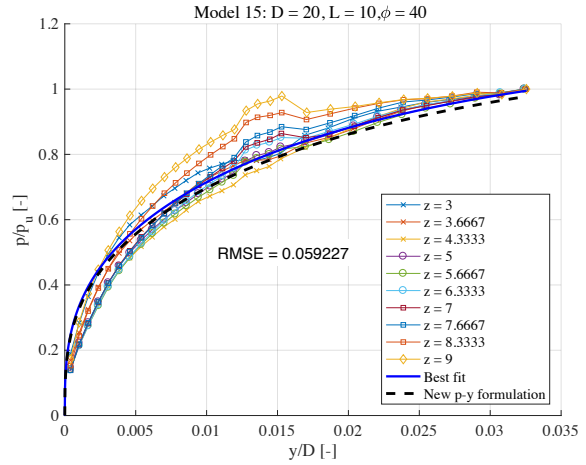
**Figure H.27:** Model 14: Best fit function vs. FE data.



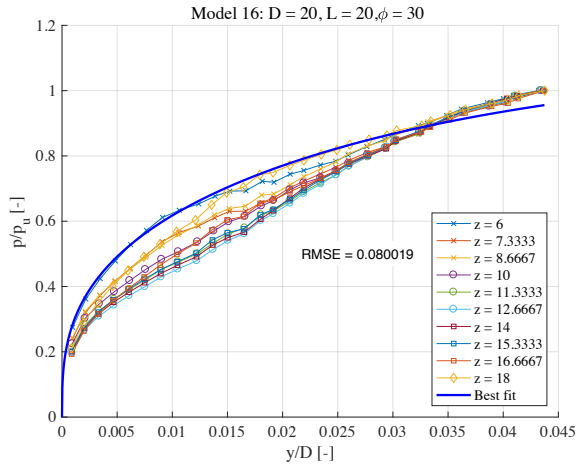
**Figure H.28:** Model 14: New p-y formulation vs. FE data.

**Model 15**

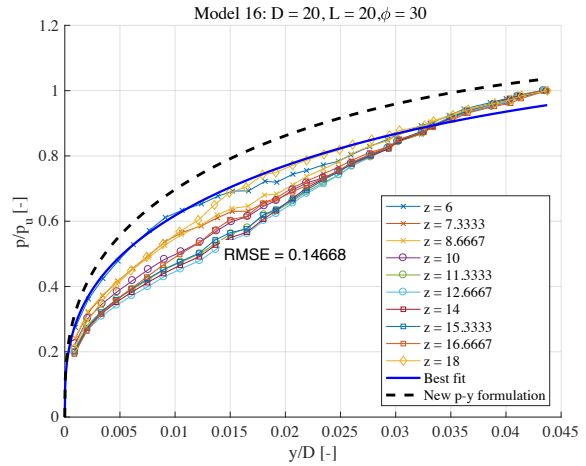
**Figure H.29:** Model 15: Best fit function vs. FE data.



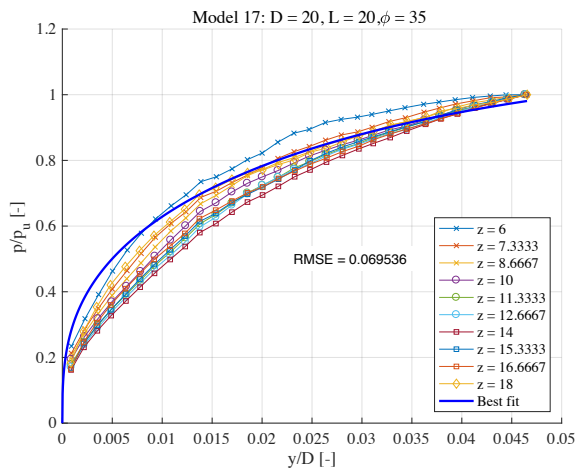
**Figure H.30:** Model 15: New p-y formulation vs. FE data.

**Model 16**

**Figure H.31:** Model 16: Best fit function vs. FE data.



**Figure H.32:** Model 16: New p-y formulation vs. FE data.

**Model 17**

**Figure H.33:** Model 17: Best fit function vs. FE data.

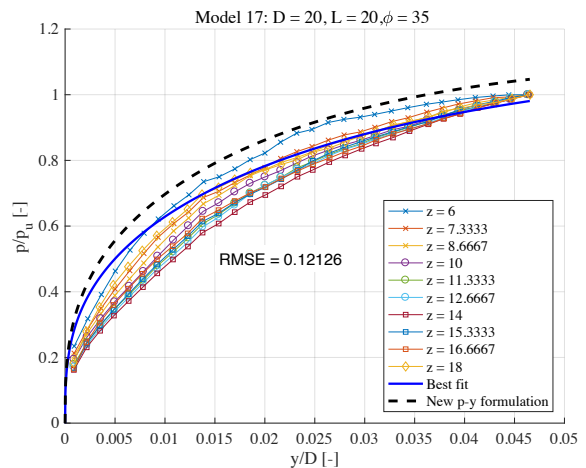


**Figure H.34:** Model 17: New p-y formulation vs. FE data.



## Model 18

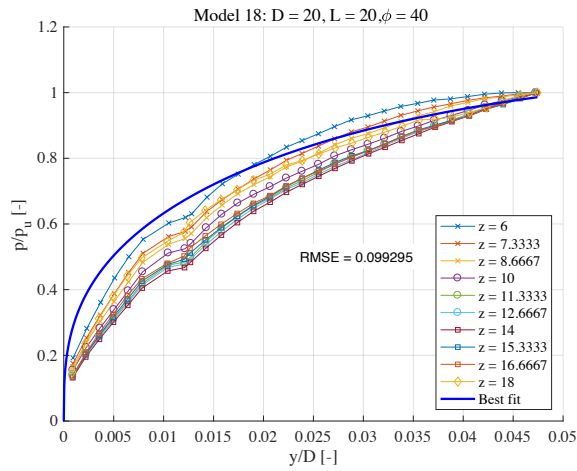


**Figure H.35:** Model 18: Best fit function vs. FE data.

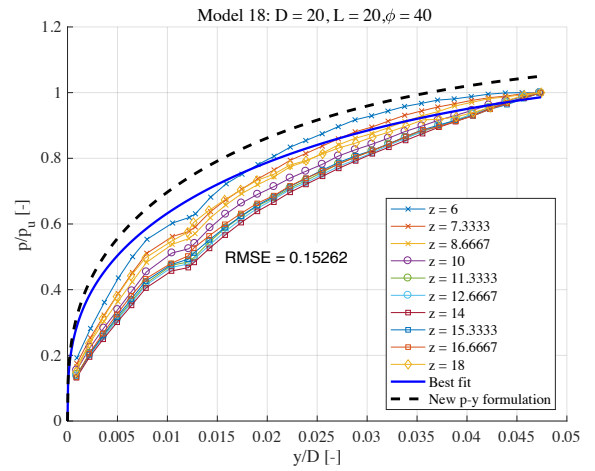


**Figure H.36:** Model 18: New p-y formulation vs. FE data.